Matrix product states and X-ray absorption

by

Yifei Shi

A dissertation submitted in partial fulfillment
of the requirements for the degree of
Doctor of Philosophy
(Department of Physics)
in The University of Virginia
2015

Doctoral Committee:

Professor Israel Klich
Professor Gia-Wei Chern
Professor Seunghun Lee
Professor Ira Herbst

ACKNOWLEDGEMENTS

I give my deepest gratitude to my advisor Prof. Israel Klich. He started to guide me at a difficult time of my Ph.D study, and has always been patient, encouraging, and inspiring. Through constant assistance and advice, he influenced me on different aspects of academic activities, and goes beyond that. His easy-going personality also makes him a best friend next door to me. I owe him my sincere thanks for all the things he has done for me.

I also give thanks to my former advisor Prof. Austen Lamacraft. He has led me into the world of condensed matter physics, when I was pretty much clueless about the academic world.

In addition, I want to express my deeply felt gratitude of the members of my thesis committee, Prof. Gia-Wei Chern, Prof. Seunghun Lee and Prof. Ira Herbst.

I also thank Prof. Paul Fendley, who is now enjoying his time at Oxford, for the many inspiring discussions on criticality and scaling. I also benefited greatly from talking with Prof. Jeffery Teo, on the subject of topological phases. And although only met for a short time, Prof. Gia-Wei Chern has helped me in many ways on numerics.

I must also thank Dr. Andrew James in University College London, for helping me on Monte Carlo simulation, DMRG, and also collaborating on RIXS calculations. And Dr. David Benjamin and Marton Kanasz-Nagy in Harvard both enlightened me on the study of RIXS.

I also give thanks to fellow condensed matter theory students, Amr Ahmadain,

Syed Raza, Alex Sirota, Sharmistha Sahoo, Gabriel Wong, Zhao Zhang, for the good time at UVa, and wish them fortune in their careers.

The support from my parents is very important to me, during the six and half years of study. They always encourage me, although I have yet to find the best way to help them understand what condensed matter really means. One more time, I say "Xiexie" to them.

TABLE OF CONTENTS

LIST OF FIGURES

Figure

LIST OF ABBREVIATIONS

MPS Matrix Product State

FCS Full Counting Statistics

TNS Tensor Network State

TI Translational Invariant

RIXS Resonant X-ray Inelastic Scattering

XAS X-ray Absorption Spectroscopy

OD Optimally Doped

UD Under Doped

MD Medium Doped

ABSTRACT

Matrix product state and X-ray absorption

by

Yifei Shi

The first part of the thesis is dedicated to the study of Matrix Product State (MPS). Initially named "finitely correlated state", MPS is the basis of the Tensor Network State that is widely used to represent quantum many-body wave functions, and is also the essential concept in powerful numerical tools like Density-Matrix Renormalization Group. It is an ansatz that only samples a very small portion of the complete Hilbert space, but can represent ground states of 1-dimensional gapped local Hamiltonians efficiently.

We will first look at the quantum fluctuation of observables in such states. In particular, we consider the Full Counting Statistics of MPS, which is separated into a bulk and boundary term. We identify a central limit theorem like behavior in the limit of large system sizes, and write the corrections of the central limit theorem for a finite size system in terms of the Edgeworth series. We also show that, for special cases of MPSs, like the famous Affleck, Lieb, Kennedy and Tasaki state, because of the topological nature of the state, this description is no longer valid. Next we look at the time-evolution of an MPS under time-dependent Hamiltonians. We show that in the "injective" case, the Schrodinger equation can be written in terms of the MPS matrices in an interesting way. We show, however, it can never produce an exact time-evolution that changes the entanglement structure of the state.

The second part of the thesis focuses on X-ray absorption and scattering. We are particularly interested in the resonant inelastic X-ray scattering (RIXS), which has been rapidly developing recently. However, there is still an on-going debate about whether the RIXS spectrum of cuprate systems shows collective or quasi-particle physics. We first use a simple perturbation method to get a basic idea about the physics of the process. Then we use a determinant method and the quasi-particle picture to study the RIXS response of a variety of cuprate systems, like CLBLCO, YBCO, and Bi-2201, and find excellent agreement with experiments. We also develop a method to account for the superconducting gap within a meanfield approach and study it in detail for a model of p-wave superconductor. Although the gap is small compared to other band structure parameters, the effect of the gap is rather significant.

CHAPTER I

Introduction to Matrix Product State

1.1 The fundamental problem in condensed matter physics, and the MPS approach

A fundamental problem in condensed matter physics is the extremely large number of degrees of freedom in the system. For a system of N spin 1/2 particles, the Hilbert space is 2^N dimensional. Modern computational techniques can deal with $N \sim 30$, considering that in reality there are $N \sim 10^{22}$ particles on a macroscopic level, it becomes completely impossible to solve the problem exactly, other than in very special models. Even if we consider a system with only 100 spins, which in some cases is just enough to show statistical behavior, there will be a 10^{30} dimensional Hilbert space. If we ever try to store an exact state of the system into a computer, assuming each coefficient is represented by a double-precision number that takes 8 bytes, then a total disk space of $\sim 10^{19}$ Terabytes (TB) is needed. If a 1TB hard drive weights 0.5 pounds, then the total mass of the hard drives needed is about 400 times larger than the mass of Mount Everest.

To deal with this problem, theoretical methods like mean field theory, perturbation theory are commonly used, and numerically, methods like Monte Carlo and density matrix renormalization group (DMRG) are the main tools. DMRG is proven to

be really effective in 1 dimension [78], it is a variational method based on matrix product state (MPS), an ansatz of states that is particularly simple but effective [60], at representing the ground state of local gapped Hamiltonians. Here "local" means the interaction terms in the Hamiltonian decay at least exponentially in space, and gapped means the excited states have finite energy difference from the ground state, even in the thermodynamic limit (the gap will always exist for a finite system without degeneracy). In Chap I and Chap II, we focus on the basic concepts and applications of MPS, to get an idea about how MPS can deal with the fundamental problem.

1.1.1 The AKLT state, where everything started

We start from the most famous example of MPS, the Affleck, Lieb, Kennedy and Tasaki (AKLT) state [1], the Hamiltonian is a spin-1 chain:

$$H = \sum_{<i,j>} \vec{S_i} \cdot \vec{S_j} + \Delta(\vec{S_i} \cdot \vec{S_j})^2 \tag{1.1}$$

At $\Delta = \frac{1}{3}$, the Hamiltonian is special and can be written in term of "projectors". Consider that for spin-1, $(\vec{S_i} + \vec{S_j})^2 = 2S^2 + 2\vec{S_i} \cdot \vec{S_j}$, it has eigenvalues 6, 2 or 0 if the total spin is 2, 1, or 0. An operator in this form: $P_{i,j} = \frac{1}{24}(\vec{S_i} + \vec{S_j})^2((\vec{S_i} + \vec{S_j})^2 - 4)$, would give 1 if the total spin is 2, and 0 if the total spin if 1 or 0. P_{ij} is then called a projector onto the spin-2 subspace. We found that at $\Delta = \frac{1}{3}$, H is just a sum of projectors: $H = \sum_i (\frac{1}{6} P_{i,i+1} - \frac{1}{3})$, where $P_{i,i+1}$ projects from the Hilbert space of two spin-1 degree of freedom to the subspace where neighboring spin-1s have a total spin 2. Since the projector always has a non-negative expectation value, to minimize the energy, all the projectors should give 0, i.e. the neighboring spin-1s always have total spin 0 or 1. This can be satisfied by imagining that there are 2 spin-$\frac{1}{2}$s on each site, in order to give a total spin of 1. these spins are restrained to be in a triplet state. Neighboring spin-$\frac{1}{2}$s on different sites are taken in a singlet state Then the total spin

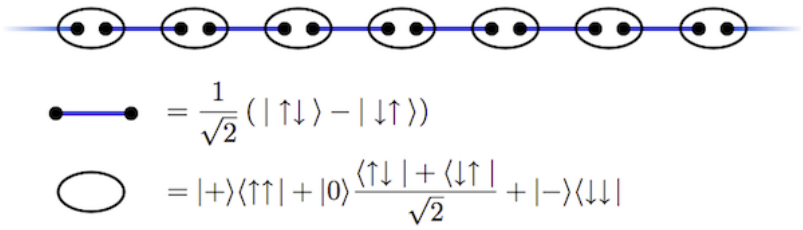

Figure 1.1: The AKLT state. Black circles represent the physical spin-1 space on each site, which is considered as two spin-1/2s and then projected onto total spin-1 subspace. Blue line means the two auxiliary spin-1/2s are in a singlet state. This makes sure the projector $H_{i,i+1}$ gives 0.

of 2 spin-1s on neighboring sites would be the addition of 2 spin-1/2s, which is always 1 or 0, as shown in Fig 1.1 [79]. Below, spin-1 states are denoted by $+, 0, -$ and spin-$\frac{1}{2}$ states by $\uparrow, \downarrow$.

With the help of this picture we can write the state explicitly. Define the following matrices for each spin-1 state:

$$A^+ = \begin{pmatrix} 1 & 0 \\ 0 & 0 \end{pmatrix} \begin{pmatrix} 0 & 1 \\ -1 & 0 \end{pmatrix} = \begin{pmatrix} 0 & 1 \\ 0 & 0 \end{pmatrix}$$

$$A^0 = \frac{1}{\sqrt{2}} \begin{pmatrix} 0 & 1 \\ 1 & 0 \end{pmatrix} \begin{pmatrix} 0 & 1 \\ -1 & 0 \end{pmatrix} = \begin{pmatrix} -\frac{1}{\sqrt{2}} & 0 \\ 0 & \frac{1}{\sqrt{2}} \end{pmatrix}$$

$$A^- = \begin{pmatrix} 0 & 0 \\ 0 & 1 \end{pmatrix} \begin{pmatrix} 0 & 1 \\ -1 & 0 \end{pmatrix} = \begin{pmatrix} 0 & 0 \\ -1 & 0 \end{pmatrix}$$

Here the A matrices act on the spin-$\frac{1}{2}$ Hilbert space, they are written as mutiplication of 2 matrices, the first one is the projection onto spin triplet state, as the black circle in Fig 1.1, the second one takes $|\uparrow\uparrow\rangle + |\downarrow\downarrow\rangle$ to $|\uparrow\downarrow\rangle - |\downarrow\uparrow\rangle$, so the As eventually projects from the maximally entangled state of the spin-$\frac{1}{2}$ state to the desired spin-1 states.

And we can write:

$$| AKLT\rangle \propto \sum_{\{s_i\}} \mathrm{Tr}(\prod_i A^{s_1} A^{s_2} ... A^{s_n}) |s_1 s_2 ... s_n\rangle \tag{1.2}$$

We use $\{s_i\}$ to represent a spin configuration, $|s_1, s_2, ..., s_i, ..., s_N\rangle$, and the summation is over all position spin configuratinos $\{s_i\}$. States with this form are called Matrix Product States. The coefficient of a spin configuration is given by the trace of product of matrices for this configuration. This form can be generalized to any 1-dimensional system. If we have a spin chain of N sites, and the physical space on each site has dimension d, we break it into an auxiliary Space of $D \times D$, with 2 auxiliary spins. Neighboring auxiliary spins are in a maximumly entangled state: $\sum_{i=1}^{D} |i\rangle|i\rangle$.

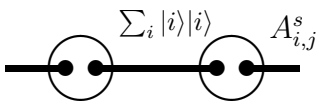

Next we use matrix $(A^{s_k}_{[k]})_{i,j}$ to project from $D \times D$ dimensional auxiliary space to d dimensional physical space. Here $[k]$ is the site number, s_k is the spin on site k. i and j are the indices of the matrix. We get:

$$| \Psi_M\rangle = \sum_{\{s_i\}} \prod_i \mathrm{Tr}(A^{s_1}_{[1]} A^{s_2}_{[2]} ... A^{s_N}_{[N]}) |s_1, s_2, ..., s_N\rangle (\mathrm{PBC}) \tag{1.3}$$

for periodic boundary condition(PBC), and

$$| \Psi_M\rangle = \sum_{\{s_i\}} \prod_i A^{s_1}_{[1]} A^{s_2}_{[2]} ... A^{s_N}_{[N]} |s_1, s_2, ..., s_N\rangle (\mathrm{OBC}) \tag{1.4}$$

for open boundary condition(OBC). Here $A_{[1]}$ and $A_{[N]}$ are row and column vectors respectively.

1.1.2 Schmidt decomposition and Conanical form

Here we look at a useful way of treating a many-body wave function, which is especially convenient for MPSs. If we have a wave function on N sites, if we divide system into subsystem A(L sites) and B($N-L$ sites), we can always write:

$$\mid \psi\rangle = \sum_{i=1}^{d^L} \sum_{j=1}^{d^{N-L}} C_{ij} |i\rangle_A \otimes |j\rangle_B \tag{1.5}$$

$\mid i\rangle$ and $\mid j\rangle$ are some basis set for A and B. We can do a single value decomposition: $C = UDV$, U and V are unitary, and D is diagonal with semipositive elements, called Schmidt coefficients λ_α. Then the wave function is:

$$\begin{aligned} |\psi\rangle &= \sum_{\alpha=1}^{\chi} \lambda_\alpha (\sum_{i=1}^{d^L} U_{i\alpha} |i\rangle_A) \otimes (\sum_{j=1}^{d^{N-L}} V_{\alpha j} |j\rangle_B) \\ &= \sum_{\alpha=1}^{\chi} \lambda_\alpha |\phi_\alpha^{[A]}\rangle \otimes |\phi_\alpha^{[B]}\rangle \end{aligned} \tag{1.6}$$

χ is the number of non-zero Schmidt coefficients. The basis functions ϕ are orthonormal: $\langle \phi_\beta^{[A]} | \phi_\alpha^{[A]} \rangle = \delta_{\alpha\beta}$ and $\langle \phi_\beta^{[B]} | \phi_\alpha^{[B]} \rangle = \delta_{\alpha\beta}$. Eq (1.6) is called the Schmidt decomposition. If the state is written in this form, we look at the reduced density matrix of subsystem A, then:

$$\rho_A = \sum_{\alpha=1}^{\chi} \lambda_\alpha^2 \mid \phi_\alpha^{[A]} \rangle \langle \phi_\alpha^{[A]} \mid \tag{1.7}$$

and the rank of $\rho_{A(B)}$ is just χ.

For a MPS, the Schmidt decomposition is particularly usefull. If we divide the state into left and right part,

$$\mid \Psi_M \rangle = \sum_{\alpha=1}^{D} \mid \phi_\alpha^{left} \rangle \otimes \mid \phi_\alpha^{right} \rangle \tag{1.8}$$

with

$$\begin{aligned}\phi_\alpha^{left} &= \sum_{\{s_1,...s_i\}} A_{[1]}^{s_1} A_{[2]}^{s_2} ... A_{[i]}^{s_i} |s_1, s_2, ..., s_i\rangle \\ \phi_\alpha^{right} &= \sum_{\{s_{i+1},...s_N\}} A_{[i+1]}^{s_{i+1}} A_{[i+2]}^{s_{i+2}} ... A_{[N]}^{s_i} |s_{i+1}, s_{i+2}, ..., s_N\rangle \end{aligned} \tag{1.9}$$

It already looks like the form in Eq (1.6), but ϕ_α may not be orthonormal. On the other hand, if we change $A_{[i]} \to X_i^{-1} A_{[i]} X_{i+1}$, the state is invariant, this is some type of gauge freedom. So we have the freedom to choose X_i, and can choose the gauge so that Eq (1.8) is exactly the Schmidt decomposition. This gauge is called the canonical gauge. In the case of PBC and $A_{[i]}^{s_i}$ are the same for every site, we can drop the subscript $[i]$, the canonical form has the following property [60]: the A^{s_i}s have a block diagonal form:

$$A^{s_i} = \begin{pmatrix} \lambda_1 A_1^{s_i} & 0 & 0 \\ 0 & \lambda_2 A_2^{s_i} & 0 \\ 0 & 0 & ... \end{pmatrix}$$

$1 \geq \lambda_i > 0$, and $A_j^{s_i}$ obey the constrains:

$$\sum_i A_j^{s_i} A_j^{s_i \dagger} = \mathbb{I} \tag{1.10}$$

$$\sum_i A_j^{s_i \dagger} \Lambda_j A_j^{s_i} = \Lambda_j \tag{1.11}$$

where j is the index of the diagonal block, and Λ_j is a positive diagonal matrix with trace equal to 1. In this thesis, we are most interested in the case that the As only have 1 block, since this is the "irreducible" case. We can then drop the j index and

write:

$$\begin{aligned} \sum_i A^{s_i} A^{s_i\dagger} &= \mathbf{I} \\ \sum_i A^{s_i\dagger} \Lambda A^{s_i} &= \Lambda \end{aligned} \tag{1.12}$$

where Λ is diagonal, positive, full rank and has trace 1. This is also called the injective case.

1.1.3 Properties of MPS

In this section we derive some important properties for a translational invariant MPS with PBC:

$$\mid \Psi_A\rangle = \sum_{\{s_i\}} \mathrm{Tr}(\prod_i A_{s_i}) |\{s_i\}\rangle \tag{1.13}$$

First the overlap of the MPSs Ψ_A and Ψ_B is:

$$\begin{aligned} \langle \Psi_B \mid \Psi_A \rangle &= \sum_{\{s_i\}} \mathrm{Tr}[(\prod_i A_{s_i})] \mathrm{Tr}[(\prod_i B^*_{s_i})] \\ &= \mathrm{Tr}(E_{AB}^N) \end{aligned} \tag{1.14}$$

where $E_{AB} = \sum_i \bar{A}_{s_i} \otimes B_{s_i}$. In particular when $A = B$, $|\Psi_A|^2 = \mathrm{Tr}[(E_A)^N]$,

$$E_A = \sum_i \bar{A}_{s_i} \otimes A_{s_i} \tag{1.15}$$

which is also called transfer matrix of MPS. Assume E_A can be diagonalized, $E_A = V^{-1} D V$, where D is diagonal, then only the largest eigenvalues matter in the thermodynamic limit $N \to \infty$. We are mostly interested in the case that the largest eigenvalue is not degenerate, or the injective case [60], in this case the only largest eigenvalue λ_M must be 1 if the state is normalized.

The expectation value of an operator $\hat{O}$ can also be written in a nice way:

$$\begin{aligned} \langle \hat{O}_i \rangle &= \mathrm{Tr}((E_A)^{N-1} E_A^O) \\ \langle \hat{O}_i \hat{O}'_j \rangle &= \mathrm{Tr}(E_A^O (E_A)^{j-i-1} E_A^{O'} (E_A)^{N-j+i-2}) \end{aligned} \tag{1.16}$$

where $E_A^O = \sum_{i,j} O_{i,j} A_{s_i} \otimes \bar{A}_{s_j}$. An interesting quantity to look at is the two point function: $C(r) = \langle \hat{O}_0 \hat{O}_r \rangle - \langle O \rangle^2$, from Eq (1.16), when r is large enough, $C(r) \sim \lambda_2^r \sim exp(-r/\xi)$, where λ_2 is the second largest eigenvalue of E_A, and $\xi = \log(1/\lambda_2)$. So the correlation for MPS can only decay exponentially (injective case) or stay as a constant. We know that in a critical system, the correlation will in general be a power law decay, so MPS can not truely represent a critical system, but instead will give an effective correlation length of $\xi \sim \log D$. In practice, methods like DMRG can still simulate ground states of gapped system effectively nonetheless.

As an example, let's look the AKLT state in Eq (1.2), the E_A matrix can be calculated as: $E = \begin{pmatrix} \frac{1}{2} & 0 & 0 & 1 \\ 0 & -\frac{1}{2} & 0 & 0 \\ 0 & 0 & -\frac{1}{2} & 0 \\ 1 & 0 & 0 & \frac{1}{2} \end{pmatrix}$, the eigenvalues of E are 1.5, -1/2, -1/2, -1/2. That means that the state is not normalized yet, to normalize it we should multiply the As by a factor of $\sqrt{\frac{2}{3}}$, and the eigenvalues become: 1, -1/3, -1/3, -1/3. The correlation of AKLT state decays as $C_r \sim (-1)^r e^{-r/log(3)}$, the $(-1)^r$ factor means it is anti-ferromagnetic.

1.2 Effectiveness of MPS

In Sec 1.1 we see that for a spin chain with N sites, MPS uses $\sim N$ number of parameters to describe a state, instead of the full Hilbert space dimension $\sim e^N$, this is an extremely small portion when N is large. Then how do we know the MPS

representation is useful at all? It turns out that if the Hamiltonian is a 1D local Hamiltonians with a gap, MPS is a good approximation to the ground state[72]. The reason is that for a subsystem of any size, MPS is only keeping a maximum of D states, where D is the dimension of the matrices. And in 1D, it is believed that for the ground state of gapped Hamiltonian, the Schmidt coefficients of the subsystem decays exponentially [62], and only the states with largest coefficients matter. Unfortuanatly this is not true in 2 or higher dimension.

1.3 Generalization of MPS

1.3.1 Graphic representation

MPS can be graphically represented, we denote the matrix A on each site by a circle, and denote every index of the matrix by a leg, each connected leg means summing over the associated index:

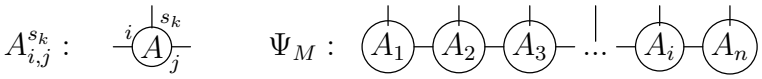

The calculation of the normalization of a state can also be graphically represented:

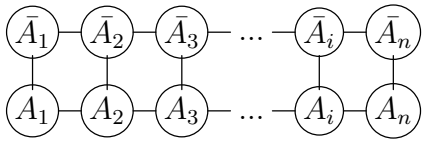

1.3.2 Tensor Network States

With the graphical method we can easily create states made of tensors. They are called Tensor Network State (TNS), an example is shown in Fig 1.2. If we cut the system into two parts, then entanglement between the two parts can be roughly estimated by counting the number of legs that are cut by the partition. Note that

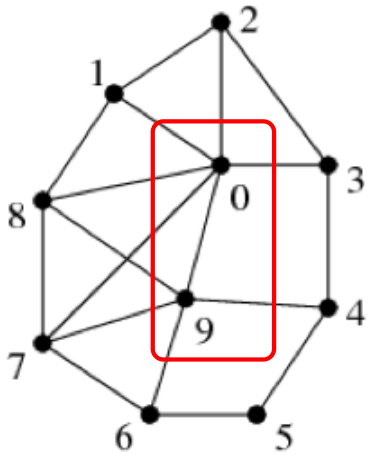

Figure 1.2: A TNS, every dot represents a tensor, and every leg represents a index. If we make a cut, the red line, the entanglement $S \sim \#$ of legs cut by the partition.

if this kind of partition is made in 1D, there can only be two legs that are cut, but in two or higher dimension this number increases with the length of the boundary between the two parts.

One commonly used TNS is the straightforward generalization of MPS to 2D, which is called Projected Entanglement Pair State (PEPS)[73], as shown in Fig1.3. In a 2D PEPS, there's a tensor (instead of a matrix as in MPS) on site r of the lattice, $A^{[r]}_{ijkl}$, the 4 indices of the tensor connects to each of the 4 neighbors. Unlike the simple case in MPS, the normalization of PEPS is computationally hard, and there's no general rule on whether there exists a canonical form [74], the reason is that in 1D, if one cuts the MPS into 2 parts, the number of legs cut by the partition is always 2, while in 2D, this number grows as the partition grows larger, and the computational cost grows accordingly. To calculate the normalization and operator expectation values, methods like tensor renormalization group are commonly used [52].

The other example of TNS is the Multi-scale entanglement renormalization ansatz (MERA)[75], shown in Fig1.4. It is designed to describe critical systems. The structure of MERA consists of many layers, corresponding to a coarse graining, or real

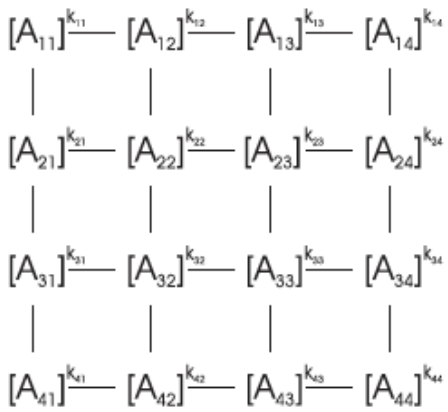

Figure 1.3: Graphic representation of PEPS, in 2 dimension, it cal also describe critical systems.

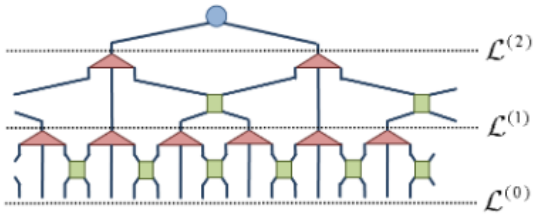

Figure 1.4: Graphic representation of MERA. It has many layers, representing the real space renormalization procedure.

space renormalization procedure: the bottom layer($\mathcal{L}^{\{0\}}$) is the initial state of the system, then a "disentangler"(green box) is used to disentangle neighboring sites and a projector (red triangle) is used to reduce the number of sites in the system by a factor of 3, to get the next layer($\mathcal{L}^{\{1\}}$). This procedure is repeated to get the final state (blue dot), and the final state has no entanglement. In this system, if one makes a partition in the bottom, then the minimal cut is to go up several layers until all the cut area is in the same site, then go back to the bottom layer. The number of legs cut by the partition is then: $\sim \log_3 L$, with L being the size of the cut region. Since the entanglement of the subsystem for 1D system generally goes as $\sim \log L$ [29], this structure has advantages when dealing with critical systems.

CHAPTER II

Full Counting Statistics and time evolution of Matrix Product States

In Chap I we saw that MPSs are useful for describing the ground states of 1 dimensional local Hamiltonians. On the other hand, there are still many open problems in this field, like what is the manifold of 1D MPS with a fixed matrix dimension D, and what is the best MPS to approximate a certain state. In this chapter we study MPS by exploring some interesting properties, the Full Counting Statistics [65] in Sec 2.1 and time evolution in Sec 2.2.

2.1 Full Counting Statistics for Matrix Product State

2.1.1 Introduction to Full Counting Statistics

To formally introduce full counting statistics, we consider a discrete probability distrubution $P(N)$, $\sum_N P(N) = 1$, and a cumulant generating function:

$$\chi(\lambda) = \langle e^{i\lambda N} \rangle = \sum_N e^{i\lambda N} P(N) \tag{2.1}$$

the cumulants are defined as the Taylor expansion of $\log(\chi(\lambda))$:

$$\log(\chi(\lambda)) = \sum_n C_n \frac{(i\lambda)^n}{n!} \tag{2.2}$$

The first few cumulants are: $C_1 = \langle N \rangle$, $C_2 = \langle N^2 \rangle - \langle N \rangle^2$, $C_3 = \langle (N - \bar{N})^3 \rangle$.

With the advantage of precision experiments in condensed matter physics, it is now possible to probe the nature of correlated quantum systems to ever higher degrees of detail and precision. This is especially apparent in cold atom systems, where in addition to refined correlation measurements, we also have fine control of the Hamiltonian parameters themselves. One of the most useful ways of studying detailed correlations in the intermediate regime between the macroscopic, thermodynamic properties, and the microscopic, atom by atom level, is through the full counting statistics functions. These describe the full probability distribution of suitable observables, such as the magnetization of a block of spins in a spin chain or the total excess charge flowing through a quantum point contact.

The full counting statistics function (FCS) contains detailed information about the properties of the state. It has been a useful tool to analyze quantum states, from it's original appearance in quantum optics, in the theory of photon detectors [30, 56] in quantum optics to counting statistics of electrons in mesoscopic systems introduced by Levitov and Lesovik [54]. The full counting statistics has studied in numerous electronic systems theoretically [58, 7, 63, 47, 53] as well as in experiments [13, 25]. The utility of full counting statistics for cold atoms was pointed out in [17]. It has also been demonstrated that in certain cases counting statistics may be used to characterize block entanglement entropy in fermions states and spin states [43, 42, 66]. Recently, the analyticity properties of the "bulk" component of the full counting statistics of classical Ising and quantum XY spin chains has been used as an alternative characterization of phases [38].

2.1.2 FCS for MPS

Here, we explore the quantum noise in MPS [55]. MPS has convenient properties that allow a thorough study of correlations and fluctuations in them, for example, an analog of the Wick's theorem has been demonstrated for generic translationally invariant MPS in [35]. Finally, we remark that our results also hold for certain other states as long as the probability distribution of certain measurements may be described in terms analogous to MPS, a prominent example for which is the exact solution of the 1D asymmetric exclusion process [21], in a recent paper, the full counting statistics for the asymmetric exclusion model was considered in [31].

Here, we concentrate on the corrections to the central limit theorem (CLT). The central limit theorem is a description of the statistics of averages of independent random variables, stating that properly weighted average tend to a Gaussian distribution when the number of random variables is large. Since the correlation length in an MPS, say, is finite, one may expect gaussian-like behavior for the magnetization of large blocks of spins. We find that the simple structure of the MPS allows us to not only do this but much more: we can controllably identify how the central limit of magnetization is reached, what are the main corrections (a consequence of entanglement in the system) and show how CLT may sometimes completely fail in cases of topological states.

The distribution of magnetization approach to Gaussian behavior at large spin blocks is substantially more intricate for the MPS as opposed to independent random variables. To address this behavior we concentrate on deriving the asymptotic probability distribution and corrections to it. While in many cases, even when the distribution seems Gaussian in the infinite block size limit, the corrections due to finite block size are modified. Such corrections are described, for independent, identically distributed variables using various asymptotic series such as the Gram-Charlier A series and the Edgeworth series [46, 11]. The Edgeworth series has been extensively

studied in the mathematical literature, with the focus on ensuring it's applicability when dealing with random identically distributed variables, which may have divergent moments, see e. g. [24, 61, 12]. Here, we derive an expression for the asymptotic corrections to the central limit error function of MPS in analogy to the asymptotic Edgeworth series. We start by deriving formulas for the full counting statistics generating function.

2.1.3 General formula

Let us consider an MPS with periodic boundary conditions on N spins, defined as follows:

$$\psi = \Sigma_{\{\sigma\}} \mathrm{Tr}\left(A_{\sigma_1} A_{\sigma_2} .. A_{\sigma_N}\right) \left|\sigma_1 \sigma_2 ... \sigma_N\right\rangle \tag{2.3}$$

where $A_\sigma \in \{A_1, ..A_S\}$, S is the spin index, and $\sigma_1 \in \{1, ..S\}$. The matrices A are of size $D \times D$, where D is called the bond dimension.

To express the full counting statistics of the spin variable σ, we define:

$$E(\lambda) = \Sigma_\sigma e^{i\lambda\sigma} \bar{A}_\sigma \otimes A_\sigma. \tag{2.4}$$

The full counting statistics generating function of the magnetization of a block of l sites is then given by

$$\chi(\lambda; l; N) \equiv \textstyle\sum_n \mathrm{prob}(\text{total spin of block} = n) e^{i\lambda n} = \ = \left\langle e^{i\lambda \hat{\mathcal{S}}_l} \right\rangle = \frac{\mathrm{Tr} E(\lambda)^l E(0)^{N-l}}{\mathrm{Tr} E(0)^N}.$$

Here $\hat{\mathcal{S}}_l = \Sigma_{i=1}^l \hat{\sigma}_i$ where $\hat{\sigma}_i$ is a spin operator at site i. When considering the thermodynamic limit, we add, as is usual, the demand that:

$$\Sigma_{\sigma=1}^S A_\sigma A_\sigma^+ = I \tag{2.5}$$

This ensures that the largest eigenvalue of $E(0)$ is $\lambda = 1$. In addition, when dealing with problems in the thermodynamic limit we assume this largest eigenvalue is non degenerate. In the thermodynamic limit, we define:

$$\chi(\lambda; l) \equiv \lim_{N\to\infty} \chi(\lambda; l; N) \tag{2.6}$$

The existence of the limit is assured by the conditions above. To compute $\chi(\lambda; l)$ we define $P(\lambda)$ to be the matrix which brings $E(\lambda)$ to it's Jordan form, with Jordan blocks J_k arranged such that the block with the largest eigenvalue is J_1. Note that the number of blocks as well as eigenvalues depend on λ. We have:

$$E(\lambda)^l = P(\lambda)(\oplus_{k=1} J_k^l)P^{-1}(\lambda). \tag{2.7}$$

We assume $\langle i|$ and $|i\rangle$ are the left and right eigenvectors of $E(\lambda)$, and $i = 1$ corresponds to the largest eigenvalue, and note that if there is no degeneracy,

$$E(0)^N \to P(0)|1\rangle\langle 1|P^{-1}(0). \tag{2.8}$$

Therefore, the full counting statistics function is given by:

$$\chi(\lambda; l) = \langle 1|P^{-1}(0)P(\lambda)(\oplus_{k=1} J_k^l)P^{-1}(\lambda)P(0)|1\rangle \tag{2.9}$$

Let $\alpha_k(\lambda)$ be the diagonal value of J_k. We can compute explicitly the power of a Jordan block, obtaining after some algerba the formula:

$$\chi(\lambda, l) = \sum_{k=1}\sum_{i=1}^{d_k}\sum_{\nu=0}^{min(l,d_k)-i} C_\nu^l Q_{k,i,\nu}\alpha_k^{l-\nu} \tag{2.10}$$

where C_ν^l are the binomial coefficients, d_k the dimension of Jordan block k and

$$Q_{k,i,\nu}(\lambda) = \langle i+\nu+\sum_{n=0}^{k-1} d_n | P^{-1}(\lambda)P(0)|1\rangle \times \quad \langle 1|P^{-1}(0)P(\lambda)|i+\nu+\sum_{n=0}^{k-1} d_n\rangle.$$

Note that in (2.10), Q, α_k as well as the limits in the sum depend on λ implicitly.

Since the largest eigenvalue 1 of $E(0)$ is non-degenerate, we have that $Q_{1,1,0}(0) = 1$ and $Q_{k,i,\nu}(0) = 0$ for all other value of k, i, ν. It is also important to note that since, generically, eigenvalues do not cross, we expect that we may set $d_k = 1, \nu = 0$ in (2.10) for almost all values of $\lambda \in [-\pi, \pi]$, unless some special symmetry or constraint is present.

Let us now consider the limit of large block size l. As with any thermodynamic quantity, computed in a system with finite correlation length, we expect a gaussian distribution of observables according to the CLT. For a matrix product state, of course, the spins are not independent, and so the central limit distribution receives contributions from two types of corrections: due to correlations and due to finite size. Bellow we establish this behavior and derive the appropriate asymptotic description of the probability distribution for large but finite blocks.

In the limit of large l, if the largest eigenvalue of the matrix $E(\lambda)$ is non degenerate, $E(\lambda)^l$ is dominated by the largest eigenvalue $\alpha_1(\lambda)$ and we may write that:

$$\chi(\lambda; l) \sim \chi_0(\lambda)\chi_1(\lambda)^l \; as \; l \to \infty \tag{2.11}$$

where:

$$\chi_1(\lambda) = \alpha_1(\lambda) \; ; \; \chi_0(\lambda) = Q_{1,1,0}(\lambda)$$

It is possible to take into account the corrections due to the smaller eigenvalues of $E(\lambda)$ as well, giving additional exponentially small corrections.

We are now in position to describe the probability distribution of block magnetization. Let us define:

$$\hat{M}_l = \frac{1}{\sqrt{l}} \frac{\hat{\mathcal{S}}_l - l\mu(l)}{var(\sigma, l)} \tag{2.12}$$

where $\mu(l)$ is the average magnetization per site, and $var(\sigma, l)$ is the variance *per site*. We note that since the spin variables on different sites are not independent, both $\mu(l)$ and $var(\sigma, l)$ depend explicitly on the size of the block. Let

$$F_l(M) = Prob(M_l \leq M) \tag{2.13}$$

be the probability distribution of measuring $\hat{M}_l$. To find $F_l(M)$, we now focus on the FCS for $\hat{M}_l$, defined as:

$$\chi_M(\lambda; l) = \langle e^{i\lambda \hat{M}_l} \rangle. \tag{2.14}$$

Since we assume that the largest eigenvalue of $E(\lambda)$ is non degenerate at $\lambda = 0$, this eigenvalue is analytic in a neighborhood of $\lambda = 0$. Indeed both $\chi_0(\lambda), \chi_1(\lambda)$ are analytic in the domain $\lambda \leq |\lambda_*|$ where λ_* is the smallest λ (in the complex plain) for which the largest eigenvalue of $E(\lambda)$ becomes degenerate (see, e.g. [49]). We can therefore expand $log(\chi_1(\lambda)), log(\chi_0(\lambda))$ near $\lambda = 0$. Noting that $\chi_0(\lambda) = \chi_1(\lambda) = 1$ we have the "cumulants" κ_r and ξ_r in:

$$\begin{aligned} log(\chi_0(\lambda)) &= \sum_{r=1}^{\infty} \frac{\xi^r (i\lambda)^r}{n!} \\ log(\chi_1(\lambda)) &= \sum_{r=1}^{\infty} \frac{\kappa^r (i\lambda)^r}{n!}. \end{aligned} \tag{2.15}$$

We see that for a block of l spins, $\mu(l) = \langle \sigma \rangle = \kappa_1 + \xi_1/l$, and $var(\sigma, l) = \sqrt{\langle \sigma^2 \rangle - \langle \sigma \rangle^2} = \sqrt{\kappa_2 + \xi_2/l}$. We also recognize χ_0 as boundary (or "Edge") term that characterize

the effect of the rest of the chain on the chosen l spins, and χ_1 as the bulk term that is not effected by other spins.

Here χ_1 plays, formally, the role of the local independent random variable in the usual derivation of the central limit theorem. However, it is important to note that in a generic MPS, χ_1 is not the full counting statistics of a valid probability distribution. Indeed, for that, the associated distribution, given by the Fourier transform of χ_1 must be a positive real function.

Let us briefly explore how close χ_1 is to a valid probability distribution. To do so we write the counting statistics of a block of size 1 as:

$$\chi(\lambda, 1) = \chi_1(\lambda) + \chi_\delta(\lambda), \tag{2.16}$$

and define the pseudo-probabilities:

$$\tilde{p}_{n,i} = \frac{1}{2\pi} \int_{-\pi}^{\pi} \mathrm{d}\lambda \ \chi_i(\lambda)\, e^{-i\lambda n} \ ; \ i = 1, \delta. \tag{2.17}$$

Associated with the various eigenvalues of the $\chi_1(\lambda), \chi_\delta(\lambda)$. Thus $\tilde{p}_{n,1}$ is the effective probability distribution which would have generated the asymptotic behavior described by the central limit behavior. We can establish the following properties:

1) From the definition of χ_1, we can immediately infer that the associated distribution is discrete.

Indeed, observe that since $E(\lambda)$ is periodic, we can choose $\chi_1(\lambda)$ to be periodic: $\chi_1(\lambda) = \chi_1(\lambda + 2\pi)$, which is associated with discrete, integer, spins.

2) The distribution is real (however it is in general not necessarily positive).

The second property is established by noting that:

$$E(-\lambda) = \tau \overline{E(\lambda)} \tau \tag{2.18}$$

where τ swaps $v_1 \otimes v_2 \to v_2 \otimes v_1$. Therefore

$$specE(-\lambda) = spec\overline{E(\lambda)} \tag{2.19}$$

and, in particular $\chi_1(-\lambda) = \chi_1^*(\lambda)$, ensuring the Fourier transform is real. It is, however, in general not associated with a probability distribution, since the Fourier transform is, in general, not strictly positive.

3) $\sum_n \tilde{p}_{n,1} = 1$ and $\sum_n \tilde{p}_{n,\delta} = 0$. To prove this note that $\chi_\delta(0) = 0$ since $\chi(0,1) = \chi_1(0) = 1$. Now use that $\sum_n \tilde{p}_{n,\delta} = \chi_\delta(0)$.

2.1.4 Edgeworth series

We now proceed to derive the Edgeworth series for our MPS. Using the definition (2.12) and Eq (2.11), we can find the cumulants for the distribution of $\hat{M}_l$:

$$\begin{aligned} log\chi_M(\lambda; l) &= \frac{(i\lambda)^2}{2} + \frac{(i\lambda)^3(l\kappa_3 + \xi_3)}{6(l\kappa_2 + \xi_2)^{3/2}} \\ &+ \frac{(i\lambda)^4(l\kappa_4 + \xi_4)}{24(l\kappa_2 + \xi_2)^2} + \frac{(i\lambda)^5(l\kappa_5 + \xi_5)}{120(l\kappa_2 + \xi_2)^{5/2}} + ... \end{aligned} \tag{2.20}$$

We note that for the normal distribution, we have:

$$log(\phi(\lambda)) = \frac{(i\lambda)^2}{2} \tag{2.21}$$

Combine the two equations, and collect terms according to the power of l, we have

$$\begin{aligned} log\frac{\chi_M(\lambda)}{\phi(\lambda)} &= \frac{1}{l^{1/2}}\frac{(i\lambda)^3\kappa_3}{6\kappa_2^{3/2}} + \frac{1}{l}\frac{(i\lambda)^4\kappa_4}{24\kappa^2} \\ &+ \frac{1}{l^{3/2}}[\frac{(i\lambda)^5\kappa_5}{120\kappa_2^{5/2}} + \frac{(i\lambda)^3}{6}(\xi_2 - \frac{3\xi_3}{2\kappa_2})] + ... \end{aligned} \tag{2.22}$$

Exponentiate the above equation, we have

$$\chi_M(\lambda; l) = (1 + \sum_{j=1}^{\infty} \frac{q_j(i\lambda)}{l^{j/2}}) e^{-\lambda^2/2} \tag{2.23}$$

where q_j is a polynomial of degree $3j$.

Finally, to obtain F_l in (2.13), we do the inverse Fourier transformation to get the probability density, and integrate it over x to get the probability distribution. Defining

$$\Phi(x) \equiv \int_{-\infty}^{x} \frac{\mathrm{dq}}{\sqrt{2\pi}} e^{-\frac{1}{2}q^2} \tag{2.24}$$

to be the error function. We obtain:

$$F_l(x) = \Phi(x) + \sum_{j=1}^{\infty} \frac{q_j(-\partial_x)}{l^{j/2}} \Phi(x). \tag{2.25}$$

In general q_j is a complicated polynomial, which can be compute to all orders. Here we write explicitly the first few terms:

$$\begin{aligned} q_1 &= -\frac{\kappa_3(\partial_x)^3}{6\kappa_2^{3/2}} \\ q_2 &= \frac{\kappa_4(\partial_x)^4}{24\kappa_2^2} + \frac{\kappa_3^2(\partial_x)^6}{72\kappa_2^3} \\ q_3 &= -\frac{\kappa_3^3(\partial_x)^9}{1296\kappa_2^{9/2}} - \frac{\kappa_3\kappa_4(\partial_x)^7}{144\kappa_2^{7/2}} - \frac{\kappa_5(\partial_x)^5}{120\kappa_2^{5/2}} \\ &\quad - \frac{(\partial_x)^3}{6}(\xi_2 - \frac{3\xi_2}{2\kappa_2}) \end{aligned} \tag{2.26}$$

Comparing the above result with the usual Edgeworth series [46, 11], we find the first two terms are the same as those appearing in the Edgeworth expansion for l independent measures with cumulants κ_i, the correction from the boundary term χ_0 only effects the third and higher order terms.

It is important to note that the parameters κ_i, ξ_i are, in principle, measurable. For example, κ_2, ξ_2 can be obtained from the total noise in the measurement of l and $l+1$ spins as $\kappa_2 = \langle \Delta \mathcal{S}_{l+1}^2 \rangle - \langle \Delta \mathcal{S}_l^2 \rangle$ and $\xi_2 = (l+1)\langle \Delta \mathcal{S}_l^2 \rangle - l \langle \Delta \mathcal{S}_{l+1}^2 \rangle$, where $\Delta \mathcal{S}_l \equiv \mathcal{S}_l - \langle \mathcal{S}_l \rangle$.

Alternatively, by considering $\chi_0(\lambda)$ as a differential operator acting on the Fourier transform of χ_1, and combining the Taylor series for $\chi_0(\lambda) = \sum_{k=0}^{\infty} \frac{f_k}{k!} \lambda^k$ with the Edgeworth series for χ_1^l, we may write explicitly

$$\tilde{F}_l = \text{Prob}\left(\frac{\mathcal{S}_l - l\kappa_1}{\sqrt{\kappa_2 l}} \leq x \right) = \sum_{L=0}^{\infty} \frac{1}{l^{L/2}} \sum_{m=0}^{L} \frac{i^m f_m \mathcal{G}_{L-m,m}}{{\kappa_2}^{m/2} m!} \tag{2.27}$$

where $\mathcal{G}_{k,m}(x)$ is given by $\mathcal{G}_{0,m} = (-\partial_x)^m \Phi(x)$:

$$\mathcal{G}_{k,m} = \sum_{\substack{\{p_1, .. p_k\} \in \mathbb{Z}_+^k \\ \Sigma l p_l = k; \Sigma p_l = j}} \frac{(-\partial_x)^{k+m+2j} \Phi(x)}{p_1! .. p_k!} \left(\frac{\kappa_3}{3!} \right)^{p_1} .. \left(\frac{\kappa_{k+2}}{(k+2)!} \right)^{p_k}.$$

We can now compute F_l by using the expression (2.27), combined with:

$$F_l(x) = \text{Prob}\left(\frac{\mathcal{S}_l - l\mu(l)}{(var(\mathcal{S}_l)/l)\sqrt{l}} \leq x \right) =$$
$$\text{Prob}\left(\frac{\mathcal{S}_l - l\kappa_1}{\sqrt{\kappa_2 l}} \leq \frac{1}{\sqrt{1 + \frac{\xi_2}{l\kappa_2}}} x - \frac{\xi_1}{\sqrt{l}\kappa_2} \right) = \tilde{F}_l \left(\frac{1}{\sqrt{1 + \frac{\xi_2}{l\kappa_2}}} x - \frac{\xi_1}{\sqrt{l}\kappa_2} \right)$$

To illustrate these ideas, let us consider the following spin 1 MPS, given by the properly normalized matrices:

$$A^+ = \sqrt{\frac{1}{3}} \begin{pmatrix} 1 & 1 \\ 0 & 0 \end{pmatrix}; A^0 = \sqrt{\frac{1}{6}} \begin{pmatrix} -1 & 1 \\ 1 & 1 \end{pmatrix}; A^- = \sqrt{\frac{1}{3}} \begin{pmatrix} 0 & 0 \\ -1 & -1 \end{pmatrix}$$

Plugging these matrices in the definition (2.4) we find that:

$$E(\lambda) = \frac{1}{6}\begin{pmatrix} 2e^{i\lambda}+1 & 2e^{i\lambda}-1 & 2e^{i\lambda}-1 & 2e^{i\lambda}+1 \\ -1 & -1 & 1 & 1 \\ -1 & 1 & -1 & 1 \\ 2e^{-i\lambda}+1 & 2e^{-i\lambda}+1 & 2e^{-i\lambda}+1 & 2e^{-i\lambda}+1 \end{pmatrix}$$

At $\lambda = 0$ we find that the largest eigenvalue is 1, and that it is separated by a gap from the next eigenvalue $1/3$.

In Fig 2.1. we compare the probability distribution for magnetization computed numerically from the ground state wave function, with the probability distribution obtained from our Edgeworth series (2.25). Here, the exact probability distribution $F_l(M)$ was found numerically by doing an inverse Fourier transformation of Eq (2.5). In the example depicted in Fig 2.1, for a block of 20 spins, it is evident that the Edgworth series works extremely well, capturing the essence of the correction already at first order. We also exhibit the pseudo-probabilities in Fig 2.2, computed according to Eq (2.17).

Next, we consider an example where the full counting statistics is not described by a Gaussian of finite width, although the system is gapped. In this example, the variance *per site* actually vanishes as $1/l$. Consider the AKLT state in Eq (1.2), the properly normalized form has:

$$A^+ = \sqrt{\frac{2}{3}}\begin{pmatrix} 0 & 1 \\ 0 & 0 \end{pmatrix}; A^0 = \sqrt{\frac{1}{3}}\begin{pmatrix} -1 & 0 \\ 0 & 1 \end{pmatrix}; A^- = \sqrt{\frac{2}{3}}\begin{pmatrix} 0 & 0 \\ -1 & 0 \end{pmatrix}$$

which gives:

$$E(\lambda) = \frac{1}{3}\begin{pmatrix} 1 & 0 & 0 & 2e^{i\lambda} \\ 0 & -1 & 0 & 0 \\ 0 & 0 & -1 & 0 \\ 2e^{i\lambda} & 0 & 0 & 1 \end{pmatrix}.$$

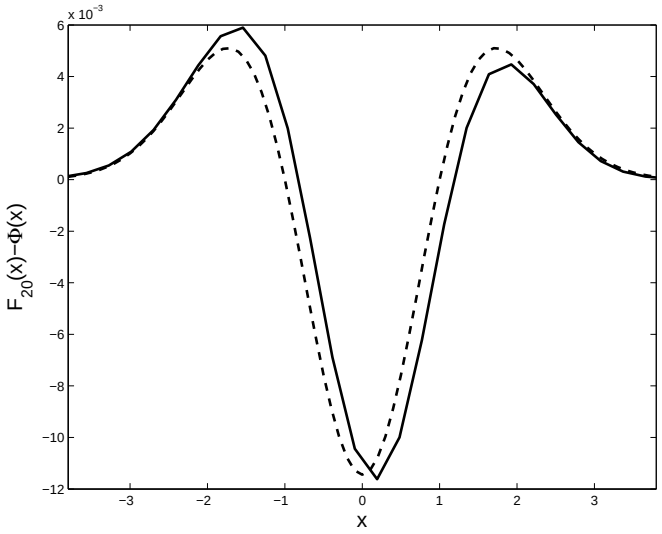

Figure 2.1: Correction to the central limit distribution (i.e,$F_l(M) - \Phi(M)$). Solid line represent the exact result by calculating the probability distribution, dashed line shows the first order correction using Edgeworth series.

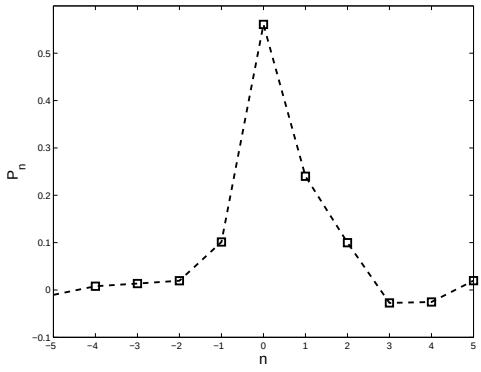

Figure 2.2: First few Fourier components of χ_1, showing small but finite negative pseudo-probabilities.

Computing the eigenvalues of $E(\lambda)$, we see that they are $1, -\frac{1}{3}, -\frac{1}{3}, -\frac{1}{3}$, independent on λ. In the limit of $N, l \to \infty$, $e^S(\lambda, l, N) \to \frac{1+cos\lambda}{2}$, we find that the counting statistics does not depend on l.

This result reflects the topological nature of the AKLT state, the total spin of the block depends only on the "edge modes" which are the only ones which are allowed to fluctuate.

In general, the absence of scaling of fluctuations, appears whenever we have a correspondence of the form

$$E(\lambda) = V(\lambda)E(0)V^{-1}(\lambda) \tag{2.28}$$

For some matrix V. In such a case, $\chi_1(\lambda) \equiv 1$, and the entire contribution comes from the edge $\chi(\lambda; l) = \chi_0(\lambda)$. In this case $\log \chi(\lambda)$ is clearly not extensive in the

block size l.

To summarize, Matrix product states supply a very natural class of probability distribution which are not IID, but are still quite amenable to treatment and computation. In this section we have studied the full counting statistics of spin in matrix product states. We explored the finite size correction to the Gaussian counting statistics expected on large scales. We showed how an Edgeworth type series may be used describe these asymptotic corrections and checked it numerically on an explicit example. Finally, we showed that in special cases, such as the AKLT model, the fluctuations in the system do not scale linearly with system size, and the Edgeworth description is not valid whenever it is based on variance and mean which were measured on any finite size block.

2.2 Time evolution of Matrix Product States

In the last section, we were able to exactly calculate the FCS of a matrix product state in a variety of cases. While it is rare for a physical problem to be exactly solvable, exact solutions of physical problems, even fine tuned ones are often of high value. These can teach us a lot about the corresponding phase, or serve as a starting point for a perturbative expansion.

In particular, it is even harder to find solutions of explicit time-dependent problems. We now pose the following natrual question: given a time-dependent MPS, can this MPS be the exact solution to some time-dependent Schrodinger equation with a local Hamiltonian? Considering that numerical methods like time evolving block decimation (TEBD)[76, 85] approximates the time evolution of interacting systems with a time-dependent MPS.

On the other hand, this problem helps us to understand phase transitions in 1D. It is argued that any two states are connected by a local unitary evolution [15], or evolution generated by a local Hamiltonian for a finite time, they are always in the

same phase. And 1 dimensional gapped phases can be classified using this definition within the MPS formalism [16].

Here we show that, in contrast to, say the Hartree-Fock variational states, which can be evolved using non-interacting time-dependent Hamiltonians, MPS are more restrictive, and require the entanglement entropy of blocks to remain constant.

2.2.1 Nonlinear equation for the Hamiltonian

We will assume a translationally invariant (TI) MPS, with a bond dimension D, a spin dimension S and representative matrices A_{σ_i}, $i \in \{1, S\}$, S is the physical dimension on site. The state is a special case of Eq (1.3):

$$\psi = \Sigma_{\{\sigma\}} \mathrm{Tr}\left(A_{\sigma_1} A_{\sigma_2} .. A_{\sigma_N}\right) \left|\sigma_1 \sigma_2 ... \sigma_N\right\rangle \tag{2.29}$$

where the set of matrices on different sites are the same. We further assume that the MPS is injective, which means that the transfer matrix in Eq (1.15): $E = \sum_i \bar{A}_{\sigma_i} \otimes A_{\sigma_i}$ has a non-degenerate largest eigenvalue which is 1. Remember that E is related to the normalization: $\langle\psi|\psi\rangle = \mathrm{Tr}(E^N)$. The canonical form Eq (1.12), also implies that the left and right eigenvectors corresponding to the largest eigenvalue are:

$$(L| = \sum_\alpha \lambda_\alpha \langle\alpha|\langle\alpha| \tag{2.30}$$

$$|R) = \sum_\beta |\beta\rangle|\beta\rangle \tag{2.31}$$

$\lambda_\alpha = \Lambda_{\alpha\alpha}$. Here parenthesis are used to indicate that $(L|$ and $|R)$ are not normalized. $|\alpha\rangle$ is the basis vector that only αth element is 1 and all others are 0. λ_α is the αth diagonal element of the Λ matrix in Eq (1.12).

To see this, consider that $E_{mm',nn'} = \sum_i \bar{A}^{\sigma_i}_{mn} A^{\sigma_i}_{m'n'}$, so Eq (1.12) means that:

$$\begin{aligned}(\sum_i A^{s_i} A^{s_i\dagger})_{mn} &= \sum_k E_{nm,kk} = \delta_{mn} \\ (\sum_i A^{s_i\dagger} \Lambda A^{s_i})_{mn} &= \sum_k \lambda_k E_{kk,mn} = \lambda_m \delta_{mn}\end{aligned} \tag{2.32}$$

so that:

$$E|R) = \sum_{\alpha\beta\gamma} E_{\alpha\gamma,\beta\beta} |\alpha\rangle|\gamma\rangle = |R) \tag{2.33}$$

$$(L|E = \sum_{\alpha\beta\gamma} \lambda_\alpha E_{\alpha\alpha,\beta\gamma} \langle\beta|\langle\gamma| = (L| \tag{2.34}$$

So indeed, $|R)$ and $(L|$ are the right and left eigenvectors of E, corresponding to the eigenvalue 1. We assume the state is in a canonical form at $t = 0$, but not necessarily canonical at $t > 0$.

Now assume the state evolves under a translational invariant, time-dependent two-site interaction Hamiltonian, $H = \sum_i H^{[i,i+1]}(t)$, $H^{[i,i+1]}(t)$ acts on sites i and $i+1$. If we assume that the state remains a MPS with a fixed bond dimension, so that now the As are all time-dependent. Then we have:

$$\langle\{\sigma_i\}|\frac{\partial}{\partial t}|\psi\rangle = \sum_i \mathrm{Tr}(\frac{d}{dt}(A_{\sigma_i}) A_{\sigma_{i+1}} A_{\sigma_{i+2}} ... A_{\sigma_N} A_{\sigma_1} ... A_{\sigma_{i-1}}) \tag{2.35}$$

$$\begin{aligned}\langle\{\sigma_i\}|\hat{H}|\psi\rangle = \sum_i \mathrm{Tr}((\sum_{\sigma_i',\sigma_{i+1}'} H^{[i,i+1]}_{\sigma_i\sigma_{i+1},\sigma_i'\sigma_{i+1}'} A_{\sigma_i} A_{\sigma_{i+1}}) \times \\ A_{\sigma_{i+2}} ... A_{\sigma_N} A_{\sigma_1} ... A_{\sigma_{i-1}})\end{aligned} \tag{2.36}$$

Here $\langle\{\sigma_i\}|$ is the basis state with spin configuration $\{\sigma_i\}$, we also used the cyclic property of trace. For the rest of the section, we write A_i instead of A_{σ_i}, and $H_{ij,i'j'}$

instead of $H^{[i,j]}_{\sigma_i\sigma_j,\sigma_i'\sigma_j'}$ (since H does not depend on the sites i and j) for short. Now we see that from Eq (2.35) and (2.36), the Schrodinger equation can be satisfied by requiring:

$$\frac{\mathrm{d}}{\mathrm{dt}}(A_iA_j) = -2\mathrm{i}\sum_{kl} H_{ij,kl}A_kA_l \tag{2.37}$$

or equivalently, in an integral form:

$$A_i(t)A_j(t) = \sum_{kl} U_{ij,kl}A_k(0)A_l(0) \tag{2.38}$$

where $U = \mathrm{e}^{-2\mathrm{i}\int_0^t H(t)dt}$.

Eq (2.37) is sufficient, but not necessary, to satisfy the Schodinger equation. However, we use that that the product: $\prod_{k!=i,i+1} A_{\sigma_k}$ is "dense", so that

$$\mathrm{Tr}[H_{ii+1,i'i'+1}A_{i'}A_{i'+1} + 2i\frac{d}{dt}(A_iA_{i+1})]X = 0$$

for any matrix X (except for a gauge transformation), which is another way of saying the state is injective, then Eq (2.37) must be satisfied, as explained below. So our question becomes that: can we find a set of matrices that satisfy Eq (2.37)?

Before trying to answer it, we first notice that in the injective case, it is shown [60] that for a certain length $l > l_0$, the product $A_{i_1}A_{i_2}...A_{i_l}$ for all S^l different configurations of $i_1i_2..i_l$ form a complete basis of all $D \times D$ matrices. Here we take $l_0 = 2$ for convenience, since if $l > 2$, we can always group up As to make l smaller, that does not change the physics picture. Thus for any $\dot{A}_i$ one chooses for Eq (2.37), there is always a H, although may not be Hermitian, that satisfies the equation.

Next we require this Hamiltonian to be Hermitian, or U to be unitary. In this case,

we find:

$$\begin{aligned}
&\textstyle\sum_{i,j} A_i(t)A_j(t)(A_i(t)A_j(t))^\dagger \\
&= \textstyle\sum_{i,j}\sum_{k,l,k',l'} U_{ij,kl}U^*_{ij,k'l'}A_k(0)A_l(0)(A_{k'}(0)A_{l'}(0))^\dagger \\
&= \textstyle\sum_{kl} A_k(0)A_l(0)(A_k(0)A_l(0))^\dagger = I
\end{aligned} \tag{2.39}$$

The last line we used the canonical condition. We only assume at $t = 0$ the state is in canonical form, but at $t \neq 0$ it is not.

And the same goes the other way:

$$\begin{aligned}
&\sum_{i,j}(A_i(t)A_j(t))^\dagger A_i(t)A_j(t) \\
&= \sum_{i,j}(A_i(0)A_j(0))^\dagger A_i(0)A_j(0) = \text{const.}
\end{aligned} \tag{2.40}$$

Now we can relate equation (2.39) and (2.40) to the matrix E, it is straightforward to check that:

$$[\sum_{i,j} A_i(t)A_j(t)(A_i(t)A_j(t))^\dagger]_{\alpha\beta} = \sum_\gamma (E(t)\times E(t))_{\alpha\beta,\gamma\gamma} \tag{2.41}$$

$$[\sum_{i,j}(A_i(t)A_j(t))^\dagger A_i(t)A_j(t)]_{\alpha\beta} = \sum_\gamma (E(t)\times E(t))_{\gamma\gamma,\beta\alpha} \tag{2.42}$$

Eq (2.39) and Eq (2.40), combined with Eq (2.30), gives:

$$E^2(t)|R) = |R) \tag{2.43}$$

$$(L|E^2(t) = (L| \tag{2.44}$$

So $|R)$ and $(L|$ are also the eigenvectors of $E^2(t)$ corresponding to eigenvalue 1, which is still the largest eigenvalue because of normalization. Although we assumed the Hamiltonian to be a 2-site interaction Hamiltonian, and thus in Eq (2.39) and (2.40)

we have product of two As, we can easily take the interaction to act on more sites, and the same argument still applies, so that $|R)$ and $(L|$ are eigenvectors of $E^n(t)$, where n can be an arbitrary integer. So, they must be eigenvectors of $E(t)$ itself. Since the largest eigenvalue and eigenvectors play the most important role for a MPS in the thermodynamic limit, we can already imagine that the state is not really evolving in an interesting way. To make this clear, consider the two-body reduced density matrix for a chain of N sites:

$$\rho_{ij,kl}(t) = \mathrm{Tr}((A_i(t) \otimes \bar{A}_k(t))(A_j(t) \otimes \bar{A}_l(t))E^{N-2}(t)) \tag{2.45}$$

At the limit where $N \to \infty$, only the largest eigenvalue matters in the trace, and because it is 1, we can write the above equation as:

$$\begin{aligned} \rho_{ij,kl}(t) &= (L|(A_i(t) \otimes \bar{A}_k(t))(A_j(t) \otimes \bar{A}_l(t))|R) \\ &= \mathrm{Tr}[\Lambda A_i(t)A_j(t)(A_k(t)A_l(t))^\dagger] \end{aligned} \tag{2.46}$$

for the second line we plugged in the explicit form for $(L|$ and $|R)$. Now we can have an equation of motion for the reduced density matrix, using equation (2.37):

$$\begin{aligned} \frac{d}{dt}\rho_{ij,kl}(t) &= \mathrm{iTr}[\Lambda \sum_{ij} H_{ij,i'j'}(t)A_{i'}(t)A_{j'}(t)(A_k(t)A_l(t))^\dagger] \\ &\quad - \mathrm{iTr}[\Lambda A_i(t)A_j(t) \sum_{k'l'} H_{kl,k'l'}(t)(A_{k'}(t)A_{l'}(t))^\dagger] \\ &= \mathrm{i}[H(t), \rho(t)]_{ij,kl} \end{aligned} \tag{2.47}$$

We see that, the two-body reduced density matrix is evolving under a unitary matrix: $\rho_2(t) = U_2(t)\rho_2(0)U_2(t)^\dagger$. As a consequence, all the eigenvalues of $\rho(t)$ remain constant, which means the entanglement spectra are constant. Remember, we assumed the Hamiltonian to be a two-site interaction, but we can always assume it acts on

more sites, and the same is true for 3 or more site reduced density matrices. So the state is not actually evolving in an interesting way: no correlation are generated beyond the range of interaction.

That also means, if we start from an MPS with certain bound dimension, as soon as one turns on the interaction, the state (in thermodynamic limit) can not be written exactly as any finite dimension MPS.

2.2.2 Exact time evolution in non-injective case

In the last section, we see that there can not be non-trivial exact time-evolution under the conditions: the state is translational invariant and injective. Without these conditions, of course MPS can represent an exact time-evolution. And here we show a simple example. We now consider the spin-1/2 XXZ model:

$$H = \sum_{<ij>} s_i^x s_j^x + s_i^y s_j^y + \Delta s_i^z s_j^z \tag{2.48}$$

$$= \sum_{<ij>} \frac{1}{2}(s_i^- s_j^+ + s_i^+ s_j^-) + \Delta s_i^z s_j^z \tag{2.49}$$

the state:

$$\Psi_p = \frac{1}{\sqrt{N}} \sum_{n=1}^{N} e^{ipn} |n\rangle \tag{2.50}$$

where N is the number of sites and $|n\rangle$ denotes the state that all spins are up except the nth spin, and $p = 2\pi k/N$, k = 0, 1, 2, ... N. Those states are all eigenstates of the model, with energy $E_p = 2cos(k) + \Delta(N-2)$. Consider the state $\Psi = \Psi_{p_1} + \Psi_{p_2}$, it evolves under the Hamiltonian as $\Psi(t) = \Psi_{p_1} e^{-iE_1 t} + \Psi_{p_2} e^{-iE_2}$, assume $E1 < E2$ and $\delta = (E2 - E1)/N$, upto an overall factor $e^{iE_1 t}$, the state can be written as a MPS:

$$\Psi(t) = Tr(X \prod A_\sigma)|\sigma_i\rangle \tag{2.51}$$

where

$$A_\uparrow = \begin{pmatrix} e^{ip_1} & 0 & 0 & 0 \\ 0 & 1 & 0 & 0 \\ 0 & 0 & e^{ip_2+\delta} & 0 \\ 0 & 0 & 0 & e^{i\delta} \end{pmatrix} \quad A_\downarrow = \begin{pmatrix} 0 & 1 & 0 & 0 \\ 0 & 0 & 0 & 0 \\ 0 & 0 & 0 & e^{i\delta} \\ 0 & 0 & 0 & 0 \end{pmatrix}$$

and $X = \begin{pmatrix} 0 & 0 & 0 & 0 \\ 1 & 0 & 0 & 0 \\ 0 & 0 & 0 & 0 \\ 0 & 0 & 1 & 0 \end{pmatrix}$

One can check that although the matrices are site independent, the state is not translational invariance because of the boundary we put. Notice that this time evolution does not obey (2.37), since the matrices here do not satisfy the injective condition. We can also learn from this example that, if a time evolution of non-translational invariant MPS, that involves 2 eigenstates of a Hamiltonian:

$$\Psi_M(t) = \phi_0 + \phi_1 e^{-iEt} \tag{2.52}$$

where ϕ_0 and ϕ_1 are eigenstates of the Hamiltonian, and assuming ϕ_0 has eigenvalue 0 and ϕ_1 with $E > 0$, then at time $t = 0$ and $t = \tau$ the states $\phi_0 + \phi_1$ and $\phi_0 + \phi_1 e^{-i\tau E}$ are both MPSs. So the difference of them, $\phi_1(1 - e^{-iE\tau})$, or ϕ_1, is also a MPS.[1] Then ϕ_0 and ϕ_1 are both MPSs. Then same reasoning goes on with an exact time evolution that evolves any finite number of eigenstates. However, these MPSs are in general NOT injective, and do not fit into our definition of "interesting" time evolution.

To summarize, in this section, we write a nonlinear equation for the time evolution of translational invariant injective MPS. This equation allows nontrivial time evolution under non-Hermitian local Hamiltonians, but not for Hermitian local Hamil-

[1]This is because for 2 MPSs with matrix sets A_i and B_i, their superposition can always be expressed as another MPS: $\phi_C = \phi_A + \phi_B$, where $C = A \oplus B$. But ϕ_C is not injective since it has 2 blocks now.

tonians.

CHAPTER III

X-ray scattering and absorption in condensed matter systems

To experimentally understand a condensed matter system, we need to look the response of the system to external perturbations. There are many ways to add perturbations, like adding a magnetic field, electric field, changing pressure. One commonly used way is to probe the system with particle scattering and look at the spectrum, which is the cross section as a function of energy. There are many different particles that people use to study the scattering, X-ray(photon), electron, neutron... In the rest of the thesis we focus on the X-ray absorption and scattering, in the former case the photon is absorpt by the system, and in the latter case the photon transfers energy into the system and then is scattered. We are particularly interested in resonant inelastic X-ray scattering. In Chap III basic knowledge about X-ray absorption and scattering spectroscopy are introduced, and in Chap V and Chap IV we look at some specific examples.

3.1 X-ray absorpsion in 1D, edge singularity

3.1.1 Theoretical formalism

In an X-ray absorption experiment, a photon is scattered into material, exciting a core electron into an empty valence band, and then another electron from an occupied valence band decay back into the core state. In X-ray terminology, "edge" is used to indicate the state of the core electron. For K-edge, the core electron is in the $1s$ state, while at L-edge the core electron is in $2s$ or $2p$ state. When the core-hole is present, it produces a screened Coulomb potential.

3.1.1.1 Dipole interaction

Here we start to look at the Hamiltonian of the system, which includes the electrons and photons. The photons can be represented by a vector potential $\mathbf{A}(\mathbf{r})$, it is quantized as:

$$\mathbf{A}(\mathbf{r}) = \sum_{\mathbf{k},\epsilon} \sqrt{\frac{1}{2\omega_k}} (\epsilon a_{\mathbf{k}\epsilon} e^{i\mathbf{kr}} + \epsilon^* a^\dagger_{\mathbf{k}\epsilon} e^{-i\mathbf{kr}}) \tag{3.1}$$

The free photon Hamiltonian is a collection of harmonic oscillators:

$$H_{ph} = \sum_{\mathbf{k}\epsilon} \hbar\omega_k (a^\dagger_{\mathbf{k}\epsilon} a_{\mathbf{k}\epsilon} + 1/2) \tag{3.2}$$

The Hamiltonian of the full system is:

$$H_{tot} = \sum_i \frac{(\mathbf{p}_i + e\mathbf{A}(\mathbf{r}_i))^2}{2m} + U(\mathbf{r}_i) + H_{ph} \tag{3.3}$$

where the first term is the electron kinetic energy in the presence of the electromagnetic field, and $U(\mathbf{r})$ is the potential energy. We can write the interaction between the photon and electron as a perturbation: $H_{total} = H_0 + H'$, where the interaction

term is

$$H' = \sum_i \frac{e}{2m}(\mathbf{p}_i \cdot \mathbf{A}_i + \mathbf{A}_i \cdot \mathbf{p}_i) + \frac{e^2}{2m}\mathbf{A}(\mathbf{r}_i)^2 = \frac{e}{m}\mathbf{p_i} \cdot \mathbf{A}(\mathbf{r}_i) + \frac{e^2}{2m}\mathbf{A}(\mathbf{r}_i)^2 \qquad (3.4)$$

Coulomb gauge $\nabla \cdot \mathbf{A} = 0$ is used so $\mathbf{A} \cdot \mathbf{p} = \mathbf{p} \cdot \mathbf{A}$. Assume the incident X-ray have uniform momentum $\mathbf{k}$, the initial state would have a single photon and final state has none. The term proportional to $\mathbf{A}^2$ has no contribution since it change the photon number of the inital state by 2, 0, or -2. Furthermore, the term proportional to $a^\dagger_{\mathbf{k}\epsilon}$ in $\mathbf{A} \cdot \mathbf{P}$ also vanishes since it creates a photon to the initial state. So only the $a_{\mathbf{k}\epsilon}$ term in $\mathbf{A}$ contributes, by destroying a photon from the initial state. We can treat $a_{\mathbf{k}\epsilon}$ just as a number if it is only sandwiched between states with one and zero photons, so the photon potential $\mathbf{A}$ is reduced to $\mathbf{A}(\mathbf{r}_i) = \frac{1}{\sqrt{2\omega_k}}\epsilon e^{i\mathbf{k}\mathbf{r}_i}$. In the dipole limit, one makes the approximation that: $e^{i\mathbf{k}\mathbf{r}_i} \sim e^{i\mathbf{k}\mathbf{R}_i}$, where $\mathbf{R}_i$ is the position of the ion the electron is bond to, so it is a number instead of an operator. We get for the dipole interaction, the transition operator is:

$$\mathcal{D} = \frac{1}{im\omega_k}\sum_i e^{i\mathbf{k}\cdot\mathbf{r}_i}\epsilon \cdot \mathbf{p}_i \qquad (3.5)$$

we can further write $\mathcal{D} = \epsilon \cdot \mathbf{D}$, where $\mathbf{D} = \sum_i \frac{1}{im\omega_k}e^{i\mathbf{k}\cdot\mathbf{r}_i}\mathbf{p}_i$. Notice that:

$$\begin{aligned}\langle f|\frac{1}{im\omega_k}\mathbf{p}|i\rangle &= \langle f|\frac{1}{\hbar\omega_k}[\frac{\mathbf{p}^2}{2m}, \mathbf{r}]|i\rangle \\ &= \langle f|\frac{1}{\hbar\omega_k}(E_f - E_i)\mathbf{r}|i\rangle \sim \langle f|\mathbf{r}|i\rangle\end{aligned}$$

the last step is due to energy conservation, so that finally, we can replace $\mathbf{D}$ by:

$$\mathbf{D} = \sum_i e^{i\mathbf{k}\mathbf{R}_i}\epsilon \cdot \mathbf{r}_i \qquad (3.6)$$

3.1.1.2 Scattering intensity

The transition coeffecient from initial state $|i\rangle$ to final state $|f\rangle$ can be calculated as:

$$W(n) = \langle n|\mathcal{D}|i\rangle \tag{3.7}$$

The scattering intensity, according to Fermi's golden rule, is then:

$$\begin{aligned} I(\omega) &\propto \sum_f |\langle f|\mathcal{D}|i\rangle|^2 \delta(\omega - E_f + E_i) \\ &= \sum_f |\langle f|\epsilon \cdot \mathbf{D}|i\rangle|^2 \delta(\omega - E_f + E_i). \end{aligned} \tag{3.8}$$

Here $|i\rangle$ is the initial state, $|f\rangle$ is a possible final state of the system, usually taken as a complete set of eigenstates of the final Hamiltonian. The delta function imposes energy conservation.

We see from Eq (3.8) that the intensity depends both on the physics of the system and the geometry of the experiment. If the transition is Copper L edge $2p \rightarrow 3d$, then we need to calculate $\epsilon \cdot \langle 3d|\mathbf{r}|2p\rangle$. In this section we are mostly interested in the physics of the system that does not depend on geometry. Detailed calculation on the geometric dependence is worked out in Sec 3.2.

Assume the electron system is described by a simple band model, with the initial Hamiltonian:

$$H_i = -t \sum_i c_i^\dagger c_{i+1} + \text{h.c} + \mu \sum_i c_i^\dagger c_i, \tag{3.9}$$

here we neglect electron spin in this section just to show the basic idea. The effect of the dipole transition operator is to create a core-hole and a band electron, when only considering the band electrons, we take it just as the electron creation operator $c^\dagger$, and because of translational invariance, we can just assume the core-hole is at site

$r = 0$, so that then intensity is:

$$I(\omega) \quad \propto \quad \sum_f \langle i|c_0|f\rangle\langle f|c_0^\dagger|i\rangle\delta(\omega - E_f + E_i) \tag{3.10}$$

After a core hole is created, the core hole has some effective potential V at site $i = 0$, and the Hamiltonian becomes,

$$H_f = -t\sum_i c_i^\dagger c_{i+1} + \text{h.c} + \mu\sum_i c_i^\dagger c_i + V c_0^\dagger c_0 \tag{3.11}$$

Using $\delta(z) = \frac{1}{2\pi}\int_{-\infty}^{\infty} e^{izt}dt$, one can write the intensity as:

$$\begin{aligned} I(\omega) \quad &\propto \quad \int_{-\infty}^{\infty} e^{i(\omega - E_f + E_i)t}\langle i|c_0|f\rangle\langle f|c_0^\dagger|i\rangle\delta(\omega - E_f + E_i) \\ &= \quad \int_{-\infty}^{\infty} e^{i\omega t}\langle c_0 e^{-iH_f t}c_0^\dagger e^{iH_i t}\rangle dt = \int_{-\infty}^{\infty} G(t)e^{i\omega t}dt \end{aligned} \tag{3.12}$$

Here we used $\sum_f e^{-iE_f t}|f\rangle\langle f| = e^{-iH_f t}$, and $|i\rangle e^{iE_i t} = e^{iH_i t}$, since E_i and E_f are the energy eigenvalues of H_f and H_i. Here $E_{i(f)}$ are numbers but $H_{i(f)}$ are operators. The integrand $G(t) = \langle c_0 e^{-iH_f t}c_0^\dagger e^{iH_i t}\rangle$ is similar to the electron propagator. $c_0^\dagger$ creates a valence band electron at site $i = 0$. Since the Hamiltonians $H_{i(f)}$ all have quadratic form, this can be calculated exactly. For a certain temperature $\frac{1}{\beta}$ the intensity is:

$$I(\omega) = \int_{-\infty}^{\infty} e^{i\omega t}\mathrm{d}t\mathrm{Tr}(c_0 e^{-iH_f t}c_0^\dagger e^{iH_i t}e^{-\beta H_i})/\mathrm{Tr}(e^{-\beta H_i}). \tag{3.13}$$

3.1.1.3 Determinant method

To calculate the trace, we use the formula:

$$\mathrm{Tr}(e^A e^B) = \det(1 + e^a e^b) \tag{3.14}$$

Here the variable in capital letters represent any quadratic operator, and lower case letters represent the matrix containing the coefficient of the quadratic terms:

$$A = \sum_{ij} a_{ij} c_i^\dagger c_j \tag{3.15}$$

Notice that the dimension of A is the Hilbert space dimension of the Hamiltonian, 2^N, but the dimension of a is just N. To calculate Eq (3.13), we use the commutational relationship:

$$e^{-iH_f t} c_0^\dagger = \sum_m (e^{-iH_f t})_{m0} c_m^\dagger e^{-iH_f t} \tag{3.16}$$

to move $c_0^\dagger$ to the left of the numerator of Eq (3.13), and put c_0 and $c_0^\dagger$ together, and the numerator in Eq (3.13) is now:

$$\sum_m (e^{-iH_f t})_{m0} \mathrm{Tr}(c_0 c_m^\dagger e^{-iH_f t} e^{iH_i t} e^{-\beta H_i}) \tag{3.17}$$

Using

$$c_0 c_m^\dagger = \frac{\partial}{\partial \alpha} e^{\alpha M}|_{\alpha=0} \tag{3.18}$$

where $\mathcal{M} = |0\rangle\langle m|$, we can use Eq (3.14) again to get:

$$\mathrm{Tr}(c_0^\dagger c_m e^{-iH_f t} e^{iH_i t} e^{-\beta H_i}) = \det(1 + e^\omega)(\frac{1}{1+e^\omega})_{0m} \tag{3.19}$$

where $e^\omega = e^{-iH_f t} e^{iH_i t} e^{-\beta H_i}$. Next we define $N = (1 + e^{\beta h_i})^{-1}$, so that:

$$\mathrm{Tr}(c_0^\dagger e^{-iH_f t} c_0^\dagger e^{iH_i t} e^{-\beta H_i}) = \det(1 + e^{-ih_f t} e^{ih_i t} \frac{N}{1-N})(\frac{1}{1+e^{-\omega}} e^{-iH_f t})_{00} \tag{3.20}$$

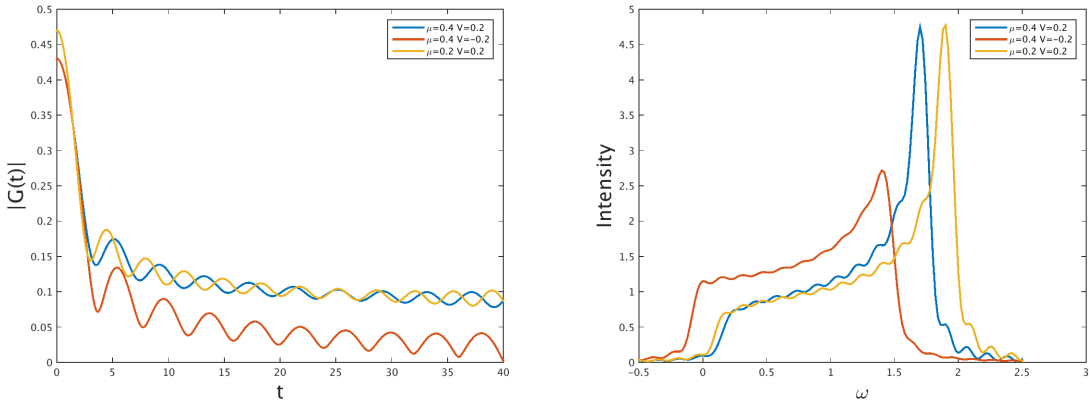

Figure 3.1: X-ray absorption edge. Left: absolute value of $G(t)$ for different set of parameters. Blue curve, $t = -1$, $\mu = 0.4$, $V = 0.2$, red curve, $t = -1$, $\mu = 0.4$, $V = -0.2$, yellow curve, $t = -1$, $\mu = 0.2$, $V = 0.2$. Right: the intensity calculated from the Fourier transform of $G(t)$.

The denominator in Eq (3.13) is $\det(\frac{1}{1-N})$, finally we have,

$$I(\omega) = \int_{-\infty}^{\infty} e^{i\omega t} \det(1 - N + e^{-ih_f t} e^{ih_i t} N)((1 + e^{-\omega})^{-1} e^{-iH_f t})_{00} \mathrm{d}t \tag{3.21}$$

The determinant and trace can be calculated numerically on finite size systems.

A famous result in X-ray absorption is the Fermi edge singularity [59, 28], it means that, the propagator $G(t)$ in Eq (3.12) behaves as a power-law in large t limit, $G(t) \to t^{-\gamma}$, so that the Fourier transform of $G(t)$, the absorption intensity, has a power law singularity at the absorption threshold. Here it is important to assume that V is much smaller than the bandwidth.

Assuming the energy spectrum is linear in k, and using Bosonization, the intensity can be calculated theoretically [64], the propagator is:

$$G(t) = \exp\{(1 + V\rho)^2 \frac{1}{N} \sum_k \frac{1}{k} (e^{-i(k/\rho)t} - 1)\} \tag{3.22}$$

ρ is the density of states around Fermi sea. According to [64], $G(t)$ behaves as: $G(t) \to (t)^{-\gamma}$ when $t \to \infty$, where $\gamma = (1 + V\rho)^2$.

Here we reproduce the Fermi edge singularity using our determinant method, by look at the tight-binding Hamiltonian (3.9) on a chain with N sites. Fig.3.1 shows the numerical calculation on a chain of $N = 100$ sites, at zero temperature. We see that the edge singularity is around $\omega \sim 2$, when μ is changed, the position of the edge is also changed, which is reasonable since it controls the threshold energy. When V is decreased, the peak is less sharp, which is consistent with the prediction in Eq (3.22), and it also affects the position of the peak since it creates an effective chemical potential term.

3.1.2 X-ray absorption with a superconducting pairing

A particularly interesting family of systems for X-ray experiments are superconductors, especially High Tc superconductors, where a gap exists because of the superconducting pairing. Next, we consider adding a pairing term in the Hamiltonian to represent superconducting phase. The new Hamiltonian is:

$$H_i = -t \sum_i c_i^\dagger c_{i+1} + \Delta \sum_i c_i^\dagger c_{i+1}^\dagger + h.c - \sum_i \mu c_i^\dagger c_i \tag{3.23}$$

To deal with this kind of Hamiltonian with the preferred determinant method, we introduce Majorana fermions, related to the usual fermion creation and annihilation operators by:

$$\begin{aligned} a_i &= c_i + c_i^\dagger \text{ i=0,2,...N-1} \\ a_i &= i(c_i^\dagger - c_i) \text{ i=N,...2N-1} \end{aligned} \tag{3.24}$$

Where a_i stands for Majorana fermions and c_i for ordinary fermions. Majorana fermions, or real fermions, have the property that they are Hermitian. They are named after Italian physicist Ettore Majorana[80]. Although not famous during his

time, he did groundbreaking works in different areas of physics. Besides the suggestion of Majorana fermions, in 1932 he wrote a paper in the field of atomic spectroscopy concerning the behaviour of aligned atoms in time-varying magnetic fields. Rabi and others studied the same problem and developed an important sub-branch of atomic physics. In 1933 nuclear physics experiments suggested the existence of an unknown particle, which was considered to be gamma ray by some. Majorana first proposed that the particle should be a chargeless counterpart of proton, the neutron. Fermi once told him to write a paper, but he didn't bother. Later that year James Chadwick proved the existence of the neutron and was eventually awarded the Nobel prize for that. In 1959, Majorana disappeared suddenly under mysterious circumstances while going by ship from Palermo to Naples. His work on Majorana fermion was not appreciated at that time, like many of his other works. However, recently the search of Majorana fermions became a really hot topic in condensed matter physics, especially in topological systems [26].

In this thesis we will only use Majorana fermions as a mathematical tool to deal with gapped systems. Using Eq (3.24), H_i can be written in form of a_i and still be quadratic, only now there are $2N$ Majorana fermions.

$$H_i = -\frac{i}{4}(t+\Delta)(a_i a_{i+N+1} - a_{i+N+1} a_i) - \frac{i}{4}(\Delta - t)(a_{i+N} a_{i+1} - a_{i+1} a_{i+N}) - \frac{i\mu}{4}(a_{i+N} a_i - a_i a_{i+N}) \tag{3.25}$$

We still use $H_f = H_i + V c_0^\dagger c_0$. The trace formula for Majorana fermions now reads:

$$\mathrm{Tr} e^{A_{ij} a_i a_j} = \sqrt{det(1 + e^{4A})} \tag{3.26}$$

Now A is an antisymmetric matrix of size $2N \times 2N$. And we can carry out similar

calculations for the propagator:

$$G(t) = \langle c_0 e^{-iH_f t} c_0^\dagger e^{iH_i t} \rangle \tag{3.27}$$

We first commute a_i with e^{iH_i} by:

$$a_i e^{ih_{mn}a_m a_n} = e^{ih_{mn}a_m a_n} a_j (e^{4ih})_{ij}$$

Then we calculate the trace: $\mathrm{Tr}(e^{A_{ij}a_i a_j} a_m a_n)$, this can be done by noticing that $a_m a_n = \frac{a_m a_n - a_n a_m}{2} + \delta_{mn}$, so we write

$$\mathrm{Tr}(e^{A_{ij}a_i a_j} a_m a_n) = \mathrm{Tr}(e^{A_{ij}a_i a_j}(\frac{1}{2}\frac{d}{d\alpha} e^{\alpha M_{ij} a_i a_j}|_{\alpha=0} + \delta_{nm}))$$

Where $M = |m\rangle\langle n| - |n\rangle\langle m|$, is an antisymmetric matrix. We can again use Eq (3.26) to write

$$\begin{aligned}
\mathrm{Tr}(e^{A_{ij}a_i a_j} \frac{d}{d\alpha} e^{\alpha M_{ij} a_i a_j}|_{\alpha=0}) &= \frac{d}{d\alpha} \mathrm{Tr}(e^{A_{ij}a_i a_j} e^{\alpha M_{ij} a_i a_j})|_{\alpha=0} \\
&= \frac{d}{d\alpha} e^{\frac{1}{2}\mathrm{Tr} log(e^{4A} e^{4\alpha M})} = \frac{1}{2}\sqrt{det(1+e^{4A}e^{4\alpha M})} \frac{\mathrm{Tr}(4e^{4A}M)}{1+e^{4A}e^{4\alpha M}}|_{\alpha=0} \\
&= 2\sqrt{det(1+e^{4A}e^{4\alpha M})}\{(1+e^{-4A})^{-1}_{nm} - (1+e^{-4A})^{-1}_{mn}\}
\end{aligned}$$

And finally, we have:

$$\mathrm{Tr}(e^{A_{ij}a_i a_j} a_m a_n) = \sqrt{\det(1+e^{4A})}\{(1+e^{-4A})^{-1}_{nm} - (1+e^{-4A})^{-1}_{mn} + \delta_{mn}\} \tag{3.28}$$

Define $N = (1+e^{4\beta h_i})^{-1}$, $S = e^{-4ih_f t} e^{4ih_i t}$, $e^\omega = S e^{-4\beta h_i}$, $X = e^{4ih_i t - 4\beta h_i}\{((1 + e^{-\omega})^{-1})^T - (1+e^{-\omega})^{-1} + 1\}$, the propagator is now:

$$G(t) = \sqrt{(\det(1 - N + e^{-4ih_f t} e^{4ih_i t} N)}(X_{00} + X_{NN} - iX_{0N} + iX_{N0})/4 \qquad (3.29)$$

Next we consider how to take the limit of Eq (3.29) at zero temperature. At $\beta \to \infty$, $N \to$projection onto negetive eigenvectors of h_i. And for the limit of X, we write:

$$X = e^{4ih_i t} e^{-4\beta h_i} (\frac{1}{1 + (e^{4\beta h_i} S^{-1})^T} + \frac{e^{4\beta h_i} S^{-1}}{1 + e^{4\beta h_i} S^{-1}}) = e^{4ih_i t} (\frac{e^{-4\beta h_i}}{1 + (e^{4\beta h_i} S^{-1})^T} + \frac{S^{-1}}{1 + e^{4\beta h_i} S^{-1}})$$

Now notice that h is antisymmtric, so $e^{-4\beta h} = (e^{4\beta h})^T$, and we have:

$$X = (\frac{1 - N}{S^{-1}(1 - N) + N})^T + \frac{N}{SN + (1 - N)} \qquad (3.30)$$

Fig 3.2 shows a numerical calculation of the intensity for several Δ values. The edge singularity is at $\omega \sim 3$. This is the same for all curves. At ω around 0 there is also a jump depending on the value of Δ, when there is no pairing term the jump happens at $\omega = 0$ as in Fig 3.1 because there is no gap in the system, so that any positive energy input can excite the system. When a pairing term is present and opens a gap, the input energy has to be large enough to overcome the gap, which is $\sim 2\Delta$, so the jump starts at the value of the gap, this is consistent with the plot.

3.2 Introduction to RIXS

3.2.1 Experimental setup

In this section we look at a more complicated, and more powerful experimental technique, Resonant inelastic X-ray scattering(RIXS), which has recently attracted a large amount of research interest and proven to be useful in studying the excitations

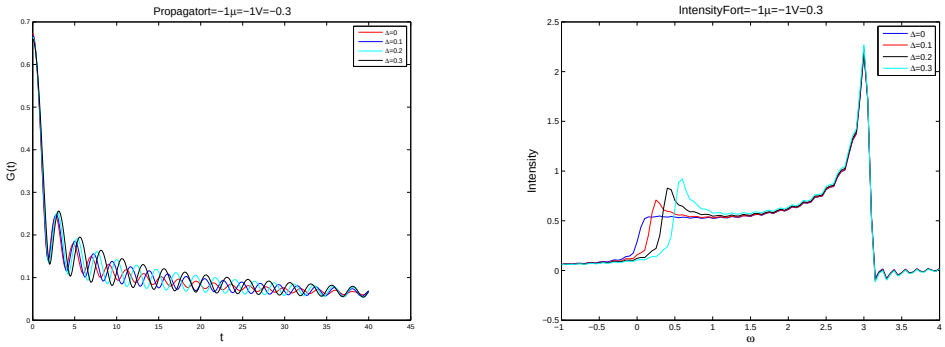

Figure 3.2: $G(t)$(left figure) and the intensity(right figure) for different Δ values. The other parameters are $t = -1$, $\mu = -1$, $V = 0.3$, $N = 150$.

in superconducting systems [50, 18, 23]. RIXS is a second order optical process, where a high energy X-ray knocks out a core election, temporarily creating a core-hole, and an electron in the valence band decays back into the core-hole and emits another photon [70]. Fig 3.3 shows an experimental setup of RIXS. RIXS is mostly performed at L and K-edges. There are 2 cases in RIXS, called direct and indirect RIXS. In the former, the core electron is excited into some valence band, and another electron from the valence band decays to fill the core-hole. In indirect RIXS, the transition from the core state to the conduction band is weak, the photon excites the electron into an empty state above the Fermi sea, and the same electron hops back. Naively it seems nothing interesting happens here, but the strong core-hole in the system would cause the system to deviate from the ground state, thus a shake-up of the system due to an abrupt appearance of a core hole potential. In the most studied example, transition metal K edge ($1s \rightarrow 4p$), the core-hole would create excitations in the $3d$ band. Fig 3.4 shows a brief description of the procedure.

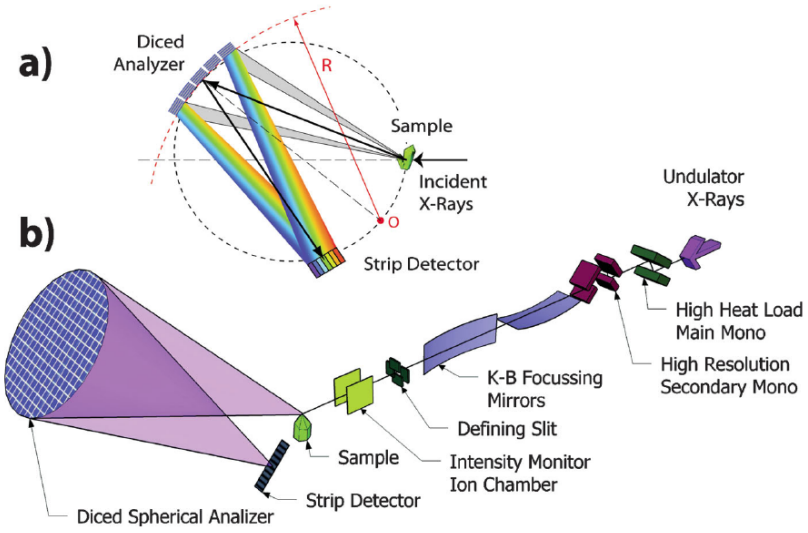

Figure 3.3: RIXS setup, from [4].

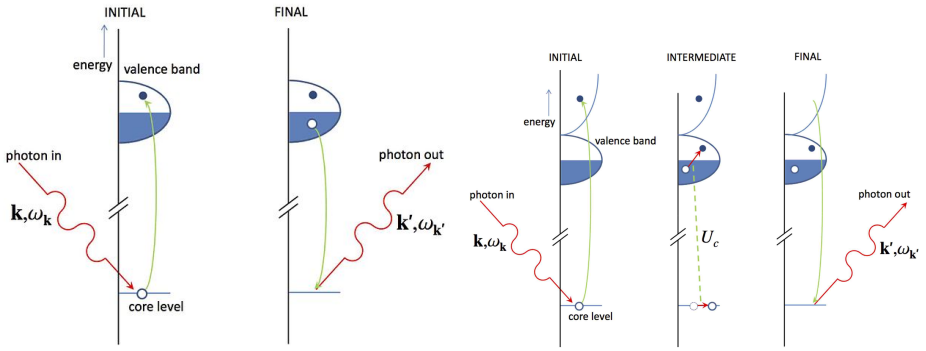

Figure 3.4: Direct(left) and indirect(right) RIXS. The figure is taken from[4].

A RIXS experiment is a lot more complicated, and expensive, than just X-ray absorption, why do we want to study it? it is main advantage is the wide range of energy scales to which it is sensitive. The different excitations that RIXS can measure are: photons $\sim$ 50meV, magnons $\sim$ 500meV, orbital excitations, $\sim$ 1.5eV, charge transfer excitations, $\sim$ 2eV. It is a bulk measurement, for X-ray of $1keV$, the penetration depth is around $0.1\mu m$. Since the photon-matter interaction is relatively strong compared to other techniques like neutron-matter interaction, a small sample size can already produce large enough cross section. It also utilizes the polarization of the photon.

3.2.2 Krammers-Heisenberg formula

The non-equilibrium processn involved in RIXS may be rather complicated, and thus the interpretation of experimental measurements may not be straightforward, as it may involve contributions which are not well described by effective low energy theories. In this section, we'll introduce the most standard formalism, the Kramers-Heisenberg cross section, although there is still a debate about what Hamiltonian should be used in this formalism. We are only interested in the "Magnon" region, where the energy transfer is $\sim$ 500meV, since it tells us about the electric and magnetic properties, and this is also the region most experiments focus on. To study the RIXS intensity, we want to put emphasis on two features of RIXS: "second order" and "resonant", which differ from the first order process in Sec 3.1. The system is excited by a photon and then emits one. Similar to the discussion in Sec 3.1, we want to treat the photon-electron interaction as a perturbation, the total Hamiltonian is:

$$H_{tot} = \sum_i \frac{(\mathbf{p}_i + e\mathbf{A}(\mathbf{r}_i))^2}{2m} + U(\mathbf{r}_i) + H_{ph} \tag{3.31}$$

H_{ph} is the same as in Eq3.2. The transition coeffecient to a final $|f\rangle$ state, up to second order, is:

$$W(N) = \langle N|H^{'}|I\rangle + \sum_{N} \frac{\langle N|H^{'}|N\rangle\langle N|H^{'}|I\rangle}{E_N - E_I} \tag{3.32}$$

Here the states denoted by capital letters $|I\rangle$ $|N\rangle$ and $|F\rangle$ are states of the total system, with electrons (which can involve different bands) and the photon. So $|I\rangle$ and $|F\rangle$ would have a photon, but the intermediate state $|N\rangle$ would have no photon, and an extra band electron, since the photon is absorpt to excite a core-electron. Later we will use lower case letters $|i\rangle$, $|n\rangle$ and $|f\rangle$ to denote the electron state. we use perturbation theory to second order: because of the "resonant" feature of RIXS, for the second order term, if $E_N \sim E_I$, there is a resonance and the intensity would have a significant boost, so this is really the term we want. Furthermore, the final state $|F\rangle$ would also have a photon coming out, and excitations in the electron system, this is different from the first order procedure in Sec 3.1. In RIXS the intensity would not only depend on the energy transferred into the system, but also the momentum transfer. Using Fermi's golden rule, we only keep the resonant part. The intensity is:

$$I = \frac{2\pi}{\hbar} \sum_{F} |\sum_{N} \frac{\langle F|H^{'}|N\rangle\langle N|H^{'}|I\rangle}{E_N - E_I}|^2 \times \delta(E_F - E_I) \tag{3.33}$$

Using the dipole approximation in Eq (3.5) and (3.6), we can write:

$$H^{'} \sim \mathcal{D} = \epsilon \cdot \mathbf{D} = \sum_{i} e^{i\mathbf{k}\cdot\mathbf{r}_i} \epsilon \cdot \mathbf{r}_i \tag{3.34}$$

Or we can write Eq (3.33)

$$I(\omega, k, k') = \sum_{F} \frac{2\pi}{\hbar} |\mathcal{F}_{FI}(k, k', \omega, \Gamma)|^2 \times \delta(E_F - E_I) \tag{3.35}$$

where

$$\begin{aligned}\mathcal{F}_F &= \sum_N \frac{\langle F|\mathcal{D}^\dagger|N\rangle\langle N|\mathcal{D}|I\rangle}{E_N - E_I + i\Gamma} \\ &= \sum_N \langle F|\mathcal{D}^\dagger G\mathcal{D}|I\rangle \end{aligned} \tag{3.36}$$

k and $k^{'}$ are the momentum of the incident and outgoing photon, $G = \sum_N \frac{|N\rangle\langle N|}{E_N - E_I + i\Gamma}$. We added an inverse core-hole lifetime Γ, it takes account of all the complicated process that are not included in the Hamiltonian that makes the intermediate state short lived. If we only consider the electron system, the initial, final, intermediate electron states are $|i\rangle$, $|f\rangle$, $|n\rangle$, and $E_N = E_n$, $E_I = E_i + \omega$, $E_F = E_f + \omega^{'}$. With this we can usually safely remove the photon, but we do have to remember that there can be multiple bands involved in indirect RIXS. Eq (3.35) is also called the Kramers-Heisenberg cross section.

3.3 A perturbative study of RIXS intensity

In this section we start to analyze the RIXS intensity using Eq (3.35), which is the basic formula in the theoretical study of RIXS spectrum. Different types of Hamiltonians have been used in the equation, in most cases in the context of high Tc superconductors, people use the t-J model [69, 70], and RIXS spectrum is understood as the dispersion of magnon excitations [70]. Here we instead use a simple band hopping Hamiltonian:

$$H_0 = \sum_{k,\sigma} \epsilon_k d^\dagger_{k,\sigma} d_{k,\sigma} \tag{3.37}$$

and demonstrate that one can use this simple model to quantitatively understand the spectrum. When the core-hole is present, it creates a screened Coulomb potential at site r: $H_r = H_0 + U_c \sum_\sigma d^\dagger_{r,\sigma} d_{r,\sigma}$, where U_c is the core-hole potential. A natural

thought is to take U_c to be small and do a perturbative expansion. In this section we study the RIXS intensity, both for direct and indirect RIXS, by doing that. But first we want to treat the dipole interaction in Eq (3.6) more carefully.

3.3.1 Dipole interaction in RIXS

The $\mathcal{F}$ function in Eq (3.36) can be written in terms of the dipole interaction:

$$\mathcal{F}_F = \sum_{F,R} \langle F | e^{i\mathbf{Q}\mathbf{R_i}} \epsilon^{'} \cdot \mathbf{D}^{'\dagger} \cdot G \cdot \epsilon \cdot \mathbf{D} | I \rangle \tag{3.38}$$

ϵ and $\epsilon^{'}$ are the polarization of incident and outgoing photons, $\mathbf{Q} = \mathbf{k} - \mathbf{k}^{'}$ is the momentum transfer. It will depend on the geometry of the experiment. Here we specifically consider copper $L3$ edge $2p \rightarrow 3d$, and calculate the geometry dependence explicitly.

For the $2p$ orbital, there are 3 states with $m = 1, 0, -1$, for the $3d$ orbital the state is $|3d_{x^2-y^2}\rangle$. The dipole matrix elements $\eta_m = \langle 3d_{x^2-y^2} | \mathbf{r} | 2p_m \rangle$ can be calculated as:

$$\eta_m = \langle 3d_{x^2-y^2} | \mathbf{r} | 2p_m \rangle = \begin{cases} 0 & (m = 0) \\ \frac{1}{\sqrt{2}}(\hat{x} \mp i\hat{y}) & (m = \pm 1) \end{cases} \tag{3.39}$$

However because of the spin-orbit interaction, m is not a good quantum number of the ground state, but the total spin of the electron $\mathbf{J} = \mathbf{s} + \mathbf{L}$ is approximately a good quantum number. The total spin should be 3/2, the 1/2 state is off resonance from the edge. So we write the transformation from the uncoupled $|1m; \frac{1}{2}s_z\rangle$ space (also

denoted as $|m,s\rangle$) to the total spin $|j,m_z\rangle$ state:

$$\begin{aligned}
|1,\uparrow\rangle &= |\frac{3}{2},\frac{3}{2}\rangle \\
|1,\downarrow\rangle &= \sqrt{\frac{1}{3}}|\frac{3}{2},\frac{1}{2}\rangle + \sqrt{\frac{2}{3}}|\frac{1}{2},\frac{1}{2}\rangle \\
|-1,\uparrow\rangle &= \sqrt{\frac{1}{3}}|\frac{3}{2},-\frac{1}{2}\rangle + \sqrt{\frac{2}{3}}|\frac{1}{2},-\frac{1}{2}\rangle \\
|-1,\downarrow\rangle &= |\frac{3}{2},-\frac{3}{2}\rangle
\end{aligned}$$

$m = 0$ states are not considered since the dipole matrix element is 0. Also since $j = 1/2$ state is off resonance at the edge, we should drop them. So that:

$$\begin{aligned}
|1,\uparrow\rangle &= |\frac{3}{2},\frac{3}{2}\rangle \\
|1,\downarrow\rangle &= \sqrt{\frac{1}{3}}|\frac{3}{2},\frac{1}{2}\rangle\rangle \\
|-1,\uparrow\rangle &= \sqrt{\frac{1}{3}}|\frac{3}{2},-\frac{1}{2}\rangle\rangle \\
|-1,\downarrow\rangle &= |\frac{3}{2},-\frac{3}{2}\rangle
\end{aligned}$$

The dipole operator $\mathcal{D}$, in the uncoupled basis, is written as:

$$\epsilon \cdot \mathbf{D} = \sum_{R,m,\sigma} e^{-i\mathbf{kR}} \hat{\epsilon} \cdot \hat{\eta}_m d^\dagger_{\mathbf{R}\sigma} p_{\mathbf{R},\sigma,m} \tag{3.40}$$

$d^\dagger$ is the creation operator for band electron and p destroys a core-electron. We can then write it in the total spin basis:

$$\begin{aligned}
\hat{\eta}_m \cdot d^\dagger_{\mathbf{R}\sigma} p_{\mathbf{R},\sigma,m} &= \hat{\eta}_1 (d^\dagger_{\mathbf{R},\uparrow} p_{\mathbf{R},3/2} + \sqrt{1/3} d^\dagger_{\mathbf{R},\downarrow} p_{\mathbf{R},1/2}) \\
&+ \hat{\eta}_{-1} (d^\dagger_{\mathbf{R},\downarrow} p_{\mathbf{R},-3/2} + \sqrt{1/3} d^\dagger_{\mathbf{R},\uparrow} p_{\mathbf{R},-1/2})
\end{aligned} \tag{3.41}$$

and the same for the final state dipole operator $\mathcal{D}'$. We plug in Eq (3.41), and notice

that each term in $\mathcal{D}$ must match up with the same term in $\mathcal{D}'$, we can also drop p and only consider the band electrons, to get:

$$\begin{aligned}\mathcal{F}_f &= \sum_{\mathbf{R}} e^{i\mathbf{QR}}\chi_{\alpha\beta}\langle f|d_{\mathbf{R},\alpha}Gd^{\dagger}_{\mathbf{R}\beta}|i\rangle \\ &= \sum_{\mathbf{R},n} e^{i\mathbf{QR}}\chi_{\alpha\beta}\langle f|d_{\mathbf{R},\alpha}\frac{|n\rangle\langle n|}{E_n-\omega-E_i+i\Gamma}d^{\dagger}_{\mathbf{R}\beta}|i\rangle \end{aligned} \tag{3.42}$$

where

$$\begin{aligned}\chi_{\uparrow\uparrow} &= \chi^*_{\downarrow\downarrow} = (\hat{\epsilon}_f\cdot\hat{\eta}_1)^*(\hat{\epsilon}_i\cdot\hat{\eta}_1) \ + (1/3)(\hat{\epsilon}_f\cdot\hat{\eta}_{-1})^*(\hat{\epsilon}_i\cdot\hat{\eta}_{-1}) \\ \chi_{\uparrow\downarrow} &= \chi_{\downarrow\uparrow} = 0 \end{aligned} \tag{3.43}$$

At this stage we only consider the electron system. We can also write the total intensity as a mix of spin-flip (SF) and none-spin-flip (NSF) intensity, with:

$$\begin{aligned}\mathcal{F}_{NSF} &\sim d_{\uparrow}Gd_{\uparrow} + d_{\downarrow}Gd_{\downarrow} \\ \mathcal{F}_{SF} &\sim d_{\uparrow}Gd_{\uparrow} - d_{\downarrow}Gd_{\downarrow} \end{aligned} \tag{3.44}$$

In experiments, the X-ray shines onto the sample with an angle. The standard terminology uses σ channel to represent X-ray polarized parallel to the surface of the sample, and π channel to represent the polarization that is perpendicular to σ channel (not perpendicular to the surface of the sample). A prime is used to indicate the outgoing photon. So $\sigma\pi'$ channel means the incoming photon is parallel to the surface of the sample but outgoing photon is not. We see that the SF channel would correspond to $\sigma\pi'$ and $\pi\sigma'$ signal since the spin is flipped after scattering, and NSF channel corresponds to $\sigma\sigma'$ and $\pi\pi'$ channel. In some cases, the outgoing photon is not polarized and we take the everage of the outgoing σ' and π' channel.

3.3.2 Zeroth order expansion

We consider an incident photon with energy ω, momentum $\mathbf{k}$, and outgoing photon with energy $\omega + \Delta\omega$, momentum $\mathbf{k} + \mathbf{Q}$. From Sec 3.2.2, the intensity is:

$$I \propto \sum_F |\mathcal{F}_f|^2 \delta(E_F - E_I) \tag{3.45}$$

where

$$\mathcal{F}_f = \sum_R e^{i\mathbf{Q}\mathbf{R_m}} \chi_{\rho\sigma} \langle f | d_{m\rho} (H_m - E_i - \omega + i\Gamma)^{-1} d^\dagger_{m\sigma} | i \rangle \tag{3.46}$$

Here H_m is the Hamiltonian after creating a core hole at site m, $H_m = H_0 + U_c \sum_\sigma d^\dagger_{m\sigma} d_{m\sigma}$, Γ is the inverse of life span of the core hole. Remember that the states $|i\rangle$ and others are the total electron states that may involve multipy bands. χ depends on experimental geometry as in Eq (3.43).

In this section, we want to write the intensity as an expansion in U_c:

$$I = I^0 + I^1 + ... \tag{3.47}$$

by expanding the propagator G:

$$G = G^0 + G^1 + ... \tag{3.48}$$

For the zeroth order approximation, we take $H_m = H_0$, the unperturbed Hamiltonian, which is just a simple band. And we write explicitly:

$$\begin{aligned} G_0 &= (H_0 - E_I + i\Gamma)^{-1} = \sum_N \frac{|N\rangle\langle N|}{E_N - E_I + i\Gamma} \\ &= \sum_n \frac{|n\rangle\langle n|}{E_n - E_i - \omega + i\Gamma} \end{aligned} \tag{3.49}$$

Again, $|N\rangle$ is the state of the complete system with electrons and photons. $|n\rangle$ is the electron state. In the case of indirect RIXS, an electron is excited from $1s$ state to $4p$ state, the core-hole causes excitations in $3d$ band. So the d_m and $d_m^\dagger$ act on the 4p band while G_0 act on 3d band, so those parts are separated, and we don't need to worry about the spin dependence, only considering the 3d band, we have:

$$\mathcal{F}_f = \sum_m e^{i\mathbf{Q}\mathbf{R_m}} \langle f| \sum_n \frac{|n\rangle\langle n|}{E_n - E_i - \omega + i\Gamma} |i\rangle \tag{3.50}$$

Here $|f\rangle$ must be the same as $|i\rangle$ for $\mathcal{F}_f$ to be nonzero. That means only elastic scattering. So the zeroth order intensity for inelastic scattering is 0. This is not surprising, since we mentioned in the introduction that for indirect RIXS, the only reason for the excitation to appear in the $3d$ band is the core-hole potential.

In the case of direct RIXS at Cu L-edge, we can forget about the 4p band and all the operators act on the 3d band. For the Hamiltonian in Eq (3.37), the single electron eigenstates are also momentum eigenstates, and it only couples electrons with same spins. Then

$$\mathcal{F}_f = \sum_m e^{i\mathbf{Q}\mathbf{R}_m} \chi_{\rho\sigma} \langle f| d_{m\rho} \sum_n \frac{|n\rangle\langle n|}{E_n - E_i - \omega + i\Gamma} d_{m\sigma}^\dagger |i\rangle \tag{3.51}$$

Assume the ground state of 3d band is $|i\rangle = \prod_{\alpha\sigma} (d_{\alpha\sigma}^\dagger)^{n_{\alpha\sigma}} |\Omega\rangle$, where Ω is the vacuum, $d_{\alpha\sigma}^\dagger$ create an electron with single electron of state $|k_\alpha\rangle$ and spin σ, and $n_{\alpha\sigma}$ is the occupation number, which is decided by the chemical potential and the temperature. Here we limit our discussion to zero temperature so $n_{\alpha\sigma} = 0, 1$. We write

$$d_{m\sigma}^\dagger = \frac{1}{\sqrt{N}} \sum_k e^{-i\mathbf{k}\mathbf{R_m}} d_{k\sigma}^\dagger$$

In order that $\mathcal{F}$ is nonzero, that means $\langle n| d_{k\sigma}^\dagger |i\rangle$ is nonzero for some k_1, so $|n\rangle$

must be a state that creates an electron with momentum and spin k_1, σ, from the ground state $|i\rangle$, i.e. $|n\rangle = d^\dagger_{k_1\sigma}|i\rangle$, and similarly $|f\rangle$ destroys an electron with k_2 from $|n\rangle$: $|f\rangle = d_{k_2\rho}|n\rangle = d_{k_2\rho}d^\dagger_{k_1\sigma}|i\rangle$. So we have:

$$\begin{aligned}\mathcal{F}_f &= \sum_m e^{i\mathbf{Q}\mathbf{R_m}} e^{i\mathbf{k_1}\mathbf{R_m}} e^{-i\mathbf{k_2}\mathbf{R_m}} \frac{1}{\epsilon_{k_1} - \omega + i\Gamma}(1 - n_{k_1\sigma})n_{k_2\rho} \\ &= \frac{1}{\epsilon_{k_1} - \omega + i\Gamma}(1 - n_{k_1\sigma})n_{k_1+Q,\rho}\end{aligned}$$

We dropped the spin part χ since it does not depend on σ and ρ. Summing over all possible final states:

$$I^0 \propto \sum_k (1 - n_k)n_{k+Q} \frac{1}{|\epsilon_k - \omega + i\Gamma|^2}\delta(\epsilon_k - \epsilon_{k+Q} - \Delta\omega) \tag{3.52}$$

We used the fact that $n^2 = n$ for fermions. The Feynman diagram is shown as:

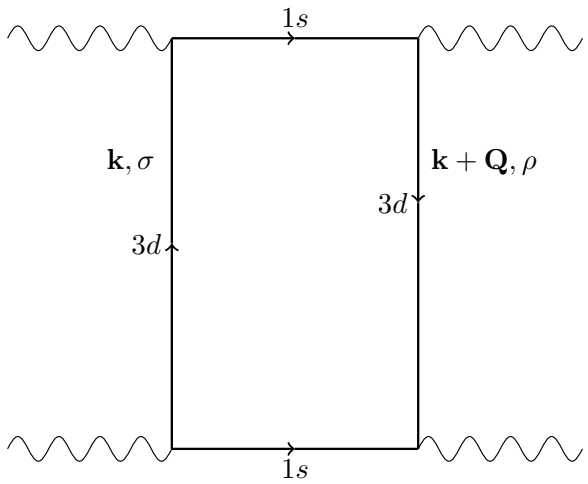

Here wavy lines are the photon propagators and solid lines are the electron propagators.

3.3.3 Leading order correction.

3.3.3.1 Indirect RIXS

We first consider the correction to indirect RIXS. Since for the first order correction $I^1 = \mathcal{F}_f^0(\mathcal{F}_f^1)^* + (\mathcal{F}_f^0)^*\mathcal{F}_f^1$, and $\mathcal{F}^0 = 0$ in the indirect case, the first order correction is 0, and the leading order is the second order.

We write:

$$\begin{aligned} G &= (H_m - E_I + i\Gamma)^{-1} = ((G^0)^{-1} + U_c(d^\dagger_{m\uparrow}d_{m\uparrow} + d^\dagger_{m\downarrow}d_{m\downarrow})^{-1} \\ &\sim G^0 - U_c G_0(d^\dagger_{m\uparrow}d_{m\uparrow} + d^\dagger_{m\downarrow}d_{m\downarrow})G_0 \\ &= G^0 + G^1 \end{aligned}$$

The first order correction of $\mathcal{F}_f$ is now:

$$\begin{aligned} \mathcal{F}_f^1 &= U_c \sum_m e^{i\mathbf{QR_m}} \langle F|G_0(d^\dagger_{m\uparrow}d_{m\uparrow} + d^\dagger_{m\downarrow}d_{m\downarrow})G_0|I\rangle \\ &= U_c \sum_{m,n,l} e^{i\mathbf{QR_m}} \langle F| \frac{|N\rangle\langle N|}{E_N - E_I - \omega + i\Gamma}(d^\dagger_{m\uparrow}d_{m\uparrow} + d^\dagger_{m\downarrow}d_{m\downarrow}) \frac{|L\rangle\langle L|}{E_L - E_I - \omega + i\Gamma}|I\rangle \end{aligned}$$

χ is dropped since the result does not depend on σ and ρ. Next we want to consider the effect of 3d and 4p bands. We use $|i\rangle$, $|f\rangle$ and $|n\rangle$ to denote 3d states. $E_n = E_{n,3d} + E_{n,4p}$, the overlap, $\langle L|I\rangle$, should be the product of 3d state overlap and 4p state overlap. Only interested in 4p band states, we can trace over 3d states.

$$\begin{aligned}
\mathcal{F}_f^1 &= U_c \sum_m e^{i\mathbf{QR_m}} \langle F|G_0(d_{m\uparrow}^\dagger d_{m\uparrow} + d_{m\downarrow}^\dagger d_{m\downarrow})G_0|I\rangle \\
&= U_c \sum_{m,n,l} e^{i\mathbf{QR_m}} \langle f| \int d\epsilon g(\epsilon) \frac{|n\rangle\langle n|}{E_n - E_i - \epsilon - \omega + i\Gamma} (d_{m\uparrow}^\dagger d_{m\uparrow} + d_{m\downarrow}^\dagger d_{m\downarrow}) \frac{|l\rangle\langle l|}{E_l - E_i - \epsilon - \omega + i\Gamma} |i\rangle \\
&= U_c \sum_m e^{i\mathbf{QR_m}} \int \frac{d\epsilon g(\epsilon)}{(E_f - E_i - \epsilon - \omega + i\Gamma)(-\epsilon + \omega + i\Gamma)} \langle f|(d_{m\uparrow}^\dagger d_{m\uparrow} + d_{m\downarrow}^\dagger d_{m\downarrow})|i\rangle
\end{aligned}$$

Where $g(\epsilon)$ is the density of state as function of energy for the 3d band.

In the above equation, $|f\rangle$ should be a state that takes one electron from $|i\rangle$ under the Fermi sea then adds a hole into the system:

$$|f\rangle = d_{k_2}^\dagger d_{k_1} |i\rangle$$

So we have:

$$\begin{aligned}
\mathcal{F}_f^1 &= \sum_m e^{i\mathbf{QR_m}} e^{i\mathbf{k_1 R_m} - i\mathbf{k_2 R_m}} \frac{U_c}{(\epsilon_{k_1} - \epsilon_{k_2} - \omega + i\Gamma)(\omega + i\Gamma)} (1 - n_{k_2}) n_{k_1} \\
&= \frac{U_c}{(\epsilon_k - \epsilon_{k+Q} - \omega + i\Gamma)(\omega + i\Gamma)} (1 - n_{k+Q}) n_k \qquad (3.53)
\end{aligned}$$

Summing over all possible $|f\rangle$ gives:

$$I^1 = \sum_f |\mathcal{F}_f^1|^2 = \int d\mathbf{k} | \frac{U_c^2 \int d\epsilon g(\epsilon)}{(\epsilon_k - \epsilon_{k+Q} + \epsilon - \omega + i\Gamma)(\omega - \epsilon + i\Gamma)} |^2 (1 - n_{k+Q}) n_k \quad (3.54)$$

Graphically, this is represented as:

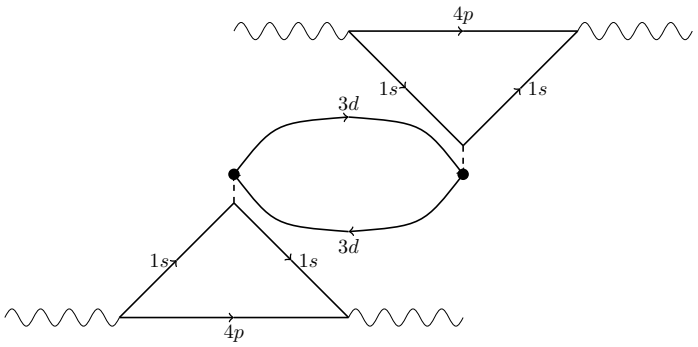

where the black dots represent the core-hole columb potential.

3.3.3.2 Direct RIXS

We now consider direct RIXS. We write:

$$\begin{aligned}\mathcal{F}_f^1 &= U_c \sum_m e^{i\mathbf{QR_m}} \chi_{\rho\sigma} \langle f | d_{m\rho} G_0 (d^\dagger_{m\uparrow} d_{m\uparrow} + d^\dagger_{m\downarrow} d_{m\downarrow}) G_0 d^\dagger_m | i \rangle \\ &= U_c \sum_m e^{i\mathbf{QR_m}} \chi_{\rho\sigma} \langle f | d_{m\rho} \frac{|n\rangle\langle n|}{E_n - E_i - \omega + i\Gamma} (d^\dagger_{m\uparrow} d_{m\uparrow} + d^\dagger_{m\downarrow} d_{m\downarrow}) \frac{|l\rangle\langle l|}{E_l - E_i - \omega + i\Gamma} d^\dagger_{m\sigma} | i \rangle\end{aligned}$$

Following the same reasoning, in order for this contribution to be nonzero: $|l\rangle = d^\dagger_{k_1\sigma}|i\rangle$, $|n\rangle = d^\dagger_{k_3\mu} d_{k_2\mu} d^\dagger_{k_1\sigma}|i\rangle$, and $|f\rangle = d_{k_4\rho} d^\dagger_{k_3\mu} d_{k_2\mu} d^\dagger_{k_1\sigma}|i\rangle$. Here $d_{k_2\mu}$ and $d_{k_3\mu}$ must have the same spin because of the form of the core-hole potential, they can only be both up or both down.

If $\sigma \neq \rho$ we have:

$$\mathcal{F}_f^1 = 2 \sum_m \frac{U_c^2 e^{i\mathbf{QR_m}} e^{i\mathbf{k_1 R_m} - i\mathbf{k_2 R_m} + i\mathbf{k_3 R_m} - i\mathbf{k_4 R_m}}}{(\epsilon_{k_3} - \epsilon_{k_2} + \epsilon_{k_1} - \omega + i\Gamma)(\epsilon_{k_1} - \omega + i\Gamma)} (1 - n_{k_1})(1 - n_{k_3}) n_{k_2} n_{k_4} \quad (3.55)$$

A factor of 2 appears, since μ can be up or down.

Now we see that the effect of the spins σ and ρ in this case, if $\sigma = \rho$, we can let $\sigma = \rho = \mu$, there is another possible $|n\rangle$ that can also give the same final state $|f\rangle$: $|n\rangle = d^\dagger_{k_3\sigma} d_{k_4\sigma} d^\dagger_{k_1\sigma}|i\rangle$, and $|f\rangle$ destroys an electron k_2, σ from $|n\rangle$. It differs from

Eq (3.56) by changing $\epsilon_{k_2} \to \epsilon_{k_4}$ in the denominator, and giving up the factor of 2:

$$\mathcal{F}_f^{1'} = \sum_m \frac{U_c^2 e^{i\mathbf{Q}\mathbf{R_m}} e^{i\mathbf{k_1}\mathbf{R_m} - i\mathbf{k_2}\mathbf{R_m} + i\mathbf{k_3}\mathbf{R_m} - i\mathbf{k_4}\mathbf{R_m}}}{(\epsilon_{k_3} - \epsilon_{k_4} + \epsilon_{k_1} - \omega + i\Gamma)(\epsilon_{k_1} - \omega + i\Gamma)} (1 - n_{k_1})(1 - n_{k_3}) n_{k_2} n_{k_4} \quad (3.56)$$

The sum over m gives the momentum conservation condition. Graphically, the two cases are represented as:

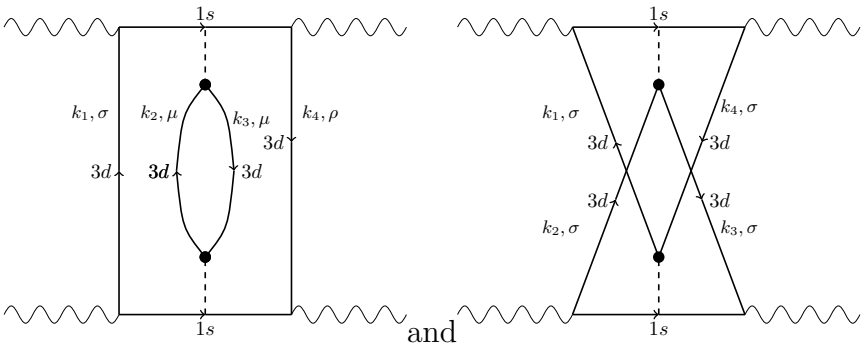

The second case only happens when $\sigma = \rho$.

For the first order correction, $I^1 = \mathcal{F}_f^0 (\mathcal{F}_f^1)^* + (\mathcal{F}_f^0)^* \mathcal{F}_f^1$, since for $\mathcal{F}_f^1$, $|f\rangle$ has a pair excitation from $|i\rangle$, but for $\mathcal{F}_f^0$, only one eletron excitaion is allowed, the product $(\mathcal{F}_f^0)^* \mathcal{F}_f^1$ is 0, and the leading order is also 2nd order. With:

$$\begin{aligned} I^1 &= \sum_f |\mathcal{F}_f^1|^2 \\ &= \int dk_1 dk_2 dk_3 dk_4 \frac{U_c^2 \delta(k_1 - k_2 + k_3 - k_4 + Q) \delta(\epsilon_{k_1} + \epsilon_{k_3} - \epsilon_{k_2} - \epsilon_{k_4} - \Delta\omega)}{|(\epsilon_{k_3} - \epsilon_{k_2} + \epsilon_{k_1} - \omega + i\Gamma)(\epsilon_{k_1} - \omega + i\Gamma)|^2} \\ &\times \quad (1 - n_{k_1}) n_{k_4} (1 - n_{k_3}) n_{k_2} \end{aligned} \quad (3.57)$$

Which is a 3-d integral. For simplicity, we only write the term in Eq (3.56), but keep in mind there could be another term in the case $\sigma = \rho$.

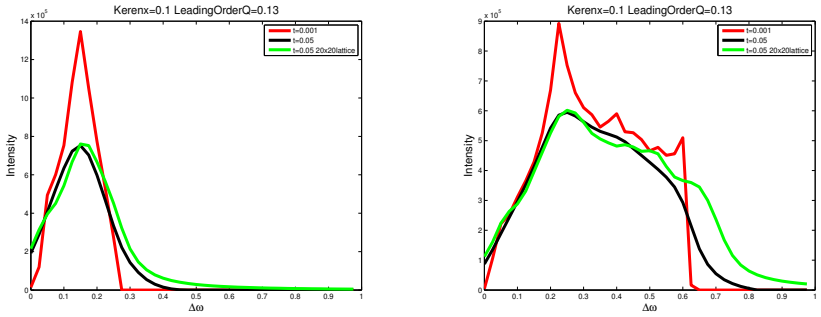

Figure 3.5: Leading order intensity. Here we used the Lorentzian to approximate the delta function in energy: $\delta(E) \sim \frac{1}{\pi}\frac{t}{t^2+E^2}$. This is to mimic the effect of the energy resolution in the experiment, mostly around $\sim$ 100meV. The red lines are close to the exact value. The black lines show the smearing effect of the delta function, and the green line is calculated on a smaller lattice to show the convergence.

3.3.4 Numerics

Now let's look at an example of CLBLCO ($(Ca_xLa_{1-x})(Ba_{1.75-x}La_{0.25+x})Cu_3O_y$) sample, we will look more closely into this material in Chap V, but for now we only care about the band energy spectrum, which is:

$$\epsilon_k = t_0 - 2t_1(cos(k_x) + cos(k_y)) - 4t_2 cos(k_x)cos(k_y) - 2t_3(cos(2k_x) + cos(2k_y)) \quad (3.58)$$

and $t_0 = 0.134$eV, $t_1 = 0.11$eV, $t_2 = -0.032$eV, $t_3 = 0.016$eV.

Fig 3.5 shows the zeroth order calculation for direct RIXS. The red and black curves are calculated on an 80 by 80 lattice and green curve on 20 by 20 lattice. Here a "damping" factor t is used when doing the Fourier transform, so the delta function in the energy conservation condition reads now: $\delta(E) \sim \frac{1}{\pi}\frac{t}{t^2+E^2}$. This is because of the energy resolution of the experiment, $\sim$ 100meV.

We notice that in the red line, for $q = 0.34$, there is a drop in the intensity, that

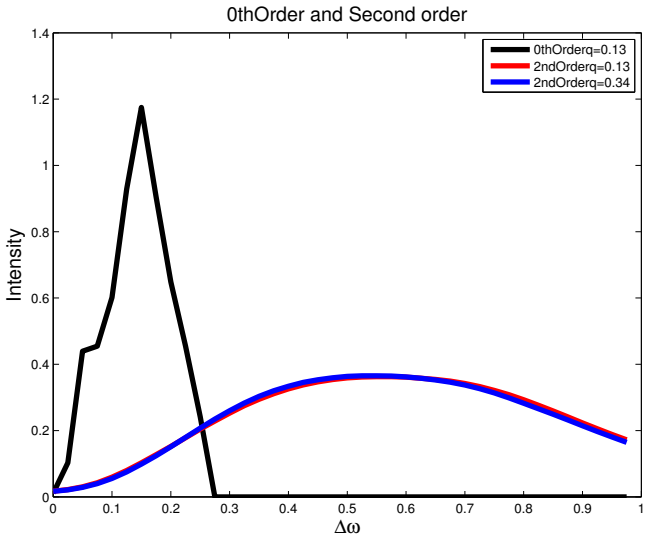

Figure 3.6: Correction for the intensity. The black curve is the leading order for $q = 0.13$, the red and blue curves are second order curves for $q = 0.13$ and $q = 0.34$ at $U_c = 1eV$. (Since the 3d integral is a lot harder, it is done on a 24×24 lattice).

comes from reaching the top of the energy band. Now we look at the corrections coming from (3.57), in the case $\sigma \neq \rho$, in Fig 3.6.

We see that the second order correction does not depend on q a lot. That's because the second order process creates 2 pairs of electron-hole excitatons and can be at any place in the Brillouin zone, as long as two of them are under the Fermi surface and two above and the total momentum adds to q, the momentum difference between the electrons can be big, even if $q = 0$. So that introducing a new momentum scale q does not change the picture too much. Also the second order intensity has a special

feature that it doesn't vanish at $q = 0$, as the leading order correction does.

CHAPTER IV

Determinant method study of RIXS spectrum in doped cuprate

In Chap III we introduced the basic experimental and theoretical knowledge about X-ray absorption and RIXS. We also used the so called "determinant method" to study the X-ray intensity. This method can also be used to study RIXS. In this chapter, we will apply this method to RIXS, particularly for cuprate systems. We will first introduce the method in Sec 4.1, and then we will apply the method to some experimental systems. In Sec 4.2 we combine it with the so called "YRZ" phenomenological Green's function to study the Bi-2201 system. In Sec 4.3 we look at the YBCO sample [41], and pay special attention to the detuning of incoming photon energy.

4.1 Introduction of method

In this chapter, we focus on the RIXS intensity in cuprate systems. We first start by introducing the determinant method used in reference [9]. If the incident photon has energy ω, momentum $\mathbf{k}$, and outcoming photon has $\omega - \Delta\omega$, $\mathbf{k}+\mathbf{Q}$, from Eq (3.42)

and Eq (3.35), the intensity is:

$$I \sim \sum_{f,m,n} e^{i\mathbf{Q}\mathbf{R}_{mn}} \chi_{\rho\sigma}\chi_{\mu\nu} \langle i|d_{n\rho}G_n d^\dagger_{n\sigma}|f\rangle\langle f|d_{m\mu}G_m d^\dagger_{m\nu}|i\rangle \delta(E_f - E_i - \Delta\omega) \tag{4.1}$$

Here $G_m = (H_m + \omega - E_i - i\Gamma)^{-1}$. Using $\delta(z) = \frac{1}{2\pi}\int e^{isz}ds$, we can replace $\sum_f |f\rangle\langle f|e^{iE_f s} \rightarrow e^{iHs}$, where H now is an operator. Also we replace $e^{iE_i}|i\rangle \rightarrow e^{-iHs}|i\rangle$. Same thing can be done for the propagator, we use $1/z = \int_0^\infty e^{-zt}dt$, so that:

$$\begin{aligned} G_m &= i\sum_m \frac{|m\rangle\langle m|}{iE_m + i\omega - iE_i - \Gamma} \\ &= i\int_0^\infty e^{(iE_m + i\omega - iE_i - \Gamma)t}|m\rangle\langle m| = \int_0^\infty e^{(i\omega - iE_i - \Gamma)t} e^{iH_m t} \end{aligned} \tag{4.2}$$

The factor $e^{iE_i t}$ can again be absorpt into $e^{iHt}|i\rangle$, finally the intensity is written in an integral form:

$$\begin{aligned} I &= \int_{-\infty}^{\infty} ds \int_{-\infty}^{\infty} dt \int_{-\infty}^{\infty} d\tau e^{i\omega(t-\tau) - is\Delta\omega - \Gamma(t+\tau)} \\ &\times \sum_{n,m} \chi_{\rho\sigma}\chi_{\mu\nu} S^{mn}_{\rho\sigma\mu\nu} \end{aligned} \tag{4.3}$$

With:

$$S^{mn}_{\rho\sigma\mu\nu} = \langle e^{\mathrm{i}H\tau} d_{n\rho} e^{-\mathrm{i}H_n\tau} d^\dagger_{n\sigma} e^{\mathrm{i}Hs} d_{m\mu} e^{\mathrm{i}H_m t} d^\dagger_{m\nu} e^{-\mathrm{i}H(t+s)} \rangle. \tag{4.4}$$

From Eq (3.43) we see that for the Cu L-edge that is relevant in this chapter, in order for χ to be nonzero, we need $\rho = \sigma$ and $\mu = \nu$, so we only use 2 spin indices and write (4.4) as $S^{mn}_{\rho\mu}$. Although Eq (4.3) looks even more complicated than Eq (3.35),

we can calculate (4.4) exactly, using Eq (3.14). The result is:

$$\begin{aligned} S^{mn}_{\rho\sigma} &= \det(F)[\langle n\rho|(1-N)^{-1}F^{-1}e^{-ih_n\tau}|n\rho\rangle \times \langle m\sigma|e^{-ihs}e^{ih_n\tau}(1-N)F^{-1}U_{mn}|m\sigma\rangle \\ &+ \langle n\rho|(1-N)F^{-1}U_{mn}|m\sigma\rangle \times \langle m\sigma|e^{ih_mt}U_0NF^{-1}e^{-ih_n\tau}|n\rho\rangle] \end{aligned} \tag{4.5}$$

Where $N = (1+e^{\beta h})^{-1}$, $U_{mn} = e^{-ih_n\tau}e^{ihs}e^{ih_mt}$, and $U_0 = e^{i(\tau-t-s)h}$, $F = 1 - N + U_{mn}U_0N$. We will not show the detailed derivation here, but we do a similar calculation in Sec 5.1. In Eq (4.3) χ depend on the experiment. The signal is split into spin-flip (SF) channel and none-spin-flip (NSF) channel. For the SF channel we want: $S^{SF} = S_{\uparrow\uparrow} + S_{\downarrow\downarrow} - S_{\uparrow\downarrow} - S_{\downarrow\uparrow}$, for the NSF channel, $S^{NSF} = S_{\uparrow\uparrow} + S_{\downarrow\downarrow} + S_{\uparrow\downarrow} + S_{\downarrow\uparrow}$. The total signal would be the mixture of the two channels and the relative weight depends on the incident and outgoing angles of the X-ray.

4.2 Auxiliary fermion approach to the RIXS spectrum in doped cuprate

4.2.1 Introduction to YRZ Green's function

An important part of the study of doped cuprates is to understand the possible structure and role of the Fermi surface. Angle-resolved Photo-Emission (ARPES) experiments suggest that the Fermi surface is made of pockets [82, 6]. A phenomenological ansatz of a retarded Green's function was proposed by Yang, Rice and Zhang (YRZ) [48, 83] to explain the formation of a hole pocket. This form of Green's function satisfies Luttinger sum rule, the complete Fermi surface is suggested to be the combination of the zeros and poles of the Green's function, and the hole doping is directly related to the volume of the hole pocket. The dramatic development in RIXS techniques has enabled a new test ground for high-temperature superconductivity

theories. And the YRZ Green's function can be helpful for understanding RIXS experiments. In [39], it is shown that the ansatz can be obtained alternatively by the slave boson mean field (SBMF) theory, and can be used to study the magnetic response contribution to RIXS in the underdoped region. In particular, the "hour-glass" behavior [27], a downwardly dispersing portion at low energy near (π, π), can also be derived.

Despite the success of the YRZ theory, it is an ansatz for the Green's function that does not directly correspond to a microscopic model. Although some key figures of the Fermi surface can be understood from the Green's function, since the theory is not free, it does not allow the calculation of some other quantities such as density-density correlations, without making further assumptions, such as the random phase approximation in [39]. In this section, we show that by introducing an auxiliary fermion, we can write a simple Hamiltonian that gives the YRZ Green's function, and allows taking into account interactions with a core hole using the methods of [9].

The YRZ ansatz starts from a t-J model,

$$H_{t-J} = -\sum_{ij\sigma} t_{ij} c^{\dagger}_{i\sigma} c_{j\sigma} + \frac{1}{2}\sum_{ij} J_H \mathbf{S_i} \cdot \mathbf{S_j} \tag{4.6}$$

The first term is a hopping term and the second term a spin-spin interaction term. The proposed ansatz for the coherent part of the Green's function is:

$$G_{\sigma}(\omega, \mathbf{k}) = \frac{g_t(x)}{\omega - \xi_0(\mathbf{k}) - \xi'(\mathbf{k}) - \frac{|\Delta(\mathbf{k})|^2}{\omega + \xi_0(\mathbf{k})}} \tag{4.7}$$

where x is the doping, or the net number of holes in a unit cell, $\xi_0(\mathbf{k}) = -2t(x)(\cos k_x + \cos k_y)$, $\xi'(\mathbf{k}) = -4t' \cos k_x \cos k_y - 2t''(\cos 2k_x + \cos 2k_y) - \mu_p$, $\Delta(\mathbf{k}) = -\Delta_0(\cos k_x - \cos k_y)$. The renormalization of the hopping parameters are: $t(x) = g_t(x)t_0 + \frac{3}{8} g_s(x) J_H \chi$, $t'(x) = g_t(x) t'_0$, $t''(x) = g_t(x) t''_0$, $\chi_{ij} = \langle c^{\dagger}_{i\sigma} c_{j\sigma} \rangle$. g_t, g_s are referred to as the Gutzwiller functions [33], and are given here by $g_t = \frac{2x}{1+x}$, $g_s = \frac{4}{(1+x)^2}$. μ_p is a chemical potential

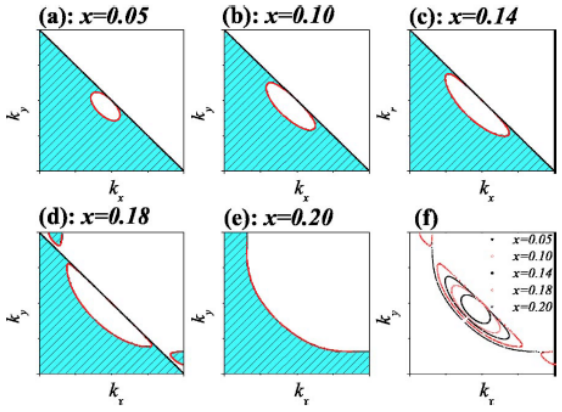

Figure 4.1: The Fermi surface, incluing zeros and poles of YRZ Green's function in reference [82]. Only a quarter of the Brillouin zone($k_x \in [0,\pi]$, $k_y \in [0,\pi]$) is showed, the Fermi surface is symmetric under $k_x \to -k_x$ and $k_y \to -k_y$. We see that the Fermi pocket grows as the doping increase, and eventually becomes a closed surface at $x = 0.20$. The parameters use here are: $\chi = 0.338t_0$, $J = 1/3t_0$, $t_0^{'} = -0.3t_0$, $t_0^{''} = 0.2t_0$.

term that is determined by the doping through Luttinger sum rule (LSR) [67]:

$$\rho = \frac{1}{2\pi^2} \int_{G(\mathbf{k},0)>0} d^2\mathbf{k} \ , \tag{4.8}$$

which states that the density of electrons is proportional to the area in momentum space where the zero-frequency Green's function $G(\mathbf{k},0) > 0$, and the boundary is determined by the lines of the zeros and poles of $G(\mathbf{k},0)$. At hole doping $x = 0$, by setting $\mu_p = 0$, the Green's function has only zeros, along the lines $k_x \pm k_y = \pm\pi$. At none zero doping, $G(\mathbf{k},0)$ begins to have poles, and as a result hole pockets begins to appear. Fig 4.1 shows the Fermi surface structrure created by a YRZ Green's function, for different doping. Shaded is the region where $G(\mathbf{k},0) > 0$. The line from $(\pi,0)$ to $(0,\pi)$ is the line that $G(\mathbf{k},0)$ is zero and the red line represents the poles.

This Green's function is not a solution for any tight binding Hamiltonian, but by introducing auxiliary fermions, the self-energy term $\Sigma(\mathbf{k}) = \frac{|\Delta(\mathbf{k})|^2}{\omega+\xi_0(\mathbf{k})}$ can be understood as the interaction between electrons and auxiliary fermions.

4.2.2 An auxilary fermion model

We can formally obtain a YRZ Green's function as a result of an action in the form:

$$S[\nu] = \int d\omega \nu_k (\omega - \xi_0 - \xi^{'} - \frac{|\Delta|^2}{\omega + \xi_0}) \bar{\nu}_k, \tag{4.9}$$

where ν_k are Grassman variables to represent the fermionic field. We have neglected the superconducting gap, which is much smaller than all other parameters we consider. We will also concentrate below on the low temperature limit, $T \to 0$. Written explicitly in a temporal representation:

$$\begin{aligned} S[\nu] &= \frac{1}{2\pi} \int d\tau \sum_k \nu_k(\tau)(i\partial_\tau - \xi_0 - \xi^{'}) \bar{\nu}_k(\tau) \\ &- \frac{1}{4\pi^2} \int d\tau_1 d\tau_2 \sum_k \nu_k(\tau_1) \bar{\nu}_k(\tau_2) h(\tau_2 - \tau_1) \end{aligned} \tag{4.10}$$

we see that this action is not local in time, with a response kernel:

$$h(\tau) = \int d\omega \frac{\Delta_k}{\omega + \xi_0} e^{i\omega\tau}. \tag{4.11}$$

In the RIXS procedure, when the X-ray knocks a core electron out and creates a core-hole, it generates a core-hole potential that exists for a certain time (decided by the core-hole life time), then the potential disappears, this quenching like process is often modeled as turning on a point interaction potential at time 0 to τ_0 [69], the action including a core-hole would be $S_{corehole} = S[\nu] + \int_0^{\tau_0} U_c \nu_r \bar{\nu}_r$. At this stage, the non-locality nature of the action in Eq (4.9) makes it awkward to analyze. To deal with this problem, we consider adding an auxiliary fermion, and write an action in

this form:

$$\begin{aligned} S[\nu,\psi] &= \int d\tau \sum_k [\nu_k(\tau)(i\partial_\tau - \xi_0 - \xi^{'})\bar{\nu}_k(\tau) \\ &+ \psi_k(\tau)(i\partial_\tau + \xi_0)\bar{\psi}_k(\tau) \\ &+ \Delta\nu_k(\tau)\bar{\psi}_{-k}(\tau) + \bar{\Delta}\psi_{-k}(\tau)\bar{\nu}_k(\tau)] \end{aligned} \tag{4.12}$$

where ν_k and ψ_k are Grassmann numbers, and ψ represents an auxiliary field. Notice that $\xi_0(-\mathbf{k}) = \xi_0(\mathbf{k})$, integrating out the ψ field would yield the action in Eq (4.9). The tight binding Hamiltonian for this action, including spin index is:

$$\begin{aligned} H_{cd} &= -\sum_{ij,\sigma=\uparrow,\downarrow} t^c_{ij} c^\dagger_{i\sigma} c_{j\sigma} - \sum_{ij,\sigma=\uparrow,\downarrow} t^d_{ij} d^\dagger_{i\sigma} d_{j\sigma} \\ &+ \sum_{ij,\sigma=\uparrow,\downarrow} \Delta_{ij} c^\dagger_{i\sigma} d_{j\sigma} + h.c. \end{aligned} \tag{4.13}$$

where the $d_{i\sigma}$ particles are the auxiliary fermions. The hopping and pairing parameters are: $t^c_{i,i\pm\hat{x}} = t^c_{i,i\pm\hat{y}} = t$, $t^c_{i,i\pm\hat{x}\pm\hat{y}} = t^{'}$, $t^c_{i,i\pm 2\hat{x}} = t^c_{i,i\pm 2\hat{y}} = t^{''}$, $t^c_{i,i} = -\mu_p$, $t^d_{i,i\pm\hat{x}} = t^d_{i,i\pm\hat{y}} = -t$, $\Delta_{i,i+\hat{x}} = -\Delta_{i,i+\hat{y}} = \Delta$. t^c_{ij} contains a nearest neighbor hopping, next nearest neighbor hopping and a chemical potential term, and t^d_{ij} only contains a nearest neighbor hopping term, which differs from that in t^c_{ij} by a sign.

With this Hamiltonian, we can now look at the RIXS spectrum with the determinant method. For the RIXS intensity with photon energy and momentum transfer $\omega \to \omega - \Delta\omega$, $\mathbf{q} \to \mathbf{q} + \mathbf{Q}$, the essential task is to calculate:

$$S^{mn}_{\rho\sigma\mu\nu} = \langle e^{\mathrm{i}H\tau} c_{n\rho} e^{-\mathrm{i}H_n\tau} c^\dagger_{n\sigma} e^{\mathrm{i}Hs} c_{m\mu} e^{\mathrm{i}H_m t} c^\dagger_{m\nu} e^{-\mathrm{i}H(t+s)} \rangle \tag{4.14}$$

$H_{m(n)}$ is the intermediate Hamiltonian with the presence of a core-hole at site $m(n)$. Usually it is assumed that core-hole gives an attractive point potential: $H_m = H_{cd} +$

$\sum_\sigma U_c c^\dagger_{m\sigma} c_{m\sigma}$, but in our case there are also auxiliary fermions, we could also try adding a core-hole potential for ds: $H_m = H_{cd} + \sum_\sigma U_c c^\dagger_{m\sigma} c_{m\sigma} + \sum_\sigma U_d d^\dagger_{m\sigma} d_{m\sigma}$. We found the latter gives a better agreement to the experiments. Γ is the inverse of core-hole life time, it represents the effects that are not taken into account, like decaying through phonon emission, here we take $\Gamma \sim 0.2eV$.

4.2.3 Plots and discussion

Fig 4.2 shows the comparison between a theoretical calculation using this method and experimental data for Bi-2201($Bi_2Sr_2CuO_{6+x}$) reported in [19], at doping $p = 0.12$. Quantitative agreement with the experiments was reported using the itinerant quasiparticle approach in [9] and with YRZ in [20], here we show how the combined approach improves on the YRZ result. With the experimental setup, there are 57% SF and 43% NSF in the π channel. Although the RIXS signal is commonly interpreted as a magnetic response [50, 18, 23], we demonstrate that by using a simple tight binding Hamiltonian, we can quantitatively understand the RIXS spectrum for various momentum transfer.

In Fig 4.3, we show the intensity along some high symmetry lines. Similar to the conclusions in [20, 32], we see that along the nodal $(1, 1)$ direction the RIXS spectrum becomes more diffused and less sensitive to momentum transfer, which is hard to understand from a magnon point of view.

Furthermore, we point out that in the case where $U_c = U_d = 0$, i.e. no core-hole, the result is similar to the dynamic susceptibility that is calculated in [39]. In Eq (3.35), if we assume Γ is larger than other energy scales of the system, the denominator $E_n - E_i - \omega + i\Gamma$ can be approximated by a constant $R(\omega, \Gamma)$ for any $|n\rangle$, and the intensity is written as the Fourier transform of the 4-point function:

$$I_{mn}(t) = R(\omega, \Gamma)\chi_{\tau\sigma}\chi_{\mu\nu}\langle \rho_{n\tau\sigma}(t)\rho^\dagger_{m\mu\nu}(0)\rangle \tag{4.15}$$

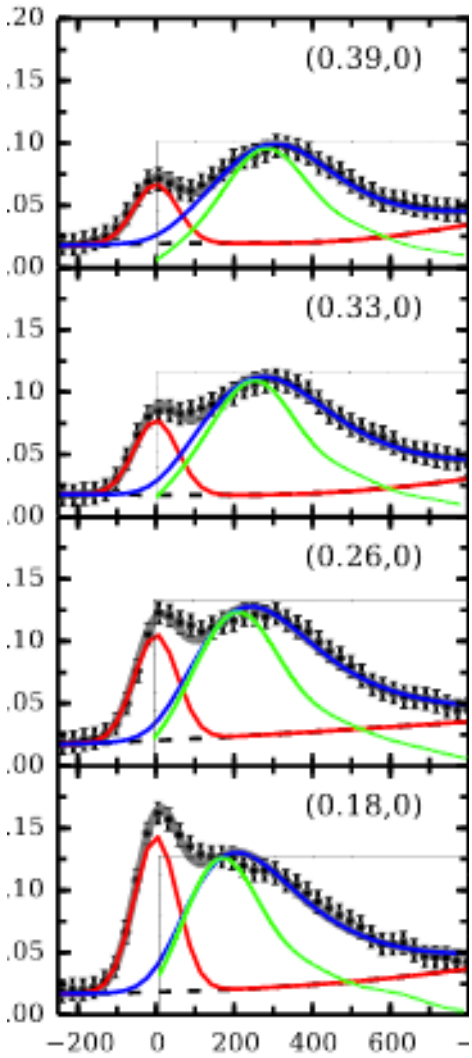

Figure 4.2: The theoretical calculation and experimental data for the Bi-2201 sample, for momentum transfer in $(1, 0)$ direction. The green curves are theoretical calculation with core-hole potential $U_c = U_d = -3eV$. Blue curves are anti-symmetrized Lorentzian capturing the magnetic scattering from [19]. Red lines are the elastic peak.

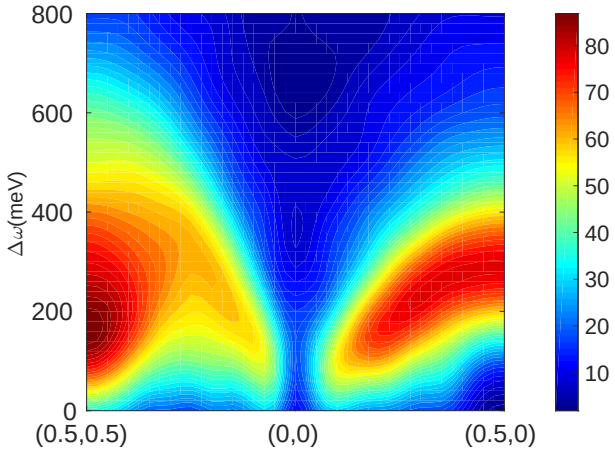

Figure 4.3: RIXS intensity along $(1,1)$ and $(1,0)$ direction. Only along the antinodal $(1,0)$ direction there exists a clear peak. The intensity along (1,1) direction can not be properly described by magnons.

where $\rho_{n\tau\sigma} = c^{\dagger}_{n\tau}c_{n\sigma}$, and we have used that $\delta(E) = \frac{1}{2\pi}\int_{-\infty}^{\infty} e^{-iEt}dt$. In [39] the irreduceble part of the magnetic susceptbility is defined as:

$$\chi^{irr}(R_{nm}, t) = \langle(\rho_{n\uparrow\uparrow}(t) - \rho_{n\downarrow\downarrow}(t))(\rho_{m\uparrow\uparrow}(0) - \rho_{m\downarrow\downarrow}(0))\rangle \tag{4.16}$$

Eq (4.15) and (4.16) are both a density-density correlation functions of the system, and have similar behavior.

We proceed to calculate the zero core-hole RIXS intensity for our tight binding model. We first solve the Hamiltonian in Eq (4.13), using a linear transformation:

$$\begin{aligned} c_{k\sigma} &= \cos\theta_k b_{k\sigma} + \sin\theta_k f_{k\sigma} \\ d_{k\sigma} &= -\sin\theta_k b_{k\sigma} + \cos\theta_k f_{k\sigma} \end{aligned} \tag{4.17}$$

$b_{k\sigma}$ and $f_{k\sigma}$ are quasi-particles, $\tan 2\theta_k = \frac{2\Delta(k)}{2\xi_0+\xi'(k)}$, the effective Hamiltonian is then just:

$$H_{bf} = \sum_k \epsilon_1(k) b^{\dagger}_k b_k + \epsilon_2(k) f^{\dagger}_k f_k \tag{4.18}$$

the energy eigenvalues are: $\epsilon_{1,2}(k) = \frac{\xi'}{2} \pm \sqrt{(\frac{2\xi_0+\xi'}{2})^2 + |\Delta(k)|^2}$. With this, Eq (3.51) can be written in terms of $b_{k\sigma}$ and $f_{k\sigma}$, which are the true excitations of the model:

$$\begin{aligned} \mathcal{F}_f &= \sum_k \langle f|(\cos\theta_k b_{k\rho} + \sin\theta_k f_{k\rho}) \sum_n \frac{|n\rangle\langle n|}{E_n - E_i - \omega + i\Gamma} \\ &\times \quad (\sin\theta_{k+Q} b^{\dagger}_{k+Q\sigma} + \cos\theta_{k+Q} f^{\dagger}_{k+Q\sigma})|i\rangle \end{aligned} \tag{4.19}$$

The final state $|f\rangle$ would have a particle-hole excitation, with four possible excitation patterns: $b_k b^{\dagger}_{k+Q}$, $b_k f^{\dagger}_{k+Q}$, $f_k b^{\dagger}_{k+Q}$, or $f_k f^{\dagger}_{k+Q}$, the total RIXS intensity would be the summation of $|A_\nu|^2$ over all possible final states $|f\rangle$.

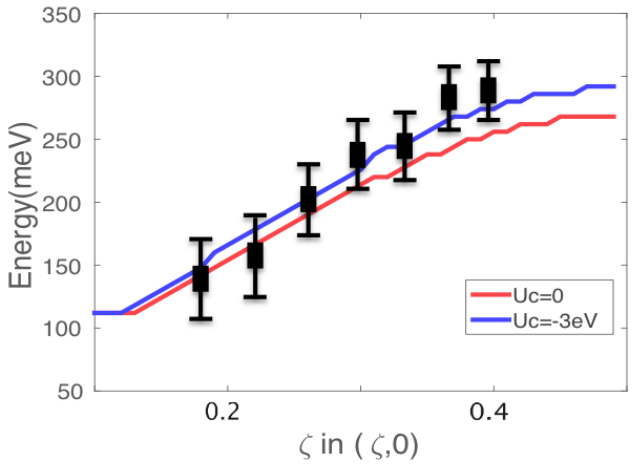

Figure 4.4: The dispersion of the energy of the paramagnon mode in Bi-2201 along $(\zeta, 0)$. The red line shows the zero core-hole calculation that gives a similar result as in [20]. The blue line shows the peak position using our calculation of spin-flip contribution with a core-hole potential $U_c = U_d = -3eV$. Experimental data reported in [20] are noted by black squares.

To argue the necessity of taking into account the core-hole interaction in the system, we show In Fig 4.4 the effect of adding a core hole, by comparing the results from Eq (4.4) and Eq (4.19), which gives results similar to the RPA calculation in [20]. We find that the core hole will push the peaks to higher energy transfer, this effect is more significant at large momentum transfer. While the RPA calculation catches the essential figure of the experiment, the inclusion of a core-hole significantly improves the agreement with the experiment. This effect can be understood as we go to first order contribution of a core-hole potential with the form $V_r = U_c \sum_\sigma c^\dagger_{r\sigma} c_{r\sigma}$ in (3.36), this term would contribute as:

$$\begin{aligned} \mathcal{F}^1_f &= U_c R(\omega, \Gamma) \sum_m e^{i\mathbf{Q}\mathbf{R}_m} \\ &\times \chi_{\rho\sigma} \langle f | d_{m\rho} (d^\dagger_{m\uparrow} d_{m\uparrow} + d^\dagger_{m\downarrow} d_{m\downarrow}) d^\dagger_m | i \rangle \end{aligned} \tag{4.20}$$

This means the final state would have two pairs of quasi particle-hole excitations, with total momentum added to $\mathbf{Q}$ and total energy $\Delta\omega$, while in the no core-hole

case, the excitations are one pair of quasi particle-hole, with the same total energy and momentum, the excitations are mostly close to Fermi surface. The core-hole allows the individual excitations to explore a larger phase space, further away from the Fermi surface, and thus the excitation energies are higher, and the peak moves to the right. This effect is much harder to analyze quantitatively, but the determinant method allows us to calculate it numerically.

In this section, we studied the non-equilibrium dynamics associated with the YRZ ansatz in the presence of X-ray absorption by introducing a phenomenological tight-binding Hamiltonian model involving auxiliary fermions. This approach allows us to resolve the non-locality of the action in time and is particularly useful when dealing with the core-hole introduced in RIXS experiments. We compare a theoretical computation based on our model with experiments on Bi-2201, and show that the core-hole moves dispersion peaks to higher energy in the $(1, 0)$ direction, giving a better agreement with the experimental data. In addition we observe that in the $(1, 1)$ direction the signal is more diffused and a well-defined magnon peak is absent.

4.3 RIXS intensity and detuning in YBCO samples

4.3.1 Introduction to YBCO

YBCO is a family of high-temperature superconductors that has been studied intensively. $YBa_2Cu_3O_7$ was the first discovered cuprate to have a $T_c \sim 93K$, above the boiling point of liquid nitrogen [81]. The discovery of YBCO led to the rapid development of several other high Tc superconductors, and started a new era in material science.

Despite the technological and scientific importance of YBCO, little is known about their overall quasi-particle band structures. Although density functional theory predicts quasi-particle dispersion near the Fermi surface reasonably well, it cannot re-

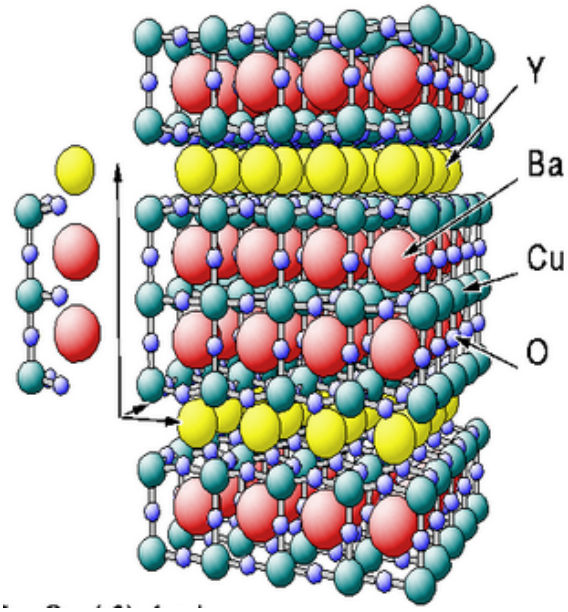

Figure 4.5: Structure of $YBCO_7$

liably capture the effect of electron-electron correlations, and thus largely overestimates the excitation energies near the top of the band [84]. On the experimental side, traditionally used band structure probes, such as angle-resolved photoemission spectroscopy (ARPES) and quantum oscillation measurements [77] probe excitations mostly in the vicinity of the Fermi surface, and provide little information on the higher energy part of the band.

In contrast, RIXS study of transition metal oxides provides a momentum-resolved access to various electronic, magnetic and phononic excitations in a large energy range with an unprecedented sensitivity. This can help us with the understanding of YBCO band structure.

4.3.2 Calculation of RIXS intensity

We use a tight-binding Hamiltonian same as in Eq (3.58), with parameters: $(t_0, t_1, t_2, t_3) = (-105,\ 29,\ -25,\ 4)$meV. Here we compare our calculation with the experimental measure of [57]. Fig 4.6 shows the intensity for different polariza-

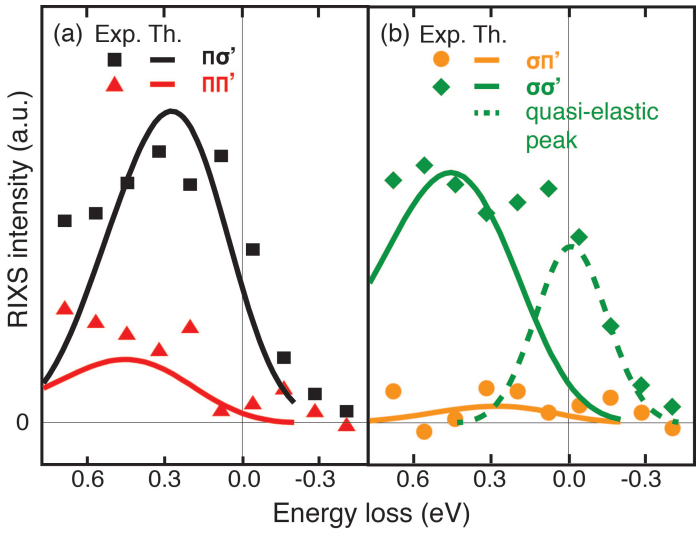

Figure 4.6: Polarization resolved RIXS spectra with incoming π (a) and σ (b) polarization on overdoped YBCO + Ca. Symbols (full lines) denote experimental (theoretical) data, whereas the dashed line in (b) corresponds to Gaussian fit to the quasi-elastic part of the $\sigma\sigma'$ channel. RIXS intensity is dominated by SF/NSF processes in the scattering geometry of (a)/(b), respectively.

tions for overdoped YBCO+Ca. We used parameters: $\mathbf{q}_{\parallel} = 2\pi\,(0.37, 0)$, $U_c = 1\,\mathrm{eV}$, $\Gamma = 250\,\mathrm{meV}$, energy resolution 95 meV HWHM, lattice size 22×22.

Experiment has also studied the dependence of RIXS intensity on incoming photon energy on $YBCO_{6+x}$. RIXS study of several $YBCO_{6+x}$ samples from the underdoped to the overdoped regime were performed, with π incoming and mixed outgoing polarization. We use ω to denote the energy shift of the photon from the maximum intensity of X-ray absorption experiment. In order to investigate the effect of the incoming photon energy on the RIXS signal, ω was tuned to be $(0, 125, 250, 375)\,\mathrm{meV}$, as shown in Fig. 4.7 (a). We find a peak near 350 meV, as well as a tail of high-energy *dd* transitions, see Fig. 4.7 (b). Up to an overall normalization factor, theoretical spectra (full lines) fit the experimental data reliably, as shown in Figs. 4.7 (c-e). Both the peak positions and the widths are reproduced for a large range of detunings: underdoped $YBCO_{6.55}$ ($p \sim 0.114$) and $YBCO_{6.79}$ ($p \sim 0.142$), optimally doped $YBCO_{6.99}$ ($p \sim 0.189$) and overdoped and YBCO + Ca ($p \sim 0.21$). Our model fails

in case of the almost undoped antiferromagnetic sample, $YBCO_{6.10}$. This is consistent with our expectations that quasi-particle theory should be only reliable on the overdoped side, and should not be applicable in the antiferromagnetic phase, where strong interactions lead to the absence of low-lying electronic excitations.

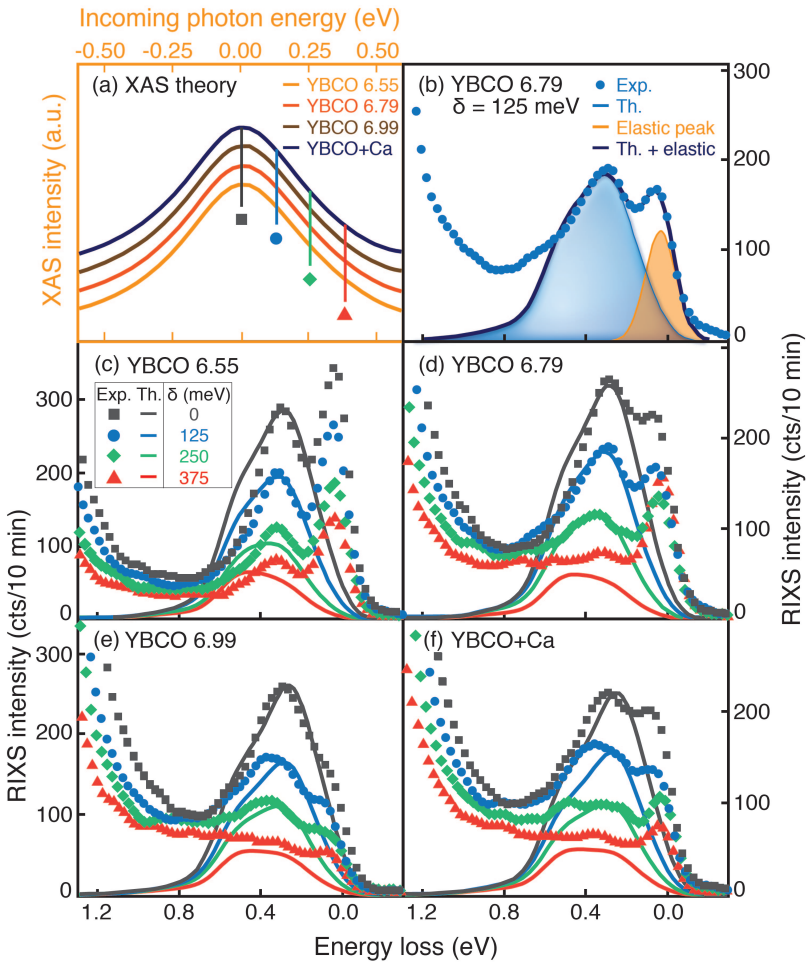

Figure 4.7: RIXS spectra of YBCO measured with π incoming polarization. The incoming photon energy is detuned $\delta = (0, 125, 250, 375)$ meV away from the XAS maximum, shown in (a). (b) The experimental RIXS data shows pronounced quasi-elastic peaks together with another peak near 300 meV, fit by our theoretical model, as well as a high-energy tail of *dd* excitaitons. (c-e) RIXS spectra at different dopings and detunings, with experimental (theoretical) data denoted by symbols (full lines).

CHAPTER V

Superconducting pairing in RIXS experiments

In Chap IV we used the determinant method to study cuprate systems. In standard BCS theory of superconductivity, the gap is present after introducing a superconducting pairing term. However, we did not consider any superconducting pairing in our models, although they are superconducting systems, based on the belief that the gap is in general small in such systems, and won't make too much of a difference. In this chapter, we will start to learn the effect of this kind of pairing, and see how it can affect the result of RIXS intensity. In Sec 5.1 we look at the CLBLCO sample and in Sec 5.2 we look at the $p + ip$ superconductor.

5.1 D-wave pairing in CLBLCO system

5.1.1 Background

The RIXS experiment in [23] is performed for $(Ca_xLa_{1-x})(Ba_{1.75-x}La_{0.25+x})Cu_3O_y$ sample, x controls the family and y controls the doping. In most of the studies on high-Tc superconductors, there are many different parameters that change dramatically simultaneously, which makes it hard to understand how the properties of the material depend on a certain parameter. In CLBLCO, we can change x or y separately, and see the effect. In particular, changing x only affects the super-exchange between Cu and O atoms, so that we can learn about how some crucial properties,

like the transition temperature, depend on the super-exchange. The structure, phase diagram and the lattice constant of the material are shown it the figure.

Underdoped(UD), medium doped(MD) and optimally doped(OD) samples are studied. Changing x from 0.1 to 0.4 would cause the T_c to increase ˜30%. T_N $T_g$and T_c are the Neel, spin-glass and superconducting transition temperature. The phase diagram for different x can be scaled into one plot [5].

5.1.2 Experiment

X-ray absorption spectroscopy(XAS) data at Cu L edge is shown it Fig 5.2, for $x = 0.1$ and $x = 0.4$ samples at different dopings. The electric field is polarized along the c-axis (with a 10° misalignment from axis). There are three peaks: peak A is almost at the same energy for all samples(only $x = 0.4$ UD is slightly off); peak B is ˜2eV higher than peak A and depends largely on doping; C peak is interpreted as the charge transfer excitations to the upper Hubbard band. The total number of holes in a unit cell including chains and planes, h, and y are estimated in this way: for the two OD samples, y is estimated from the critical temperature, and then h calculated from the relation $h = y - 6.25$; for other samples h is estimated from the relative weight of peak A and B, $B/(A + B)$, and then y calculated using the same relation.

The RIXS experiment chose the A peak as the energy of incoming X-ray, which is close to the commonly used energy for Cu L edge. The RIXS setup is shown in the figure, incoming and outgoing photons are labeled as k_i and k_f, the angle between the extension of k_i and k_f is called the two-theta angle, it is fixed to be 130°, so the momentum transfer $\mathbf{Q}$, is fixed. In order to change the momentum transfer in the parallel plane, one rotates the sample to change θ_i.

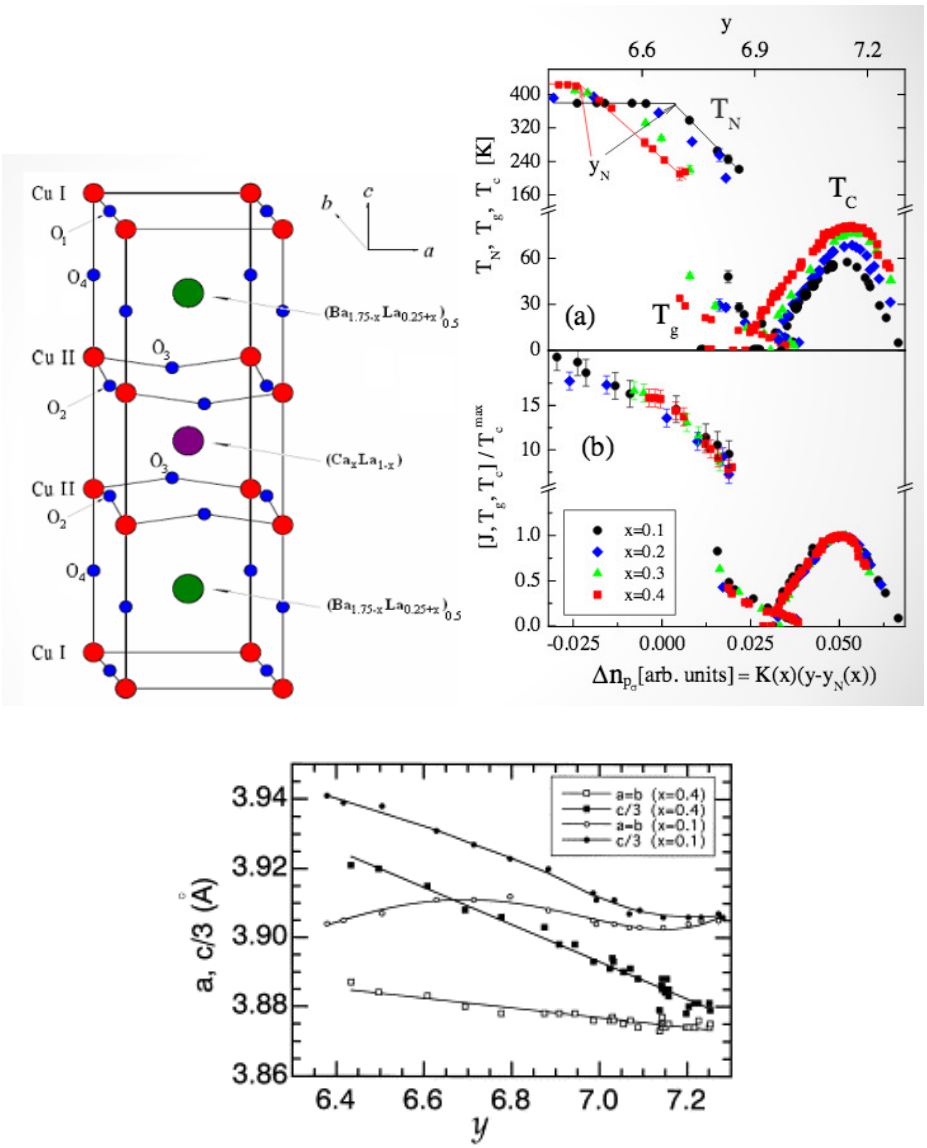

Figure 5.1: The lattice structure of CLBLCO(upper left), and it's phase diagram for several x values as a function of y(upper right). The lattice constant is shown in the lower figure [45], for different x and y values.

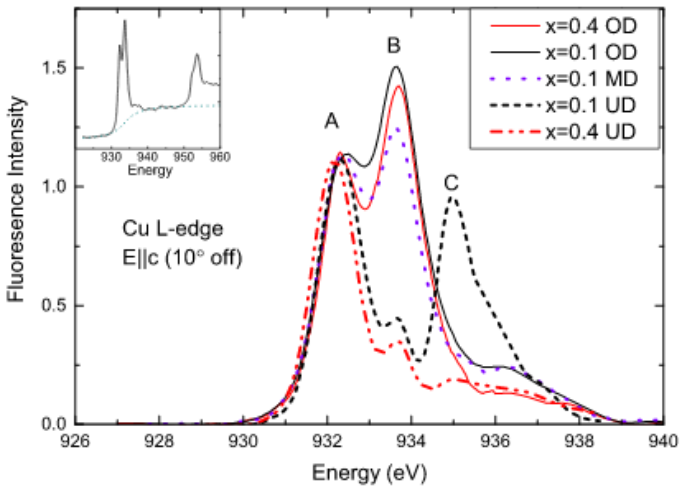

Sample	$B/(A+B)$	h	y
x=0.4 OD	0.652 ± 0.01	0.86	7.11
x=0.1 OD	0.657 ± 0.01	0.81	7.06
x=0.1 MD	0.561 ± 0.02	0.69	6.94
x=0.1 UD	0.055 ± 0.02	0.07	6.32
x=0.4 UD	0.067 ± 0.01	0.09	6.34

Figure 5.2: XAS experiment of CLBLCO(upper), three peaks appear around Cu L-edge. And the doping(lower) determined from the experiment

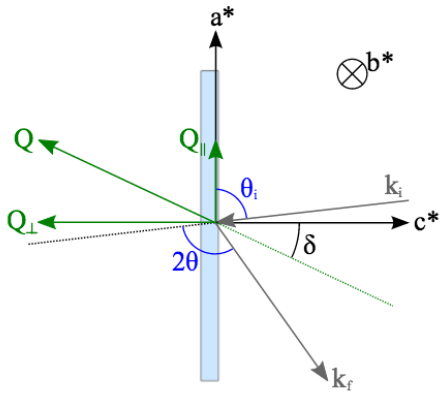

In the experiment the momentum transfer $Q = 2\pi(q, 0)$ is measured, the q values are $(0.42, 0.36, 0.28, 0.2, 0.11)$, the corresponding θ_i are $(117.4°, 107.8°, 96.9°, 87.2°, 77°)$, The lattice constant a is taken to be $3.9\mathring{A}$ for all the samples(2% error).

5.1.3 Theoretical Calculation

5.1.3.1 OD samples

Fig 5.3 show the experimental data and the theoretical calculation. The band structure parameters for $x = 0.1$ and $x = 0.4$ are:

i	$t_i^{x=0.1}$	$t_i^{x=0.4}$	$\eta_i(\mathbf{k})$
0	0.134	0.152	1
1	0.110	0.125	$-2\left[\cos\left(k_x a\right)+\cos\left(k_y a\right)\right]$
2	-0.032	-0.036	$-4\left[\cos\left(k_x a\right)\cos\left(k_y a\right)\right]$
3	0.016	0.018	$-2\left[\cos\left(2k_x a\right)+\cos\left(2k_y a\right)\right]$

The experiment[23] used π polarized spectrum, the weight of the spin-flip signal for the 5 different momentum transfer are $(84\%, 64\%, 46\%, 35\%, 28\%)$. For the theoretical calculation, lattice size 16 by 16, $\Gamma = 0.3eV$, $U_c = -1eV$, doping is $p = 0.24$ for both optimally doped samples.

5.1.3.2 Doping dependence

Here we compare the $x = 0.1$ $p = 0.24$(OD) and $p = 0.16$(MD) signal. Figure shows $q = 0.27$(left) and $q = 0.33$(right), blue curves are MD sample, and red curves are OD sample. The dependence on doping is small.

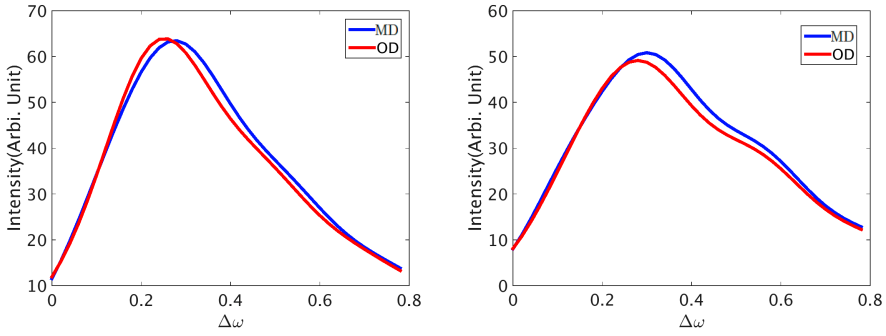

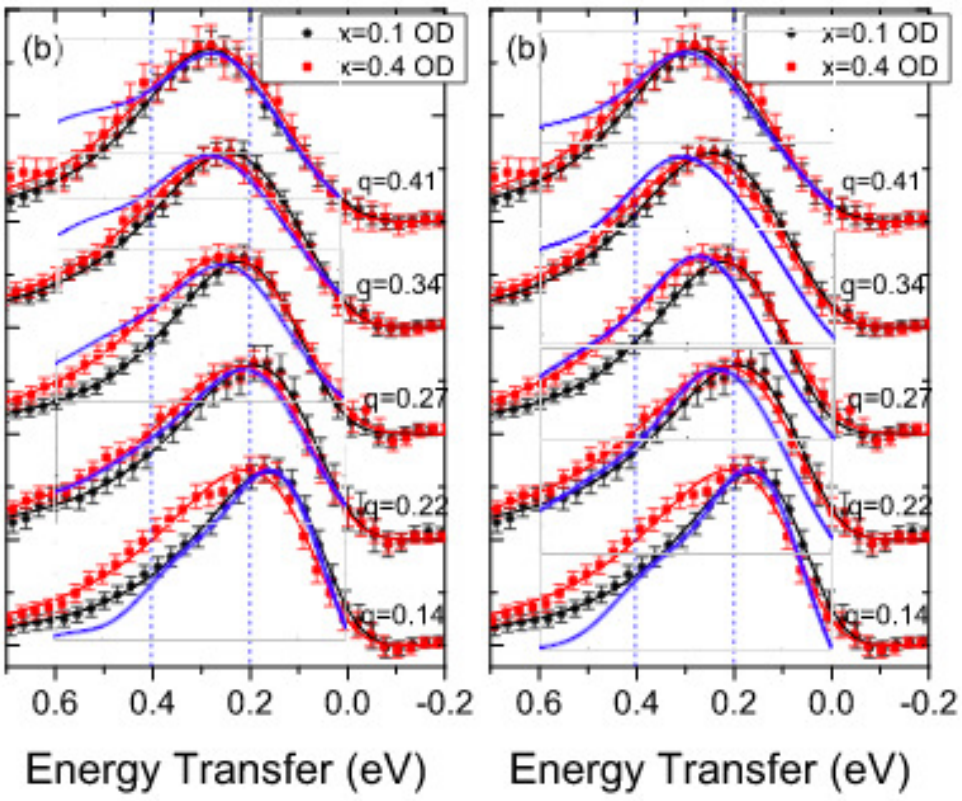

Figure 5.3: The fit to experimental curves. The black and red curves are experimental data[23] for $x = 0.1$ and $x = 0.4$ samples. The blue curves in left(right) plot shows the theoretical calculation for $x = 0.1(0.4)$ samples.

5.1.3.3 D-wave pairing

The Hamiltonian we used in the previous section is a simple band model, $H = \sum_{k\sigma} \epsilon_k d^\dagger_{k\sigma} d_{k\sigma}$, now we consider what happens if we have a superconducting pairing term: $H^d = \sum_{k\sigma} \epsilon_k d^\dagger_{k\sigma} d_{k\sigma} + \Delta_k d_{k\uparrow} d_{-k\downarrow} + h.c.$, where $\Delta_k = \Delta(\cos k_x - \cos k_y)$. In this particular case (up spin only couples to down spin in the pairing term), the Hamiltonian can still fit into the general $H = \sum_{ij} h_{ij} c^\dagger_i c_j$ form, by definding: $c_{k\uparrow} = d_{k\uparrow}$, $c_{k\downarrow} = d^\dagger_{k\downarrow}$. Then the Hamiltonian, with a core-hole at site m, becomes:

$$H^d_m = \sum_k \epsilon_k c^\dagger_{k\uparrow} c_{k\uparrow} + \epsilon_k (1 - c^\dagger_{k\downarrow} c_{k\downarrow}) + U_c c^\dagger_{m\uparrow} c_{m\uparrow} + U_c (1 - c^\dagger_{m\downarrow} c_{m\downarrow}) - \Delta_k c^\dagger_{k\downarrow} c_{-k\uparrow} + h.c. \quad (5.1)$$

Then we still want to calculate:

$$S^{mn}_{\rho\sigma} = \langle e^{\mathrm{i}H\tau} d_{n\rho} e^{-\mathrm{i}H_n\tau} d^\dagger_{n\rho} e^{\mathrm{i}Hs} d_{m\sigma} e^{\mathrm{i}H_m t} d^\dagger_{m\sigma} e^{-\mathrm{i}H(t+s)} \rangle \quad (5.2)$$

using Eq (4.5).

For the spin-flip channel, we want $S_{\uparrow\uparrow} + S_{\downarrow\downarrow} - S_{\uparrow\downarrow} - S_{\downarrow\uparrow}$, for the non-spin-flip channel we want $S_{\uparrow\uparrow} + S_{\downarrow\downarrow} + S_{\uparrow\downarrow} + S_{\downarrow\uparrow}$. But now we have to treat $S_{\uparrow\uparrow}$, $S_{\downarrow\downarrow}$ and $S_{\uparrow\downarrow}$, $S_{\downarrow\uparrow}$ seperately. If $\rho = \sigma$, we have $S^{mn}_{\rho\sigma} = \langle e^{\mathrm{i}H\tau} c_{n\rho} e^{-\mathrm{i}H_n\tau} c^\dagger_{n\rho} e^{\mathrm{i}Hs} c_{m\sigma} e^{\mathrm{i}H_m t} c^\dagger_{m\sigma} e^{-\mathrm{i}H(t+s)} \rangle$, we can use eq(4.5), and just change H correspondingly. For the down spin part, H transfers to $-H$, and also there's a numerical factor. The numerical factor mostly cancels since when calculating S, but when there's a core-hole potential, it contributes a phase factor of $e^{i(t-\tau)U_C}$.

If $\rho \neq \sigma$, then the situation is more complicated. we have to calculate:

$$\tilde{S}^{mn}_{\rho\sigma} = \langle e^{\mathrm{i}H\tau} c_{n\rho} e^{-\mathrm{i}H_n\tau} c^\dagger_{n\rho} e^{\mathrm{i}Hs} c^\dagger_{m\sigma} e^{\mathrm{i}H_m t} c_{m\sigma} e^{-\mathrm{i}H(t+s)} \rangle \quad (5.3)$$

and here we derive the formula to calculate Eq (5.3). We denote $X_1 = i(\tau - t - s)H_0$,

$X_2 = iH_m t$, $X_3 = iH_0 s$, $X_4 = -iH_n \tau$, and use composite subscript α, β , γ, δ; eg. $\alpha = n, \rho$. First we move the c and $c^\dagger$ to the left by using $e^X c_n^\dagger = (e^X)_{mn} c_m^\dagger e^X$ and $e^X c_n = (e^{-X})_{nm} c_m e^X$, we get:

$$\tilde{S}^{mn}_{\rho\sigma} = (e^{X_4})_{\beta'\beta}(e^{X_4}e^{X_3})_{\gamma'\gamma}(e^{-X_2}e^{-X_3}e^{-X_4})_{\delta\delta'}\mathrm{tr}[c_\alpha c^\dagger_\beta c^\dagger_\gamma c_\delta e^z]/\mathrm{tr}[e^{-\beta H}] \tag{5.4}$$

next we calculate $\mathrm{tr}[c_\alpha c^\dagger_\beta c^\dagger_\gamma c_\delta e^z]$. First we notice $c^\dagger_m c_n = \frac{\partial}{\partial \xi} e^{\xi M}|_{\xi=0}$, where $M = |m\rangle\langle n|$, then:

$$\begin{aligned}
\mathrm{tr}(c^\dagger_m c_n e^z) &= \frac{\partial}{\partial \xi}\mathrm{tr}(e^{\xi M}e^z) = \frac{\partial}{\partial \xi}\det(1 + e^{\xi M}e^z)|_{\xi=0} \\
&= \det(1 + e^{\xi M}e^z)\mathrm{tr}(\frac{1}{1 + e^{\xi M}e^z}Me^z)|_{\xi=0} \\
&= \det(1 + e^z)(\frac{e^z}{1 + e^z})_{mn}
\end{aligned}$$

and similar method gives:

$$\mathrm{tr}(c^\dagger_m c_n c^\dagger_p c_q e^z) = \det(1 + e^z)[(\frac{1}{1 + e^z})_{mq}(\frac{e^z}{1 + e^z})_{pn} + (\frac{1}{1 + e^z})_{mn}(\frac{1}{1 + e^z})_{pq}]$$

Combining the two results and using the fermion anti-commutational relation, we get:

$$\begin{aligned}
\tilde{S}^{mn}_{\rho\sigma} &= \det\,(F)e^{i(t-\tau)U_c}[\langle n\rho|(1 - N)^{-1}F^{-1}e^{-ih_n\tau}|n\rho\rangle \times \langle m\sigma|e^{-ih(\tau-t-s)}NF^{-1}e^{-ih_n\tau}e^{ihs}|m\sigma\rangle \\
&- \langle n\rho|(1 - N)F^{-1}e^{-ih_n\tau}e^{ihs}|m\sigma\rangle \times \langle m\sigma|e^{-ih(\tau-t-s)}NF^{-1}e^{-ih_n\tau}|n\rho\rangle]
\end{aligned} \tag{5.5}$$

Eq (4.5) and (5.5) only give $S_{\uparrow\uparrow}$ and $S_{\uparrow\downarrow}$. To find $S_{\downarrow\downarrow}$ and $S_{\downarrow\uparrow}$, notice that in the Hamiltonian (5.1) if we swap up and down spins it takes $\Delta \to -\Delta$, so we can do the

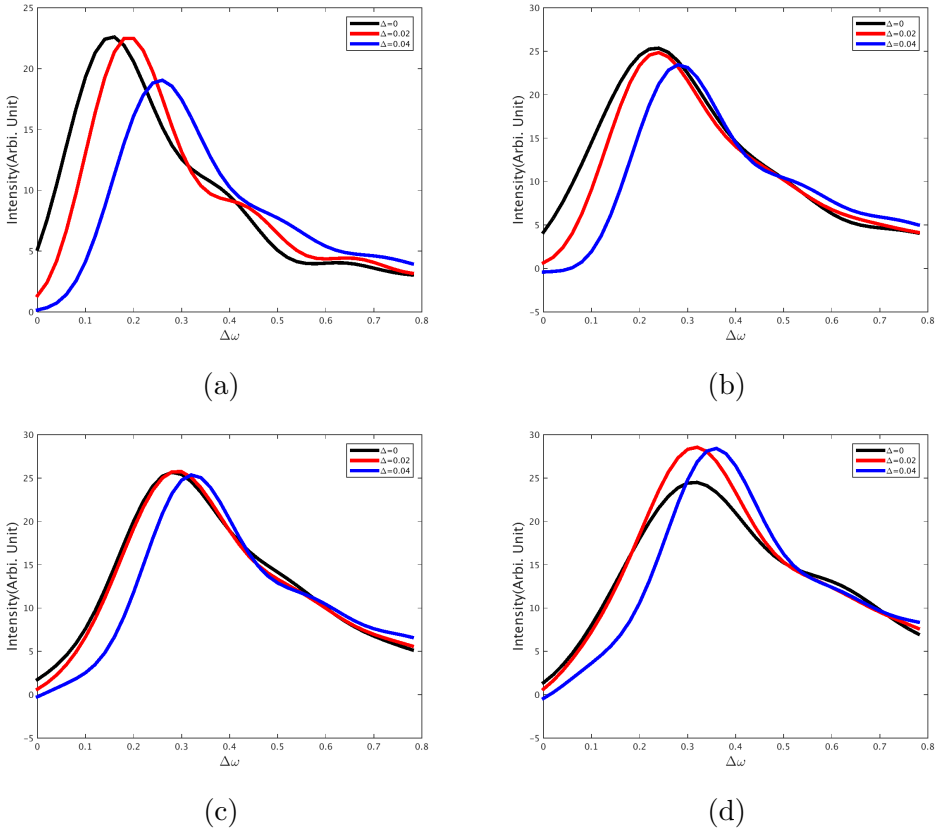

Figure 5.4: The effect of D-dave pairing term on RIXS signal in (1,0) direction. The plots are calculated for $x = 0.4$ OD sample, $q = 0.14, 0.22, 0.27, 0.34$ for (a) (b) (c) and (d). Black, red and blue curves are for $\Delta = 0, 0.02, 0.04$eV. The pairing term would shift the peak to higher energy and makes the peak sharper.

same calculation for $-\Delta$ and get the other two components.

We calculate for the $x = 0.4$ OD sample, with a pairing $\Delta = 0.02$ and $\Delta = 0.04$. Typical gap in the compound is $2\Delta \sim 0.04$eV [22]. The plots are shown in Fig 5.4. The momentum transfer are: $\mathbf{Q} = 2\pi q(1, 0)$, with $q = 0.14, 0.22, 0.27, 0.34$. In Fig 5.5 we also show a similar calculation done in (1,1) direction, $\mathbf{Q} = 2\pi q(1, 1)$, with same q values. We see that the peak is more diffused and have less dispersion.

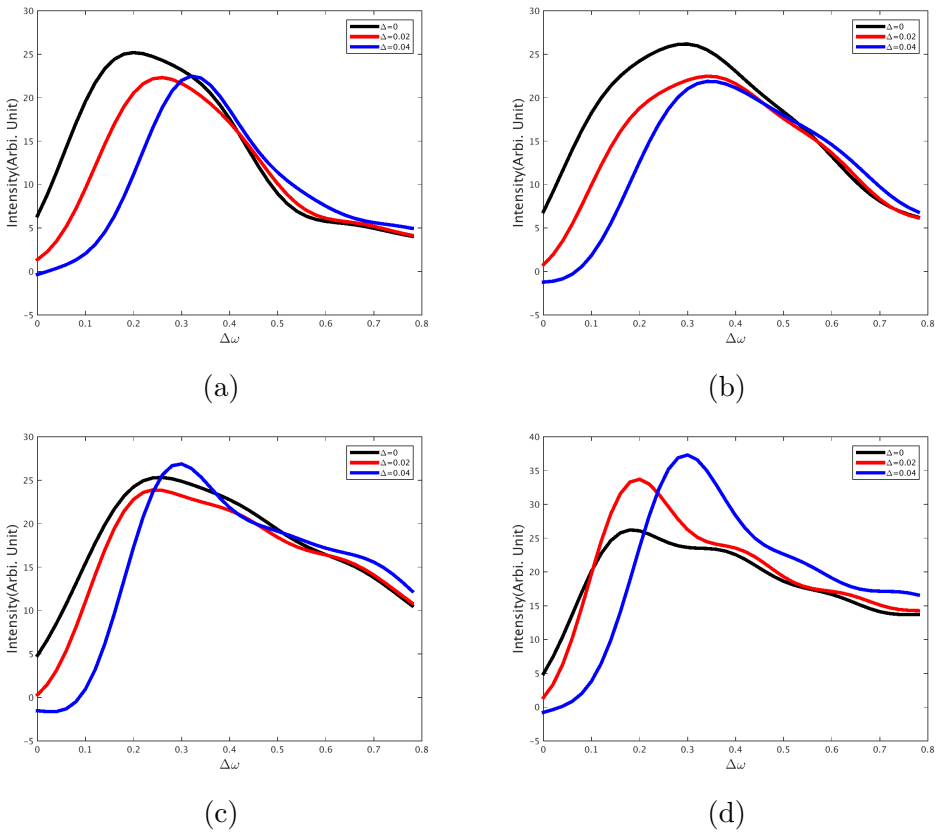

Figure 5.5: The calculation for the same sample in (1,1) direction, momentum transfer $\mathbf{Q} = 2\pi q(1,1)$, $q = 0.14, 0.22, 0.27, 0.34$ for (a), (b), (c) and (d). In this direction the peak is more diffused, but the qualitative effect of the pairing is similar

5.2 P+iP pairing and Majorana fermions

5.2.1 Model

In Sec 5.1 we considered a superconducting system with d-wave gap. However, that requires the pairing term to have specific form $\Delta_k(d_{k,\downarrow}d_{-k,\uparrow} + d_{k,\uparrow}d_{-k,\downarrow}) + h.c.$, so we can perform a simple transformation to use the determinant method. But this does not work in more general scenarios.

In this section, we will consider a general pairing term and demonstrate how changes in the presence of a gap may have an impact on RIXS measurements. To do so, we extend the method developed in [10] to describe RIXS response within a quasiparticle picture to include arbitrary pairing effects within a mean-field BCS formalism. Using the new method we show that superconducting pairing has an observable effect on the RIXS signal although the RIXS intensity is a result of an average over energy scales considerably larger than the superconducting gap. This sensitivity to pairing effects may add an important addition to the growing usefulness of the RIXS procedure in studying superconductivity related phenomena.

Recent studies of RIXS in the context of cuprates have largely considered cases of insulating phases [68, 71, 14, 71, 40]. However, RIXS experiments have been performed over a wide range of doping, including systems where itinerant electrons are present, and a description using tools developed for insulators may be insufficient. A different theoretical approach starts from the itinerant electrons, considering both direct [10] and indirect RIXS processes [8]. There the system is treated essentially as a single-band quasiparticle model. In addition, in refs [36, 32] the RIXS intensity has been calculated using the random phase approximation. In [32], it is also shown that contrary to the common interpretation, for $Bi-2212$ the magnon picture fails at a nodal direction and that a quasiparticle scenario may be an essential ingredient to understanding the RIXS data there.

In this section, we set out to examine the effect of superconducting pairing on the RIXS mechanism within a simple mean-field picture. We derive a general formula for the RIXS intensity for an arbitrary quadratic fermi Hamiltonian, with anomalous pairing Δ, as expressed in Eq (4.3) together with (5.12). This result generalizes the quasi-particle approach of [10], where the computation of RIXS spectra was performed using a model of non-interacting quasiparticles but including an interaction with a positively-charged core hole via exact determinant methods. This formalism allows us to compute the characteristics of the signal by numerically evaluating (5.12). This can be done for arbitrary band structures using relatively straightforward numerical means.

Throughout the section we will concentrate on p wave superconducting states. In particular, $p+ip$ superconductors are of great current interest. Such superconductors can support unpaired Majorana fermions at cores of (half quantum) vortices [3, 34], which obey non-Abelian statistics [37, 2]. Remarkably, we find that the RIXS signal is sensitive to the presence of a superconducting gap, although the gap scale Δ is quite small (about 5%) compared to the value of band parameters. In particular, going through the superconducting phase transition Δ acquires a non-zero value and we expect the RIXS spectra to experience a significant change.

To be concrete, we consider a minimal model for a $p+\mathrm{i}p$ superconductor. We use a two-dimensional, single band, spinless fermionic system, on a square lattice, with superconducting gap Δ. The mean field Hamiltonian is:

$$H = \sum_{i,j} h_{ij} d_i^\dagger d_j + \Delta_{ij} d_i d_j + \text{h.c.} \tag{5.6}$$

Following [51], we choose $h_{ii} = -\mu$, $h_{i,i+\hat{x}} = h_{i,i+\hat{y}} = -t_1$, $h_{i,i\pm\hat{x}\pm\hat{y}} = -t_2$, and for a $p_x + ip_y$ superconducting state, we take $\Delta_{i,i+\hat{x}} = \Delta$, $\Delta_{i,i+\hat{y}} = \mathrm{i}\Delta$, with $(\mu, t_1, t_2, \Delta) = (1.15, 0.8, 0.3, 0.05)t$, where $t \sim 0.2\text{eV}$.

In RIXS, photons with energy ω and momentum $\mathbf{q}$, are scattered, and the outgoing photons have energy $\omega - \Delta\omega$, and momentum $\mathbf{q} + \mathbf{Q}$. For spinless fermions, we write Eq (4.4) with no spin index:

$$S^{mn} = \langle e^{\mathrm{i}H\tau} d_n e^{-\mathrm{i}H_n\tau} d_n^\dagger e^{\mathrm{i}Hs} d_m e^{\mathrm{i}H_m t} d_m^\dagger e^{-\mathrm{i}H(t+s)} \rangle. \tag{5.7}$$

As long as the various stages in the time evolution are governed by quadratic fermi operators, (5.7) can be calculated by exact diagonalization methods. Consider fermions on a lattice with $N = L \times L$ sites. To handle arbitrary superconducting pairing, we represent the fermion creation and annihilation operators in terms of $2N$ Majorana fermions c_k defined as:

$$c_k = \begin{cases} d_k + d_k^\dagger & k = 1, 2, ...N \\ \mathrm{i}(d_{k-N}^\dagger - d_{k-N}) & k = N+1, N+2, ...2N \ , \end{cases} \tag{5.8}$$

and satisfying the relation $\{c_i, c_j\} = 2\delta_{ij}$. The Hamiltonian (5.6) can be re-expressed in terms of the Majorana fermions as

$$H = \sum_{ij} \mathfrak{h}_{ij} c_i c_j, \tag{5.9}$$

with $\mathfrak{h}$ the antisymmetric matrix:

$$\mathfrak{h} = \frac{1}{4} \begin{pmatrix} i\mathrm{Im}(h + 2\Delta) & i\mathrm{Re}(2\Delta + h) \\ i\mathrm{Re}(2\Delta - h) & i\mathrm{Im}(h - 2\Delta) \end{pmatrix}. \tag{5.10}$$

Traces involving quadratic Hamiltonians of the form $A = \mathfrak{a}_{ij} c_i c_j$ where $\mathfrak{a}_{ij}$ is an anti-symmetric matrix, can be calculated by using the counting statistics formulas

presented in [44]. As shown in Sec 5.3, the trace formula

$$\mathrm{Tr}(e^{A_1}...\ e^{A_n}) = \sqrt{\det(1 + e^{4\mathfrak{a}_1}...e^{4\mathfrak{a}_n})}, \tag{5.11}$$

tells us that in the direct RIXS case, the expression for S^{mn} has 3 terms $S^{mn} = S_1^{mn} + S_2^{mn} + S_3^{mn}$, the first and most important term reads:

$$\begin{aligned} S_1^{mn} &= \sqrt{\det(F)}(\Lambda_{n,m} + \Lambda_{n+N,m+N} - \mathrm{i}\Lambda_{n+N,m} - \mathrm{i}\Lambda_{n,m+N}) \\ &\quad \times(\Gamma_{m,n} + \Gamma_{m+N,n+N} - \mathrm{i}\Gamma_{m+N,n} + \mathrm{i}\Gamma_{m,n+N}). \end{aligned} \tag{5.12}$$

Here $\Lambda_{n,m}, \Gamma_{n,m}$ are elements of the $2N \times 2N$ matrices

$$\begin{aligned} \Lambda &= e^{i\mathfrak{h}s}e^{i\mathfrak{h}_m t}e^{i(\tau-t-s)\mathfrak{h}}G^{-1}(1 - N_\beta)e^{-i(\tau-t-s)\mathfrak{h}}e^{-i\mathfrak{h}_m t} \\ \Gamma &= e^{i(\tau-t-s)\mathfrak{h}}N_\beta F^{-1}, \end{aligned} \tag{5.13}$$

where $N_\beta = \frac{1}{1+e^{-4\beta\mathfrak{h}}}$, $K = e^{-4i\mathfrak{h}_n\tau}e^{4i\mathfrak{h}s}e^{4i\mathfrak{h}_m t}e^{4i(\tau-t-s)\mathfrak{h}}$, $F = 1 - N_\beta + KN_\beta$, $G = 1 - N_\beta + N_\beta K$. Here $\mathfrak{h}_m$ represent the Hamiltonian with core hole at position m (i.e. $H_m = \sum_{ij}(\mathfrak{h}_m)_{ij}c_i c_j$). The other terms have similar form, as discussed in detail in Sec 5.3. Since the term S_2 only gives an elastic scattering when there 's no core-hole, and does not depend to much on Δ, we only consider the terms S_1 and S_3.

To explore the role of the superconducting gap, we calculated the RIXS intensity across the superconducting phase transition using Eq (5.12). As is shown in Fig. 5.6, for $\mathbf{Q} = 0.15(\pi, 0)$, the main effect seems to be the shift of spectral density to higher energies: the intensity decreases for small energy transfer and increases for large energy transfer, and the shift is not simply proportional to Δ. The intensity change between the normal and superconducting state is depicted in Fig. 5.7 for different values of momentum exchange $\mathbf{Q}$ and shows the same behavior. We observe

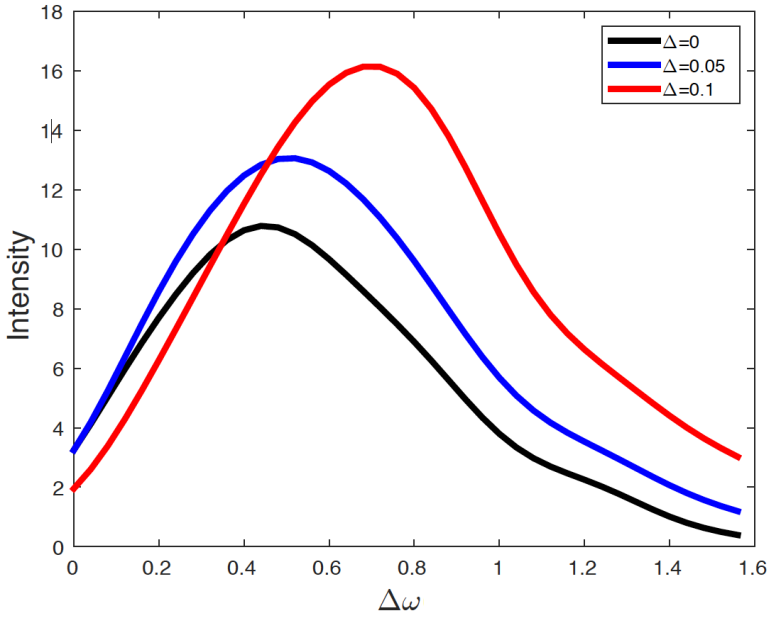

Figure 5.6: RIXS intensity across the transition for a $p_x + ip_y$ superconductor. $\mathbf{Q} = 0.15(\pi, 0)$, $U_c = t$, $\Gamma = 0.4t$, $\omega = 0$ for different values of Δ (in unit of t). Δ increase the spectral weight for higher higher energy exchanges, shifts the peak position, and also broadens the peak. Notice the shift of the peak position is not linear in Δ.

that adding a pairing term will suppress the intensity at small energy and at the same time the intensity increases at higher energy. As we explain below, this behavior can be understood by considering the problem in the absence of a core hole as follows. It turns out that the main exchanges in RIXS intensity occur due to electron-hole pairs where one of them is close to the fermi level. In the presence of pairing, electron states close to the fermi level are unavailable - the incoming photon must first overcome the energy gap, and weight is shifted to higher energies. However, as we will show below, perhaps surprisingly, the increase in intensity at a direction $\mathbf{Q}$ is not directly related to the pairing $\Delta_{\mathbf{Q}}$ at that wave vector.

Many interesting differences in the RIXS signal below and above the SC transition can be observed already for small U_c. In this limit we can compute the RIXS more efficiently using perturbation theory. We consider an expansion in terms of U_c for

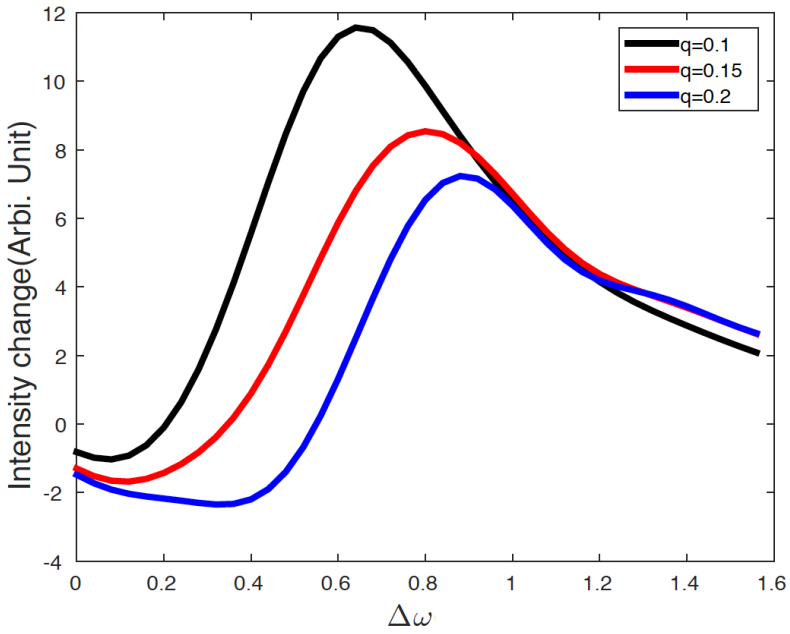

Figure 5.7: The change of intensity $I_{\Delta=0.1t} - I_{\Delta=0}$, for $\mathbf{Q} = \pi(q, 0)$ at several q values.

$\mathcal{F}_{fg}$ in (3.35). For a simple on-site core hole potential V we write:

$$\begin{aligned} G &= (H_m - E_g + i\Gamma + \omega)^{-1} \\ &\sim G^{(0)} - U_c G^{(0)}(d_m^\dagger d_m) G^{(0)} + ... \end{aligned}$$

where $G^{(0)} = (H - E_g + i\Gamma + \omega)^{-1}$, is the propagator with no core-hole. We first consider the lowest order contribution, where $U_c = 0$. The theory is then exactly solvable in terms of the eigen-states of the static problem, and we can calculate the intensity efficiently. We first solve the energy spectrum by switching to momentum space and writing the Hamiltonian in the standard Bogoliubov-de Gennes form:

$$H = \frac{1}{2}\sum_k \begin{bmatrix} d_k^\dagger & d_{-k} \end{bmatrix} \begin{bmatrix} \epsilon_k & \Delta_k \\ \Delta_k^* & -\epsilon_k \end{bmatrix} \begin{bmatrix} d_k \\ d_{-k}^\dagger \end{bmatrix} \tag{5.14}$$

where $\epsilon_k = -\mu - 2t_1[\cos(k_x) + \cos(k_y)] - 4t_2\cos(k_x)\cos(k_y)$, and $\Delta_k = 2\mathrm{i}\Delta[\sin(k_x) +$

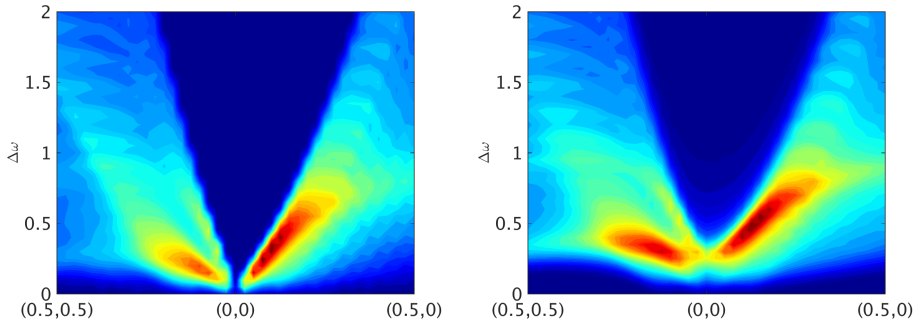

Figure 5.8: RIXS intensity map on $\mathbf{Q}$, $\Delta\omega$ plane, in the (11) and (10) directions (in units of π). Left is the normal phase($\Delta = 0$), right is the superconducting phase($\Delta = 0.05$). The calculation is done using Eq (5.16).

$i\sin(k_y)$], the Hamiltonian is diagonized by a Bogoliubov transformation:

$$\begin{aligned} d_k &= u_k^* b_k + v_k b_{-k}^\dagger \\ d_{-k}^\dagger &= -v_k^* b_k + u_k b_{-k}^\dagger \end{aligned} \tag{5.15}$$

the energy of the excitation is now $E_k = \sqrt{\epsilon_k^2 + |\Delta_k|^2}$, $|u_k|^2 + |v_k|^2 = 1$, and $\frac{u_k}{v_k} = \frac{\Delta_k}{E_k - \epsilon_k}$, the ground state is annihilated by all b_ks, and $\mathcal{F}_{fg}$ in Eq (3.46) is now given explicitly by:

$$\mathcal{F}_{fg}^0 = \sum_{\mathbf{k_1},\mathbf{k_2},\mathbf{r}} e^{i\mathbf{r}(\mathbf{k_1}-\mathbf{k_2}+\mathbf{Q})} \frac{v_{k_1} u_{k_2}}{E_{k_2} + \omega + i\Gamma} \langle f | b_{-k_1}^\dagger b_{k_2}^\dagger | g \rangle \tag{5.16}$$

As remarked before, Fig 5.7 shows the change in intensity below and above the superconducting transition [1]. From (5.16) we see in the quasiparticle picture, the contribution to RIXS intensity comes from pairs of quasiparticles with momenta $\mathbf{k}$ and $\mathbf{k} + \mathbf{Q}$, energies E_k and $-E_k + \Delta\omega$. When there is no pairing term, these are an electron and a hole, and in the presence of a pairing term, these are the Bogoliubov quasiparticles. Going to the superconducting phase, the energy spectrum becomes

[1] Calculations were carried out at zero temperature in the presence and without the gap. We have found that thermal corrections beyond the presence of the gap do not play a significant role in the RIXS signal.

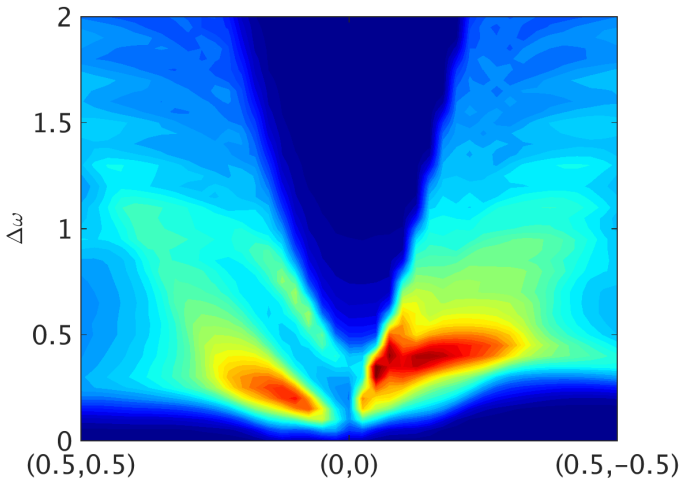

Figure 5.9: RIXS intensity map for a spinless $p_x + p_y$ type of pairing function ($\Delta_k = i2\Delta(\sin k_x + \sin k_y)$) with $\Delta = 0.05t$, in the anti-nodal $(1,1)$, and nodal directions $(1,-1)$ for $\mathbf{Q}$. In the absence of pariting the two directions should have the same intensity, thus the difference comes purely from the presence of the superconducting gap. Surprisingly, the effect is more pronounced on the nodal direction where $\Delta = 0$.

$E_k = \sqrt{\epsilon_k^2 + |\Delta_k|^2}$, when $|\epsilon_k|$ is large, the spectrum does not change too much, since $|\Delta|$ is small compared to other band parameters. Thus the change in the RIXS intensity comes mainly from pairs where at least one quasiparticle is close to the fermi sea, there the energy spectrum and density of states change significantly. For a pair of quasiparticles, one close to the fermi surface, where $|\epsilon_{k_1}| < \Delta_{k_1}$, with $E_{k_1} \sim |\Delta_{k_1}|$, and $E_{k_2} \sim \epsilon_{k_2}$, we have $\Delta\omega \sim |\Delta_{k_1}| + \epsilon_{k_2}$. The same pair without the pairing term will contribute to the intensity at $\Delta\omega \sim \epsilon_{k_2}$. In Fig. 5.8 we show the intensity as a function of $\mathbf{Q}$ and $\Delta\omega$, as calculated from the lowest order contribution (5.16) for the $p + ip$ superconducting state in comparison with it's normal state. The figure shows that for small $\mathbf{Q}$, the intensity is enhanced, which is consistent with having an energy gap forcing larger energy transfers for two quasiparticles near the Fermi sea.

A yet more intriguing situation is that of a $p_x + p_y$ superconducting order which, as opposed to the $p_x + ip_y$ order parameter allows for nodal lines. In Fig 5.9 the RIXS

intensity in the nodal and anti-nodal directions, $(1,-1)$ and $(1,1)$, respectively, are depicted for such a superconductor. There is a striking breaking of the symmetry between the two directions as a result of the pairing. In the absence of pairing, the intensity in the two directions is the same. To see this, consider an electron-hole pair with momenta (k_{x_1}, k_{y_1}), $(k_{x_1}+q, k_{y_1}+q)$, and energies ϵ_1, ϵ_2, which contributes to the intensity at $\Delta\omega$ in the $(1,1)$ direction. Another electron-hole pair with $(k_{x_1}, -k_{y_1})$, $(k_{x_1}+q, -k_{y_1}-q)$, will have the same energies, since $\epsilon(k_x, k_y) = \epsilon(\pm k_x, \pm k_y)$, but will contribute intensity in the $(1,-1)$ direction.

The effect of the pairing term can be understood by looking at $\mathcal{F}^0_{fg}$ over the Brillouin zone. In (5.16), the summation over $\mathbf{r}$ gives a delta function and we can write:

$$\mathcal{F}^0_{fg} = \sum_{\mathbf{k}} \frac{v_{\mathbf{k}} u_{\mathbf{k}+\mathbf{Q}}}{E_{\mathbf{k}+\mathbf{Q}} + \omega + i\Gamma} \tag{5.17}$$

where we took $|f\rangle = b^\dagger_{-\mathbf{k}} b^\dagger_{\mathbf{k}+\mathbf{Q}} |g\rangle$. When the system is unpaired, $|f\rangle$ describes a particle hole pair whose momenta differ by $\mathbf{Q}$ and energies differ by $\Delta\omega$.

We note that the RIXS intensity is the integral over the Brillouin zone of the function:

$$\mathfrak{F}(\mathbf{k}) = \frac{v_{\mathbf{k}} u_{\mathbf{k}+\mathbf{Q}}}{E_{\mathbf{k}+\mathbf{Q}} + \omega + i\Gamma} \delta(E_{\mathbf{k}+\mathbf{Q}} + E_{\mathbf{k}} - \Delta\omega). \tag{5.18}$$

To identify the main contributions to the signal in momentum space we now study the behavior of $\mathfrak{F}(\mathbf{k})$. In practice, we replace the delta function by: $\delta(E) \sim e^{-(E/E_{res})^2/2}$ with $E_{res} = 0.1t$, to account for the experimental energy resolution. The result is shown in Fig. 5.10. Because of the symmetry of the Hamiltonian, at $\Delta = 0$, $\mathfrak{F}_{\mathbf{k}}$ is the same at $\mathbf{Q} = (0.25, 0.25)\pi$ and $\mathbf{Q} = (0.25, -0.25)\pi$, up to 90° rotation. We can now see why for $\mathbf{Q} = (0.25, 0.25)\pi$, in the anti-nodal direction, the effect of pairing

is weaker: $\mathfrak{F}_{\mathbf{k}}$ does not change a lot after turning on the pairing, since the significant regions of $\mathfrak{F}_{\mathbf{k}}$ are far from the line $k_x = k_y$ where the pairing, $\Delta_k = 2i(\sin(k_x)+\sin(k_y))$ is most significant. However, in the nodal direction, $\mathbf{Q} = (0.25, -0.25)\pi$, a pairing term becomes much more relevant: $\mathfrak{F}_{\mathbf{k}}$ has significant contributions across the line $k_x = k_y$, and in those regions $\mathfrak{F}_{\mathbf{k}}$ is sensitive to the pairing term (noted by green circles in the plot), resulting in a substantial change in the RIXS intensity. We thus see that the effect of pairing on intensity is sensitive to the direction of the momentum transfer, and seems to be enhanced in the nodal direction.

In summary, we developed a general formalism to treat the RIXS intensity for a quadratic fermi theory with arbitrary pairing. With the introduction of Majorana fermions, all quadratic Hamiltonians can be handled within the determinant method. Focusing on p-wave superconducting states, we have shown within this approach several intriguing effects on the RIXS signal. The most important findings are a nonlinear shift of the RIXS absorption peak below the superconducting transition, and substantial breaking of symmetry when comparing the nodal and anti-nodal directions, and the effect is more pronounced in the nodal direction than the anti-nodal direction. Other paired systems can readily be studied using the current approach. It would be of interest to test the behavior described here by carrying out RIXS measurements below and above a superconducting transition.

We have confined our discussion here to mean field BCS and made no speculation about the validity of the results to strongly correlated systems and it's relevance for high-Tc superconductors. It is however of great interest to see how the present approach may affect results pertaining to the quasiparticle interpretation of RIXS results on cuprates.

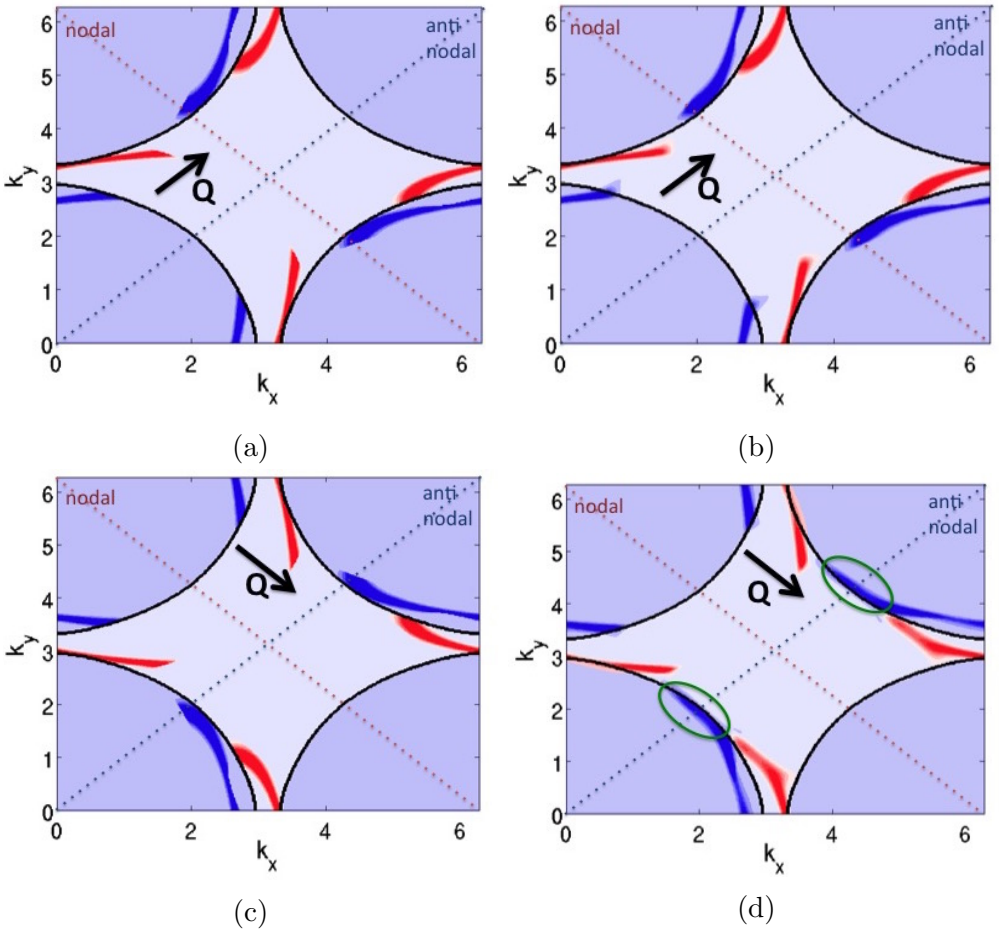

Figure 5.10: $\mathfrak{F}_{\mathbf{k}}$ over the Brillouin zone, for a $p_x + p_y$ pairing. The black lines show the original Fermi surface, red regions denote large values of $\mathfrak{F}_{\mathbf{k}}$ from electron like regions and the blue regions are the associated hole like quasiparticles. (a) and (b): $\mathbf{Q} = (0.25, 0.25)\pi$, anti-nodal direction, energy transfer $\Delta\omega = 0.35t$. (a): $\Delta = 0$, and (b): $\Delta = 0.05t$. (c) and (d): $\mathbf{Q} = (0.25, -0.25)\pi$, nodal direction, energy transfer $\Delta\omega = 0.35t$. (a): $\Delta = 0$, and (b): $\Delta = 0.05t$. The region marked with green in (d) is the most affected by the pairing.

5.3 appendix

Here we detail the calculation of (5.12). Explicitly,

$$\begin{aligned} S^{xy} &= \langle e^{iH\tau} d_y e^{-iH_y\tau} d_y^\dagger e^{iHs} d_x e^{iH_x t} d_x^\dagger e^{-iH(t+s)} \rangle \\ &= \mathrm{tr}[e^{iH\tau} d_y e^{-iH_y\tau} d_y^\dagger ... \\ &... \quad e^{iHs} d_x e^{iH_x t} d_x^\dagger e^{-iH(t+s)-\beta H}]/\mathrm{tr}[e^{-\beta H}]. \end{aligned} \tag{5.19}$$

Here, two core-holes are created at site x and y.

We first focus on the numerator. When replacing all the fermions with Majorana operators, we get a combination of terms such as:

$$\begin{aligned} \mathrm{Num} &= \Sigma_{qmnp} \mathrm{tr}[e^{iH\tau} c_q e^{-iH_y\tau} c_m e^{iHs} c_n e^{iH_x t} c_p e^{-iH(t+s)-\beta H}] \\ &= \Sigma_{qmnp} \mathrm{tr}[c_q e^{X_4} c_m e^{X_3} c_n e^{X_2} c_p e^{X_1}] \end{aligned} \tag{5.20}$$

Here the nonzero elements of Σ are

$$\begin{aligned} \Sigma_{yyxx} &= \Sigma_{y+N,y+N,x+N,x+N} = \Sigma_{y+N,y+N,x,x} = \Sigma_{y,y,x+N,x+N} = \frac{1}{16} \\ \Sigma_{y,y+N,x,x+N} &= \Sigma_{y+N,y,x+N,x+N} = -\Sigma_{y,y+N,x+N,x} = -\Sigma_{y+N,y,x,x+N} = -\frac{1}{16} \\ \Sigma_{y,y,x,x+N} &= \Sigma_{y,y+N,x,x} = \Sigma_{y+N,y+N,x+N,x} = \Sigma_{y+N,y,x+N,x+N} = \frac{i}{16} \\ \Sigma_{y,y,x+N,x} &= \Sigma_{y+N,y,x,x} = \Sigma_{y+N,y+N,x,x+N} = \Sigma_{y,y+N,x+N,x+N} = -\frac{i}{16} \end{aligned} \tag{5.21}$$

Using the relation: $c_m e^{A_{i,j} c_i c_j} = e^{A_{i,j} c_i c_j} c_{m'} (e^{4A})_{m,m'}$ (same indices are summed over), we can move all the Majorana fermions to the right, yielding:

$$\begin{aligned} \mathrm{Num} &= \Sigma_{qmnp} (e^{X_1})_{p,p'} (e^{X_2} e^{X_1})_{n,n'} (e^{X_3} e^{X_2} e^{X_1})_{m,m'} \\ &\times \quad \mathrm{tr}[e^{Z_{ij} c_i c_j} c_{m'} c_{n'} c_{p'} c_q] \end{aligned} \tag{5.22}$$

where $e^{Z_{ij}c_ic_j} = e^{X_4}e^{X_3}e^{X_2}e^{X_1}$. Now the task is to calculate traces of the form:

$$\begin{aligned} T_{mnpq} &= \mathrm{tr}[e^{Z_{ij}c_ic_j}c_mc_nc_pc_q] \\ &= \mathrm{tr}[e^{Z_{ij}c_ic_j}(\delta_{mn}+\frac{c_mc_n-c_nc_m}{2})(\delta_{pq}+\frac{c_pc_q-c_qc_p}{2})] \\ &= \mathrm{tr}[e^{Z_{ij}c_ic_j}(\frac{1}{4}\mathcal{M}\mathcal{N}+\frac{1}{2}\mathcal{M}\delta_{pq}+\frac{1}{2}\mathcal{N}\delta_{nm}+\delta_{mn}\delta_{pq})], \end{aligned} \tag{5.23}$$

where $\mathcal{M} = M_{ij}c_ic_j$. $M = |m\rangle\langle n| - |n\rangle\langle m|$, $N = |p\rangle\langle q| - |q\rangle\langle p|$. Now that M and N are anti-symmetric matrices and we can write $\mathcal{M} = \frac{\partial}{\partial\alpha}e^{\alpha\mathcal{M}}\mid_{\alpha=0}$, and use the trace formula (5.11) to calculate T. First we find:

$$\begin{aligned} &\mathrm{tr}(e^{Z_{ij}c_ic_j}\frac{d}{d\alpha}e^{\alpha M_{ij}c_ic_j}|_{\alpha=0}) = \frac{\partial}{\partial\alpha}\mathrm{tr}(e^{Z_{ij}c_ic_j}e^{\alpha M_{ij}c_ic_j})|_{\alpha=0} \\ = &\frac{1}{2}\sqrt{\det(1+e^{4Z}e^{4\alpha M})}\mathrm{tr}[\frac{4e^{4Z}M}{1+e^{4Z}e^{4\alpha M}}]\mid_{\alpha=0} \\ = &2\sqrt{\det(1+e^{4Z})}\{(1+e^{-4Z})^{-1}_{nm}-(1+e^{-4Z})^{-1}_{mn}\} \end{aligned} \tag{5.24}$$

Next, we define $B = \frac{1}{1+e^{-4Z}}$ and $\mathrm{Det} = \det(1+e^{4Z})$. Then,

$$\begin{aligned} &\frac{\partial}{\partial\beta}\frac{\partial}{\partial\alpha}\mathrm{tr}(e^Ze^{\alpha M}e^{\beta N}) \\ = &\sqrt{\mathrm{Det}}\{4\mathrm{tr}(BM)\mathrm{tr}(BN) \\ - &8\mathrm{tr}(BNBM)+8\mathrm{tr}(BMN)\} \end{aligned} \tag{5.25}$$

The last step we take $\alpha = 0$, and $\beta = 0$. Plug the result from the above two equations into Eq (5.23), we find:

$$\begin{aligned} T_{mnpq} = &\sqrt{\mathrm{Det}}\{(B_{nm}-B_{mn}+\delta_{mn})(B_{qp}-B_{pq}+\delta_{pq}) \\ &+2B_{qm}(\delta_{np}-B_{np})+2B_{pn}(\delta_{mq}-B_{mq}) \\ &-2B_{pm}(\delta_{nq}-B_{nq})-2B_{qn}(\delta_{mp}-B_{mp})\} \end{aligned} \tag{5.26}$$

Noticing that since Z is anti-symmetric, $B_{nm} + B_{mn} = \delta_{mn}$, we get:

$$T_{mnpq} = 4\sqrt{\mathrm{Det}}(B_{nm}B_{qp} + B_{qm}B_{pn} - B_{pm}B_{qn}) \tag{5.27}$$

And

$$S^{xy} = \Sigma_{qmnp}(e^{X_1})_{p,p'}(e^{X_2}e^{X_1})_{n,n'}(e^{X_3}e^{X_2}e^{X_1})_{m,m'}T_{m'n'p'q} \tag{5.28}$$

So there are in total 3 terms. We first focus on the first term:

$$S_1 = 4\Sigma_{qmnp}\sqrt{\mathrm{Det}}B_{nm}B_{qp}(e^{X_1})_{p,p'}(e^{X_2}e^{X_1})_{n,n'}(e^{X_3}e^{X_2}e^{X_1})_{m,m'} \tag{5.29}$$

We Plug it back into Eq (5.22), and define $K = e^{-4ih_n\tau}e^{4ihs}e^{4ih_m t}e^{4i(\tau-t-s)h}$, $N_\beta = \frac{1}{1+e^{4\beta h}}$, then $e^Z = K\frac{N_\beta}{1-N_\beta}$, $B = (1 + \frac{1-N_\beta}{N_\beta}K^{-1})^{-1}$. And:

$$S_1 = \Sigma_{qmnp}(e^{X_3}e^{X_2}e^{X_1}B^T(e^{X_2}e^{X_1})^T)_{mn}(e^{X_1}B^T)_{pq}, \tag{5.30}$$

where T is the matrix transpose. In order to calculate the low temperature limit($\beta \to \infty$), we have to calculate $e^{X_1}B(e^{X_1})^T$, notice that for anti-symmetric matrix h, $e^{-h} = (e^h)^T$, so

$$\begin{aligned} e^{-4\beta h}B^T(e^{-4\beta h})^T &= \frac{N_\beta}{1-N_\beta}\frac{\frac{1-N_\beta}{N_\beta}K^{-1}}{1+\frac{1-N_\beta}{N_\beta}K^{-1}}\frac{1-N_\beta}{N_\beta} \\ &= K^{-1}\frac{1}{N_\beta + (1-N_\beta)K^{-1}}(1-N_\beta) \\ &= \frac{1}{1-N_\beta+N_\beta K}(1-N_\beta) \end{aligned}$$

and

$$e^{-4\beta h}B^T = \frac{N_\beta}{1-N_\beta}\frac{1}{1+K\frac{N_\beta}{1-N_\beta}} = N_\beta\frac{1}{1-N_\beta+KN_\beta}$$

Next we define $F = 1 - N_\beta + KN_\beta$, $G = 1 - N_\beta + N_\beta K$:

$$\begin{aligned}
\Lambda &= e^{ihs}e^{ih_x t}e^{i(\tau-t-s)h}G^{-1}(1-N_\beta)e^{-i(\tau-t-s)h}e^{-ih_x t} \\
\Gamma &= e^{i(\tau-t-s)h}N_\beta F^{-1}.
\end{aligned} \tag{5.31}$$

Using the above results and summing over m, n, p, q , we have:

$$\begin{aligned}
S_1 &= \sqrt{\det(F)}(\Lambda_{y,x} + \Lambda_{y+N,x+N} - i\Lambda_{y+N,x} + i\Lambda_{y,x+N}) \\
&\times \quad (\Gamma_{y,x} + \Gamma_{y+N,x+N} + i\Gamma_{y+N,x} - i\Gamma_{y,x+N})
\end{aligned} \tag{5.32}$$

In the similar, the second term is written as:

$$\begin{aligned}
S_2 &= \Sigma_{qmnp}(e^{X_2}e^{X_1}B^T e^{-X_1})_{pn}(e^{X_3}e^{X_2}e^{X_1}B^T)_{mq} \\
&= (\Lambda^{(2)}_{y,y} + \Lambda^{(2)}_{y+N,y+N} + i\Lambda^{(2)}_{y+N,y} - i\Lambda^{(2)}_{y,y+N}) \\
&\times \quad (\Gamma^{(2)}_{x,x} + \Gamma^{(2)}_{x+N,x+N} + i\Gamma^{(2)}_{x+N,x} - i\Gamma^{(2)}_{x,x+N})
\end{aligned} \tag{5.33}$$

where $\Lambda^{(2)} = e^{-ihs}\Lambda e^{ih_x t}$ and $\Gamma^{(2)} = e^{ihs}e^{ih_x t}\Gamma$. For the third term S_3,

$$\begin{aligned}
S_3 &= \Sigma_{qmnp}(e^{X_2}e^{X_1}B^T)_{nq}(e^{X_3}e^{X_2}e^{X_1}B^T e^{-X_1})_{mp} \\
&= (\Lambda^{(3)}_{x,y} - \Lambda^{(3)}_{x+N,y+N} - i\Lambda^{(3)}_{x+N,y} - i\Lambda^{(3)}_{x,y+N}) \\
&\times \quad (\Gamma^{(3)}_{x,y} - \Gamma^{(3)}_{y+N,x+N} + i\Gamma^{(3)}_{x+N,y} + i\Gamma^{(3)}_{x,y+N})
\end{aligned} \tag{5.34}$$

where $\Lambda^{(3)} = \Lambda e^{ih_x t}$ and $\Gamma^{(3)} = e^{ih_x t}\Gamma$.

Finally, we remark that S_2 does not contribute when the core-hole potential U_c is 0. In that case, $K = \mathbb{I}$, and S_2 does only depends on t and τ, so it gives a elastic scattering. Also, S_3 would be 0 when there is no pairing, in that case the matrices $\Lambda^{(3)}$ and $\Gamma^{(3)}$ have special form that $\Lambda^{(3)}(x, y) = \Lambda^{(3)}(x + N, y + N)$, $\Lambda^{(3)}(x, y + N) = -\Lambda^{(3)}(x + N, y)$, so that S_3 vanishes.

BIBLIOGRAPHY

BIBLIOGRAPHY

[1] Ian Affleck, Tom Kennedy, Elliott H. Lieb, and Hal Tasaki. Valence bond ground states valence bond ground states in isotropic quantum antiferromagnets. *Commun. Math. Phys. 115, 477-528*, 1988.

[2] Jason Alicea. Majorana fermions in a tunable semiconductor device. *Physical Review B*, 81(12):125318, 2010.

[3] Jason Alicea. New directions in the pursuit of majorana fermions in solid state systems. *Reports on Progress in Physics*, 75(7):076501, 2012.

[4] Luuk JP Ament, Michel van Veenendaal, Thomas P Devereaux, John P Hill, and Jeroen van den Brink. Resonant inelastic x-ray scattering studies of elementary excitations. *Reviews of Modern Physics*, 83(2):705, 2011.

[5] Eran Amit and Amit Keren. Critical-doping universality for cuprate superconductors: Oxygen nuclear-magnetic-resonance investigation of (ca x la 1- x)(ba 1.75- x la 0.25+ x) cu 3 o y. *Physical Review B*, 82(17):172509, 2010.

[6] AF Bangura, JD Fletcher, A Carrington, J Levallois, M Nardone, B Vignolle, PJ Heard, N Doiron-Leyraud, D LeBoeuf, L Taillefer, et al. Small fermi surface pockets in underdoped high temperature superconductors: Observation of shubnikov–de haas oscillations in yba 2 cu 4 o 8. *Physical review letters*, 100(4):047004, 2008.

[7] W. Belzig. Full counting statistics in quantum contacts. *CFN Lectures on Functional Nanostructures Vol. 1*, pages 123–143, 2005.

[8] David Benjamin, Israel Klich, and Eugene Demler. Probing competing and intertwined orders with resonant inelastic x-ray scattering in the hole-doped cuprates. *arXiv preprint arXiv:1407.3843*, 2014.

[9] David Benjamin, Israel Klich, and Eugene Demler. Single-band model of resonant inelastic x-ray scattering by quasiparticles in high-t c cuprate superconductors. *Physical review letters*, 112(24):247002, 2014.

[10] David Benjamin, Israel Klich, and Eugene Demler. Single-band model of resonant inelastic x-ray scattering by quasiparticles in high-t c cuprate superconductors. *Physical Review Letters*, 112(24):247002, 2014.

[11] S. Blinnikov and R. Moessner. Expansions for nearly gaussian distributions. *Astronomy and astrophysics Supplement series, 130: 193–205*, 1998.

[12] SG Bobkov, GP Chistyakov, and F. Götze. Rate of convergence and edgeworth-type expansion in the entropic central limit theorem. *arXiv preprint arXiv:1104.3994*, 2011.

[13] Y. Bomze, G. Gershon, D. Shovkun, LS Levitov, and M. Reznikov. Measurement of counting statistics of electron transport in a tunnel junction. *Physical review letters*, 95(17):176601, 2005.

[14] C.-C. Chen, B. Moritz, F. Vernay, J. N. Hancock, S. Johnston, C. J. Jia, G. Chabot-Couture, M. Greven, I. Elfimov, G. A. Sawatzky, and T. P. Devereaux. Unraveling the nature of charge excitations in la 2 cuo 4 with momentum-resolved cu k-edge resonant inelastic x-ray scattering. *Physical review letters*, 105(17):177401, 2010.

[15] Xie Chen, Zheng-Cheng Gu, and Xiao-Gang Wen. Local unitary transformation, long-range quantum entanglement, wave function renormalization, and topological order. *Physical Review B*, 82(15):155138, 2010.

[16] Xie Chen, Zheng-Cheng Gu, and Xiao-Gang Wen. Classification of gapped symmetric phases in one-dimensional spin systems. *Physical Review B*, 83(3):035107, 2011.

[17] R.W. Cherng and E. Demler. Quantum noise analysis of spin systems realized with cold atoms. *New Journal of Physics*, 9(1):7, 2007.

[18] M. P. M. Dean, G. Dellea, R. S. Springell, F. Yakhou-Harris, K. Kummer, N. B. Brookes, X. Liu, Y-J. Sun, J. Strle, T. Schmitt, L. Braicovich, G. Ghiringhelli, I. Božović, and J. P. Hill. Persistence of magnetic excitations in la2- xsrxcuo4 from the undoped insulator to the heavily overdoped non-superconducting metal. *Nature materials*, 2013.

[19] MPM Dean, AJA James, RS Springell, X Liu, C Monney, KJ Zhou, RM Konik, JS Wen, ZJ Xu, GD Gu, et al. High-energy magnetic excitations in the cuprate superconductor bi 2 sr 2 cacu 2 o 8+ δ: towards a unified description of its electronic and magnetic degrees of freedom. *Physical review letters*, 110(14):147001, 2013.

[20] MPM Dean, AJA James, AC Walters, V Bisogni, I Jarrige, M Hücker, E Giannini, M Fujita, J Pelliciari, YB Huang, et al. Itinerant effects and enhanced magnetic interactions in bi-based multilayer cuprates. *Physical Review B*, 90(22):220506, 2014.

[21] B. Derrida, MR Evans, V. Hakim, and V. Pasquier. Exact solution of a 1d asymmetric exclusion model using a matrix formulation. *Journal of Physics A: Mathematical and General*, 26(7):1493, 1999.

[22] Gil Drachuck, Elia Razzoli, Rinat Ofer, Galina Bazalitsky, RS Dhaka, Amit Kanigel, Ming Shi, and Amit Keren. Linking dynamic and thermodynamic properties of cuprates: An angle-resolved photoemission study of (ca x la 1- x)(ba 1.75- x la 0.25+ x) cu 3 o y (x= 0.1 and 0.4). *Physical Review B*, 89(12):121119, 2014.

[23] David Shai Ellis, Yao-Bo Huang, Paul Olalde-Velasco, Marcus Dantz, Jonathan Pelliciari, Gil Drachuck, Rinat Ofer, Galina Bazalitsky, Jorge Berger, Thorsten Schmitt, et al. Correlation of the superconducting critical temperature with spin and orbital excitations in (ca x la 1- x)(ba 1.75- x la 0.25+ x) cu 3 o y as measured by resonant inelastic x-ray scattering. *Physical Review B*, 92(10):104507, 2015.

[24] C.G. Esseen. Fourier analysis of distribution functions. a mathematical study of the laplace-gaussian law. *Acta Mathematica*, 77(1):1–125, 1945.

[25] C. Flindt, C. Fricke, F. Hohls, T. Novotnỳ, K. Netočnỳ, T. Brandes, and RJ Haug. Universal oscillations in counting statistics. *Proceedings of the National Academy of Sciences*, 106(25):10116, 2009.

[26] Liang Fu and Charles L Kane. Superconducting proximity effect and majorana fermions at the surface of a topological insulator. *Physical review letters*, 100(9):096407, 2008.

[27] Masaki Fujita, Haruhiro Hiraka, Masaaki Matsuda, Masato Matsuura, John M. Tranquada, Shuichi Wakimoto, Guangyong Xu, and Kazuyoshi Yamada. Progress in neutron scattering studies of spin excitations in high-t c cuprates. *Journal of the Physical Society of Japan*, 81(1):011007, 2011.

[28] AK Geim, PC Main, N La Scala Jr, L Eaves, TJ Foster, PH Beton, JW Sakai, FW Sheard, M Henini, G Hill, et al. Fermi-edge singularity in resonant tunneling. *Physical review letters*, 72(13):2061, 1994.

[29] Dimitri Gioev and Israel Klich. Entanglement entropy of fermions in any dimension and the widom conjecture. *Physical review letters*, 96(10):100503, 2006.

[30] R.J. Glauber. Photon correlations. *Physical Review Letters*, 10(3):84–86, 1963.

[31] M. Gorissen, A. Lazarescu, K. Mallick, and C. Vanderzande. Exact current statistics of the asymmetric simple exclusion process with open boundaries. *Physical Review Letters*, 109(17):170601, 2012.

[32] M Guarise, B Dalla Piazza, H Berger, E Giannini, T Schmitt, HM Rønnow, GA Sawatzky, J van den Brink, D Altenfeld, I Eremin, et al. Anisotropic softening of magnetic excitations along the nodal direction in superconducting cuprates. *Nature Communications*, 5, 2014.

[33] MC Gutzwiller. Phys. re v. lett. 1963, 10, 159. *Phys. Rev*, 134:A993, 1964.

[34] M Zahid Hasan and Charles L Kane. Colloquium: topological insulators. *Reviews of Modern Physics*, 82(4):3045, 2010.

[35] R. Hübener, A. Mari, and J. Eisert. Wick's theorem for matrix product states. *arXiv preprint arXiv:1207.6537*, 2012.

[36] Jun-ichi Igarashi and Tatsuya Nagao. Analysis of resonant inelastic x-ray scattering from sr 2 iro 4 in an itinerant-electron approach. *Physical Review B*, 90(6):064402, 2014.

[37] DA Ivanov. Non-Abelian statistics of half-quantum vortices in p-wave superconductors. *Physical Review Letters*, 86(2):268–271, 2001.

[38] D.A. Ivanov and A.G. Abanov. Characterizing correlations with full counting statistics: classical ising and quantum xy spin chains. *arXiv preprint arXiv:1203.6325*, 2012.

[39] AJA James, RM Konik, and TM Rice. Magnetic response in the underdoped cuprates. *Physical Review B*, 86(10):100508, 2012.

[40] C. J. Jia, E. A. Nowadnick, K. Wohlfeld, Y. F. Kung, C. C. Chen, S. Johnston, T. Tohyama, B. Moritz, and T. P. Devereaux. Persistent spin excitations in doped antiferromagnets revealed by resonant inelastic light scattering. *Nature communications*, 5, 2014.

[41] Márton Kanász-Nagy, Yifei Shi, Israel Klich, and Eugene A Demler. Resonant inelastic x-ray scattering as a band structure probe. *arXiv preprint arXiv:1508.06639*, 2015.

[42] I. Klich and L. Levitov. Quantum noise as an entanglement meter. *Phys. Rev. Lett.*, 102(10):100502, 2009.

[43] I. Klich, G. Refael, and A. Silva. Measuring entanglement entropies in many-body systems. *Physical Review A*, 74(3):32306, 2006.

[44] Israel Klich. A note on the full counting statistics of paired fermions. *Journal of Statistical Mechanics: Theory and Experiment*, 2014(11):P11006, 2014.

[45] A Knizhnik, Y Direktovich, GM Reisner, D Goldschmidt, CG Kuper, and Y Eckstein. Transport measurements in the 1-2-3 system clblco in both the oxygen-underdoped and-overdoped regions. *Physica C: Superconductivity*, 321(3):199–206, 1999.

[46] John Kolassa. *Series Approximation Methods in Statistics*. Springer, 2005.

[47] A. Komnik and H. Saleur. Quantum fluctuation theorem in an interacting setup: point contacts in fractional quantum hall edge state devices. *Physical Review Letters*, 107(10):100601, 2011.

[48] RM Konik, TM Rice, and AM Tsvelik. Doped spin liquid: Luttinger sum rule and low temperature order. *Physical review letters*, 96(8):086407, 2006.

[49] Peter D. Lax. *Linear Algebra*. Wiley, 1996.

[50] M. Le Tacon, G. Ghiringhelli, J. Chaloupka, M. Moretti Sala, V. Hinkov, M. W. Haverkort, M. Minola, M. Bakr, K. J. Zhou, S. Blanco-Canosa, C. Monney, Y. T. Song, G. L. Sun, C. T. Lin, G. M. De Luca, M. Salluzzo, G. Khaliullin, T. Schmitt, L. Braicovich, and B. Keimer. Intense paramagnon excitations in a large family of high-temperature superconductors. *Nature Physics Phys*, 7(9):725–730, 09 2011.

[51] Samuel Lederer, Wen Huang, Edward Taylor, Srinivas Raghu, and Catherine Kallin. Suppression of spontaneous currents in sr _2 ruo _4 by surface disorder. *arXiv preprint arXiv:1404.4637*, 2014.

[52] Michael Levin and Cody P Nave. Tensor renormalization group approach to 2d classical lattice models. *arXiv preprint cond-mat/0611687*, 2006.

[53] G. C. Levine, M. J. Bantegui, and J. A. Burg. Full counting statistics in a disordered free fermion system. *Phys. Rev. B*, 86:174202, Nov 2012.

[54] LS Levitov and GB Lesovik. Charge-transport statistics in quantum conductors. *JETP letters*, 55(9):555–559, 1992.

[55] B.Nachtergaele M. Fannes and R. Werner. Finitely correlated states on quantum spin chains. *Comm. Math. Phys.*, 144(3), 1992.

[56] L. Mandel and E. Wolf. Coherence properties of optical fields. *Reviews of modern physics*, 37(2):231, 1965.

[57] M Minola, G Dellea, H Gretarsson, YY Peng, Y Lu, J Porras, T Loew, F Yakhou, NB Brookes, YB Huang, et al. Collective nature of spin excitations in superconducting cuprates probed by resonant inelastic x-ray scattering. *Physical Review Letters*, 114(21):217003, 2015.

[58] Y.V. Nazarov and M. Kindermann. Full counting statistics of a general quantum mechanical variable. *The European Physical Journal B-Condensed Matter and Complex Systems*, 35(3):413–420, 2003.

[59] Tetsuo Ogawa, Akira Furusaki, and Naoto Nagaosa. Fermi-edge singularity in one-dimensional systems. *Physical review letters*, 68(24):3638, 1992.

[60] David Perez-Garcia, Frank Verstraete, Michael M Wolf, and J Ignacio Cirac. Matrix product state representations. *arXiv preprint quant-ph/0608197*, 2006.

[61] V.V. Petrov. On local limit theorems for sums of independent random variables. *Theory of Probability & Its Applications*, 9(2):312–320, 1964.

[62] Ulrich Schollwöck. The density-matrix renormalization group in the age of matrix product states. *Ann. Phys.*, 326(1):96–192, 2011.

[63] K. Schönhammer. Full counting statistics for noninteracting fermions: Exact results and the levitov-lesovik formula. *Physical Review B*, 75(20):205329, 2007.

[64] KD Schotte and U Schotte. Tomonaga's model and the threshold singularity of x-ray spectra of metals. *Physical Review*, 182(2):479, 1969.

[65] Yifei Shi and Israel Klich. Full counting statistics and the edgeworth series for matrix product states. *Journal of Statistical Mechanics: Theory and Experiment*, 2013(05):P05001, 2013.

[66] H.F. Song, C. Flindt, S. Rachel, I. Klich, and K. Le Hur. Entanglement entropy from charge statistics: Exact relations for noninteracting many-body systems. *Physical Review B*, 83(16):161408, 2011.

[67] Alexei M Tsvelik. *Quantum field theory in condensed matter physics*. Cambridge university press, 2006.

[68] Jeroen van den Brink. The theory of indirect resonant inelastic x-ray scattering on magnons. *EPL (Europhysics Letters)*, 80(4):47003, 2007.

[69] Jeroen van den Brink and Michel van Veenendaal. Theory of indirect resonant inelastic x-ray scattering. *Journal of Physics and Chemistry of Solids*, 66(12):2145–2149, 2005.

[70] Michel Van Veenendaal. *Theory of Inelastic Scattering and Absorption of X-rays*. Cambridge University Press, 2015.

[71] F Vernay, B Moritz, IS Elfimov, J Geck, D Hawthorn, TP Devereaux, and GA Sawatzky. Cu k-edge resonant inelastic x-ray scattering in edge-sharing cuprates. *Physical Review B*, 77(10):104519, 2008.

[72] F. Verstraete and J. I. Cirac. Matrix product states represent ground states faithfully. *Phys. Rev. B 73, 094423*, 2006.

[73] Frank Verstraete, Valentin Murg, and J Ignacio Cirac. Matrix product states, projected entangled pair states, and variational renormalization group methods for quantum spin systems. *Advances in Physics*, 57(2):143–224, 2008.

[74] Frank Verstraete, Valentin Murg, and J Ignacio Cirac. Matrix product states, projected entangled pair states, and variational renormalization group methods for quantum spin systems. *Advances in Physics*, 57(2):143–224, 2008.

[75] G. Vidal. Entanglement renormalization. *Physical Review Letters*, 99(22):220405, 2007.

[76] Guifré Vidal. Efficient simulation of one-dimensional quantum many-body systems. *Physical Review Letters*, 93(4):040502, 2004.

[77] B Vignolle, A Carrington, RA Cooper, MMJ French, AP Mackenzie, C Jaudet, D Vignolles, Cyril Proust, and NE Hussey. Quantum oscillations in an overdoped high-tc superconductor. *Nature*, 455(7215):952–955, 2008.

[78] Steven R White. Density matrix formulation for quantum renormalization groups. *Physical Review Letters*, 69(19):2863, 1992.

[79] Wikipedia. Aklt model — wikipedia, the free encyclopedia, 2015. [Online; accessed 14-October-2015].

[80] Wikipedia. Ettore majorana — wikipedia, the free encyclopedia, 2015. [Online; accessed 9-November-2015].

[81] Maw-Kuen Wu, Jo R Ashburn, C_J Torng, Ph H Hor, Rl L Meng, Lo Gao, Z J_ Huang, YQ Wang, and CW Chu. Superconductivity at 93 k in a new mixed-phase y-ba-cu-o compound system at ambient pressure. *Physical Review Letters*, 58(9):908, 1987.

[82] H-B Yang, JD Rameau, PD Johnson, T Valla, A Tsvelik, and GD Gu. Emergence of preformed cooper pairs from the doped mott insulating state in bi2sr2cacu2o8+ &dgr. *Nature*, 456(7218):77–80, 2008.

[83] Kai-Yu Yang, TM Rice, and Fu-Chun Zhang. A phenomenological theory of the pseudogap state. *arXiv preprint cond-mat/0602164*, 2006.

[84] Jaejun Yu, S Massidda, AJ Freeman, and DD Koeling. Bonds, bands, charge transfer excitations and superconductivity of yba 2 cu 3 o 7-δ. *Physics Letters A*, 122(3):203–208, 1987.

[85] Michael Zwolak and Guifré Vidal. Mixed-state dynamics in one-dimensional quantum lattice systems: a time-dependent superoperator renormalization algorithm. *Physical review letters*, 93(20):207205, 2004.